R. & M. No. 3270

MINISTRY OF AVIATION

AERONAUTICAL RESEARCH COUNCIL
REPORTS AND MEMORANDA

A Study of the Effect of Leading-Edge Modifications on the Flow over a 50-deg Sweptback Wing at Transonic Speeds

By E. W. E. Rogers, C. J. Berry and J. E. G. Townsend,
of the Aerodynamics Division, N.P.L.

LONDON: HER MAJESTY'S STATIONERY OFFICE
1962
PRICE £1 12s. 6d. NET

A Study of the Effect of Leading-Edge Modifications on the Flow over a 50-deg Sweptback Wing at Transonic Speeds

By E. W. E. Rogers, C. J. Berry and J. E. G. Townsend,
of the Aerodynamics Division, N.P.L.

*Reports and Memoranda No. 3270**
May, 1960

Summary. An investigation has been made in the N.P.L. 18 in. × 14 in. Tunnel of the effects of leading-edge modifications on the flow and forces on an untapered wing of 50 deg leading-edge sweep, at stream Mach numbers between 0·60 and 1·20. Seven leading-edge profiles were tested, ranging from a drooped extension of 18 per cent of the chord of the basic sharp-nosed section to a round-nosed section with a leading-edge radius of 1·0 per cent of the basic chord.

Leading-edge droop was found to increase the wing drag near zero lift but to reduce appreciably the lift-dependent drag component, except at the highest test Mach numbers. Droop also increased the lift coefficient at which leading-edge separation occurred on the upper surface at moderate subsonic speeds, but in addition reduced the Mach number for transonic flow attachment. The appearance of the forward shock (but not the rear shock) is considerably delayed when the leading edge is drooped.

With the undrooped sections an increase in leading-edge radius was accompanied by successively earlier appearances of the forward shock, and hence the outboard shock with its attendant separation. The conditions at which the rear shock first appeared changed only slowly as the section was changed.

The variations in wing flow pattern as the leading edge is modified are discussed and related to measured changes in the wing lift and drag. An attempt is also made to estimate the local Mach numbers on some parts of the wing from the oil-flow patterns; this material is used to assess the flow conditions appropriate to shock-induced separation.

The main section of the Report concludes with a tentative discussion of the significance of the present results to the design of swept wings. In an Appendix results obtained with the wing in a sweptforward configuration are briefly considered.

1. *Introduction.* In recent years there has been a great increase in our knowledge of the flow about sweptback wings at transonic speeds, and this has led to a better understanding of the problems that must be overcome to obtain the most efficient wing designs.

Much of the advance is due to the increasing use of oil-film techniques to show up the surface flow, and with experience the patterns obtained can be interpreted to provide detailed and accurate information on such things as vortex and shock-wave positions and the occurrence and extent of

* Previously issued as A.R.C. 21,987. Published with the permission of the Director, National Physical Laboratory.

flow separations. This information is of considerable value in assessing the significance of changes in wing forces and moments, or local surface pressures, and indeed is almost essential in any fundamental investigation.

At present, the various shock waves and flow separations that may occur on swept wings at transonic speeds are comparatively well known, but there are still some doubts as to how such phenomena would be modified by changes in the wing profile. These doubts will only be resolved by means of extensive wind-tunnel tests, but as a preliminary contribution it was felt worthwhile making a simple experiment using an untapered swept wing, and progressively modifying the leading edge in seven stages, from a fairly extensive droop to an undrooped section with a large leading-edge radius.

The measurement of surface pressures was felt to complicate unduly the initial manufacture of the model and its subsequent modification, as well as extending the time required for testing in the tunnel. It was decided therefore to measure for each model state only the wing lift and drag for a wide range of incidence and Mach number, and to supplement this with an extensive series of oil-flow patterns.

As will be shown, the latter provide valuable evidence of the effect of leading-edge changes on the flow structure. Moreover in some cases, an approximate estimate can be made from the oil patterns of the local surface Mach numbers and hence the strengths of the shockwaves.

The tests were carried out at intervals between September, 1957 and June, 1958.

2. *Experimental Details.* 2.1. *The Model.* The model used for the tests was a half-wing, mounted directly on to the tunnel wall. It was without taper or twist, and the sweep (50 deg) was chosen to be representative of the region where the wing flow is likely to be most complex.

The wing was tested with the profile in seven states (A to G), which are illustrated in Figs. 1 and 2; the profile ordinates, and other section details are listed in Tables 1 and 2.

The initial state (A) consisted of a moderately large droop, with a small leading-edge radius; the first modification (to state B) almost doubled this radius with a corresponding small reduction in the extent of the droop. In state C, the leading-edge radius of state B was retained but the droop was considerably reduced.

The droop was next completely removed to form a sharp-edged basic profile (D), which was then modified to have a very small leading-edge radius (E). This was then increased to have a value typical of some modern aerofoil profiles (F). In the final state (G) the leading-edge radius was almost doubled to form a section with a comparatively blunt leading edge.

The basic section, D, which is 8 per cent thick normal to the leading edge of the wing is one of those devised by Tanner in Ref. 1, and the section modifications discussed in the present text have been designed using the methods of that Report*.

Because of the way the modifications were made the maximum thickness/chord ratio (based on the actual chord of the profile) varies with model state, changing from 4·36 per cent along the stream for state A to 5·97 per cent for state G. Moreover, since it was decided to keep the wing semi-span constant throughout the tests, there is a corresponding increase in the aspect ratio of the complete wing (2·71 to 3·72).

---

* Using the notation of Ref. 1, β was equal to 4 for the droop of states A to C, and equal to 2 for the round-nosed states E to G.

2.2. *The Tunnel.* The N.P.L. 18 in. × 14 in., with a transonic working section, was used for the tests. This has slotted walls[2], with one-eleventh of the total area open, above and below the model; the sidewalls are solid and formed by interchangeable panels of glass in steel frames.

The model was mounted directly on to a turntable set in the sidewall. Because of its comparatively large span, no attempt was made to remove or divert the tunnel-wall boundary layer ahead of the model.

The stream Mach number (M_0) was determined from the pressure measured at a previously calibrated hole in one of the slats at a position well upstream from the model.

All tests were made at a constant stagnation pressure of 31 in. mercury for a range of stream Mach numbers between 0·60 and 1·20.

2.3. *Test Procedure.* The incidence range was limited by the permitted bending stress at the wing root. The resultant test boundary, assumed for convenience to be the same for all states of the model, is shown in Fig. 3. As will be seen, a rather severe restriction is placed on the lift-coefficient range at supersonic stream Mach numbers.

No correction was applied to allow for model blockage or lift effects; these were considered to be negligible.

2.3.1. *Aeroelastic effects.* Under aerodynamic loading the wing deflects and develops a twist, corresponding to a reduction of incidence by $\delta\alpha_t$ at the tip. This incidence change was measured directly for some model states and typical results (for state G) are shown in Fig. 4. It is not easy to ensure a high degree of accuracy with measurements of this kind, but the results obtained clearly indicate that $\delta\alpha_t$ may reach -3 deg at the highest incidence and stream Mach number.

It was not possible to measure the spanwise distribution of this aeroelastic twist and the available theoretical methods for estimating this were felt to be too complex to apply to the present model. However, N.A.C.A. calculations for wings of similar sweep and thickness generally show a linear, or slightly parabolic twist distribution; the mean incidence correction may thus be somewhat less than half the measured tip twist.

The value of applying an overall incidence correction would seem to be rather doubtful, and its need is reduced by the fact that the aerodynamic twist does not vary greatly with model state, thus enabling direct comparisons to be made at nominal incidences. No incidence corrections have therefore been applied to the results presented in this Report. Nevertheless, it should not be forgotten that the effect of the twist is to reduce the aerodynamic loading at the tip compared with a similar rigid wing. The lift-curve slope of the elastic wing will be slightly smaller therefore and the appearance of shock waves or flow separations at the tip will be delayed.

2.3.2. *Boundary-layer transition band.* Except in a few instances, all the tests were made with a roughness band extending on both surfaces from the leading edge up to about 0·1 local chord*. Care was taken to see that the roughness band was promoting transition and also causing the least possible disturbance to the external flow.

* The chordwise extent of the roughness band varied slightly during the tests, since these were used to provide additional information on the minimum band width required; little effect was in fact found in the range tested (10 per cent to 7 per cent of the local chord). The band itself was prepared by spraying (dry) 320 Carborundum powder (0·0015 in. mean grain size) on to a base strip of proprietary lacquer; this technique[19] is considered to be superior to the more conventional mixture of Carborundum powder and aluminium paint.

2.3.3. *Oil-flow patterns.* For each model state an extensive series of oil-flow patterns was obtained and photographed to cover the complete range of stream Mach number and model incidence. These were used to deduce the presence of separated-flow regions, part-span and tip vortices and the various types of shock waves; in addition it is possible in some cases to make an estimate of the local Mach number by measuring the direction of the oil filaments. The oil-film pattern is often a reliable indicator of the effectiveness of the roughness band in promoting transition and can be used as a supplementary check on the more conventional sublimation techniques.

The mixture used varied slightly during the tests, but in most cases consisted of two parts of a suitable oil*, one of titanium oxide, and with a small quantity of oleic or lauric† acid[19]. The time required for the satisfactory development of a pattern was between one and two minutes.

2.3.4. *Balance measurements.* The normal and axial forces appropriate to each model state were measured on a wall-balance; the results were reduced to coefficient form and then resolved into lift and drag coefficients.

2.3.5. *Reynolds number.* At constant stagnation pressure, the test Reynolds number varies with stream Mach number, and in the present tests, because the model chord alters, there is a change with model state. The maximum variation is indicated in Table 3.

TABLE 3

Variation in Test Reynolds Number

M_0	Reynolds number $\times 10^{-6}$, based on streamwise model chord (stagnation pressure and temperature, 31 in. Hg and 283 deg K)		
	State A	State D	State G
0·6	$1{\cdot}8_5$	$1{\cdot}5_7$	$1{\cdot}3_5$
1·0	$2{\cdot}4_4$	$2{\cdot}0_7$	$1{\cdot}7_8$
1·2	$2{\cdot}5_1$	$2{\cdot}1_3$	$1{\cdot}8_3$

3. *Results.* 3.1. *Presentation of Results.* The balance results in terms of lift and drag coefficients, and lift/drag ratios are presented separately for each wing state in Figs. 5a to 5g. Before discussing these results however, it is more profitable to consider the development of the flow pattern about the wing in its various states, using the evidence provided by the oil patterns. The knowledge obtained both simplifies and broadens the subsequent analysis of the overall wing forces.

As a preliminary step, the oil-flow patterns were studied to provide a graphical representation of the main events for each wing state, when incidence and Mach number are varied. The results are set out in Figs. 6a to 6g, in the form of boundaries for the appearance of four types of shock wave,

* The oil used was Shell Vitrea 72, whose kinematic viscosity is 720 centistokes at 20 deg C.

† Lauric acid is preferable to oleic acid when used as a 'de-coagulant' since it appears to cause less deterioration of the oil mix with time. This may be associated with a lower rate of oxidisation of the acid.

together with the occurrence of flow separation behind these waves, or at the tip or at the leading edge. It is therefore convenient to consider first the influence of model state on each specific boundary.

Before doing this however, some consideration must be given to the accuracy with which these boundaries can be determined. Uncertainty arises, in fact, for two main reasons. Firstly, the main sequence of oil photographs were taken at intervals of one degree in incidence, equivalent to about $0{\cdot}05$ in C_L. Limitation on time and effort precluded any closer spacing except in a few special cases*. Secondly flow separation and shock waves can only be detected clearly when the phenomenon has developed somewhat and it is thus difficult to estimate incipient conditions.

Both these difficulties are mitigated to some extent by the fact that the growth of a separation region, or an increase in shock-wave strength, with wing lift is not particularly rapid. Thus in a sequence of patterns, it is possible by interpolation to make a reasonable estimate of the condition at which an event should first be detectable. It is true that such an estimate is to some extent subjective and presupposes a somewhat arbitrary threshold of detection; nevertheless, with care, the results obtained for different wing states should be comparable.

The characteristics of oil-flow patterns close to the beginning of flow separation, or when very weak shock waves exist, have been discussed elsewhere[3]. Briefly, for the present purposes flow separation was assumed to start at the appearance of a reattachment line[4] or a forward flow line. A shock wave was considered to appear first near a condition where the surface oil filaments become highly curved for a small chordwise distance; this is often accompanied (or even preceded) by a local increase in oil film thickness along the shock front.

With experience, it was found possible to interpret and analyse oil patterns accurately and consistently even in conditions where the traces of surface events were very faint, and to assess with some confidence the condition corresponding to the 'beginning' of flow separation or the 'first appearance' of a shock wave. The exact relationship of these estimates to the actual events on the surface wing is of course unknown for the present tests, but a similar analysis made on a pressure-plotting wing at the N.P.L. suggests that the errors involved in using an oil-pattern sequence in this way are small, and similar to those which arise in making a corresponding assessment from pressure or optical data.

One further difficulty in the analysis must be mentioned. The presence of the roughness band prevents the flow pattern from forming clearly on the surface covered by the band, and hence events happening close to the leading edge (*e.g.*, leading-edge separation) can only be detected when they pass downstream of the band. This effect, which is similar for all model states must be allowed for in assessing the oil-flow patterns.

3.2. *Upper-Surface Leading-Edge Separation and Flow Reattachment.* The upper-surface leading-edge separation boundaries, compared for the seven model states in Fig. 7, have two main sections. The first corresponds to the onset of separation with increasing incidence, and for states A to E the lift coefficient at which this occurs is almost unaffected by changes in stream Mach number. States F and G however show a marked reduction in critical C_L as M_0 increases. In both these cases, separation was first observed near the tip, and with further increase in incidence, the separation

---

* In fact over 400 oil patterns were photographed during the tests; even this coverage was found to be too coarse in many respects.

region spread inboard*. This development was characteristic too of the drooped sections (A to C), but for states D and E, separation tended to occur almost simultaneously along the whole leading edge. A subsequent increase in incidence caused the reattachment line to move rearward, more rapidly at the tip than near the root, so that the vortex was soon more highly swept than the leading edge (Fig. 7b).

The second part of the separation boundary is best regarded as denoting the change (at constant C_L and increasing M_0) from separated leading-edge flow to attached leading-edge flow, and has been called by some authors (*e.g.*, Ref. 5) a transonic flow-attachment boundary. The boundary rises very rapidly with small increases in free-stream Mach number. Fig. 7a suggests that the Mach number at which the upward rise occurs is related to the lift coefficient at which leading-edge separation takes place at a slightly lower stream Mach number. Thus for states A and B, where the critical value of C_L is about 0·35, the value of M_0 at which flow reattachment occurs is approximately 0·85. At the other extreme, the corresponding values for state E are 0·15 and 0·98. It is possible to draw a line (such as ZZ′ in Fig. 7a) through the beginnings of the upward rises and this may be of use in predicting the characteristics of sections intermediate to those tested.

The variation of both the lift coefficient at which leading-edge separation occurs, and the leading-edge attachment Mach number, with leading-edge radius have been plotted in Figs. 8a and b. The parameter ρ_n/t has been used, where ρ_n is the leading-edge radius in a direction normal to the leading edge, and t is the maximum thickness of the section; this is the square of the parameter used in Ref. 5 to correlate two-dimensional data.

The present results are inadequate to draw any reliable conclusions, apart from the deterioration of the sections of large leading-edge radii at high stream Mach number. A curve placed through the available points in Fig. 8b for the plain sections does have a minimum near $\rho_n/t = 0{\cdot}09$, which is the value at which the minimum occurs for a similar plot of two-dimensional results[5]; further work is required to establish firmly this connection however.

3.2.1. *Comparison between two- and three-dimensional results.* Boundary diagrams similar to Figs. 6 and 7 have been used extensively by those concerned with two-dimensional aerofoils at subsonic and transonic speeds and it is perhaps relevant to make some comparison between the present results and those obtained elsewhere from suitable two-dimensional sections.

The leading-edge separation curve for the wing with a sharp-edged section (state D) has been replotted in Fig. 9a, in terms of the component of Mach number normal to the leading edge ($M_0 \cos \Lambda_{L.E.}$) and the .equivalent geometric incidence of the wing section in that direction ($\alpha/\cos \Lambda_{L.E.}$). Ref. 5 contains some N.A.C.A. data for transonic flow attachment on circular-arc aerofoils and Fig. 9a contains a curve for profiles having about the same leading-edge half-angle (λ) as the section of state D. There is an appreciable difference between the values of $M_0 \cos \Lambda_{L.E.}$ in the two cases (about 0·65 and 0·75). The N.A.C.A. curve is in remarkably good agreement with the corresponding part of a curve obtained by Henshall and Cash[6] for a 4 per cent biconvex aerofoil, and confirms the contention of Ref. 5 that the leading-edge angle is not of primary importance. Different tests conditions in the two cases probably exist and hence to some extent the closeness

* This growth in the separation region near the wing tip with incidence is sufficiently rapid to allow the variation in wing aspect ratio to be neglected, and Figs. 6a to g are based on results from the wings as tested (*i.e.*, for constant wing semi-span).

of the agreement may be fortuitous. It should be noted that a roughness band was not used by Henshall and Cash (nor, most probably, by the N.A.C.A. workers) in contrast to the swept-wing tests of the present Report.

The section of the curve due to Henshall and Cash and appropriate to low-speed, leading-edge separation shows a decrease in critical incidence with increasing stream Mach number in contrast to the almost constant value of $\alpha/\cos \Lambda_{L.E.}$ for state D in that condition. The reason for this may be due partly to the fact that the curve for the aerofoil was derived from noting the divergence of the trailing-edge pressure and hence will reflect to some degree the fact that the bubble length grows with M_0 at constant incidence. The first appearance of leading-edge separation may well be at a more constant incidence.

A 4 per cent biconvex aerofoil was used for the wing section of a wing-body combination tested by Scott-Wilson[12], and the corresponding separation boundary is shown as a broken line in Fig. 9a. The wing in this case had a leading-edge sweep of 11 deg ($\cos \Lambda_{L.E.} = 0{\cdot}982$), a gross aspect ratio of $3{\cdot}5$ and a taper ratio of $0{\cdot}5$. A leading-edge roughness band was used. The difference between this curve and that for the corresponding aerofoil is large and is presumably attributable to the effect of the finite aspect ratio.

Two-dimensional tests have been made at the N.P.L. by Tanner* on some of the sections in the family from which states D to G were chosen. One of Tanner's models was of a profile intermediate between states D and E, having a leading-edge radius of $0{\cdot}1$ per cent chord, and the boundaries for the appearance of leading-edge separation, the shockwave, and shock-induced separation are given in Fig. 9b. A comparison is made in this Figure between these results and those for states D and E, using the modified incidence and Mach number scales.

Tanner's tests were unfortunately made without a leading-edge transition band and this in addition to differences in the techniques of determining separation makes difficult any detailed comparison of the two sets of results. Despite quantitative differences in the boundaries, the basic separation boundary shapes (including shock-induced separation behind the rear and aerofoil shocks) are similar and are of the form sketched in the inset to Fig. 9b. The general relationship between the two sets of boundaries is similar to that for state D and Henshall and Cash's curve in Fig. 9a.

An attempt has been made in Fig. 9c to compare the chordwise shock positions in the wing and aerofoil tests considered in Fig. 9b. The aerofoil was at an incidence of $4{\cdot}0$ deg and the wing at $2{\cdot}6$ deg ($\alpha/\cos \Lambda_{L.E.} = 4{\cdot}05$ deg); the tunnel speed parameter is $M_0 \cos \Lambda_{L.E.}$. The wing rear shock for convenience was measured at $0{\cdot}7$ of the semi-span, but in these flow conditions the shock is nearly parallel to the leading edge. The agreement between the two curves is not good and this may well be because the rear shock on this wing is far more influenced by the root flow (*see* Section 3.3.1 below) than on a wing of higher aspect ratio when true yawed-wing flow might be more closely approached.

State F of the present wing perhaps corresponds most closely to the profile of a typical modern high-speed section. The relevant leading-edge separation boundary is plotted in Fig. 9d where it is compared with boundaries† from two-dimensional tests[5] on NACA 64A009‡ and 64A012 aerofoils. As in earlier comparisons made in this section, the swept-wing leading-edge separation line occurs

* This work is at present unpublished but is quoted extensively by Pearcey in Ref. 18.

† Almost certainly obtained without a roughness band on the models.

‡ The maximum thickness of NACA 64A009 and the chordwise section of state F are at $0{\cdot}40c$ and $0{\cdot}397c$; the leading-edge radii are $0{\cdot}0058c$ and $0{\cdot}0059c$ respectively. State F section is $8{\cdot}46$ per cent thick.

at a higher value of the incidence parameter and the transonic-flow attachment section of the boundary at too low a value of the Mach number parameter. Crudely this can be regarded as a failure of the wing to achieve the full benefit of the leading-edge sweep effects, due to the influence of the root and tip, and this viewpoint could be extended to allow the use of an 'effective wing sweep' with a value somewhat lower than the geometric wing sweep.

Alternatively the higher values of effective incidence for low-speed separation obtained with the swept wing may be regarded more as a delay in the onset of separation effects beyond that suggested by simple sweep theory. This approach is put forward in Ref. 7, where the phenomenon is attributed to the relieving effect of the lateral flow in the boundary layer*.

Though quantitative agreement is not obtained the shape of the swept-wing boundary is similar to that for the two-dimensional models, the latter having a characteristic trough often associated[11] with moderately thick sections. In contrast the flat shape typical[11] of a 'thin' (4 per cent) section[10] is shown in Fig. 9d. It is interesting to note that the leading-edge separation curve for the swept wing of Refs. 3 and 15 is very similar to that of state F despite differences in wing planform and section†.

Finally in Fig. 9e a comparison is made between the separation boundary obtained from Tanner's two-dimensional tests on the section of the present wing in state G, and the results from the wing itself. The broken line (which is obtained from combining the leading-edge and shock-induced separation boundaries) is similar to the wing boundaries for leading-edge separation and shock-induced separation behind the outboard shock. No separation behind the rear shock was observed for this wing state because of the large spanwise extent of the outboard shock. Once again the techniques used to determine the onset of separation were different.

The comparisons made in Fig. 9 suggest therefore that quantitative agreement on separation boundaries is unlikely between related two- and three-dimensional results, unless care is taken to avoid the effects of the wing tip and root. Although the present results are by no means conclusive, it appears that simple geometric analogies are insufficient, and perhaps this is not surprising in view of the complexity of the phenomenon. The nature of leading-edge separation and transonic flow attachment are not well understood for two-dimensional aerofoils, despite the valuable contributions contained in Refs. 5, 8 and 9 and the extension to swept leading edges seems even more difficult. Obviously further work is required on this matter. Nevertheless, it is felt that qualitative agreement based on the general shape of the separation boundary may well be possible and this in fact could form a valuable link between wing design and aerofoil research. In the latter field, it is possible to relate, in a general way, the profile characteristics with the separation boundary.

3.2.2. *Inboard leading-edge separation.* An unusual feature of the flow for some states at low supersonic stream Mach numbers was the simultaneous occurrence of separated flow over the *inboard* region of the wing, with attached flow *outboard*. This was most marked for the sharp-edged

---

* This explanation may also be applied to the transonic flow-attachment boundary. The latter too could be related to the *minimum* stream Mach number component for which pressure recovery from a shock-induced separation is possible; this involves an extension of two-dimensional ideas. An early flow attachment as M_0 increases would imply that relatively good pressure recovery has been obtained on the swept wing.

† The wing of Refs. 3 and 15 had a leading-edge sweep of $53\frac{1}{2}$ deg, a taper ratio of $\frac{1}{3}$ and a 6 per cent RAE 102 section along the stream. The latter becomes a 7·7 per cent thick profile normal to the leading edge; state F of the present tests is actually 8·46 per cent thick in this direction.

section D, and its range, in terms of Mach number and incidence, is indicated in Fig. 6d. A typical oil-pattern sequence at $M_0 = 1{\cdot}05$ showing the transition to complete leading-edge separation ($\alpha = 9{\cdot}6$ deg) is shown in Fig. 10. The final stage (between Figs. 10c and d) was usually very abrupt and was accompanied in the tests by a violent oscillation of the model, which was self-sustaining and showed in some cases a tendency to diverge*.

This inboard separation phenomenon was also present to some extent with states E, F and C, though in the last two cases it is difficult to distinguish this from flow separation to the rear of the forward shock; indeed the phenomenon may in some cases arise directly from this cause. With state E however, the phenomenon was only a little less marked than for state D.

Similar flow changes and wing oscillations were observed when the roughness band was removed.

3.3. *Shock Waves.* In addition to the bow wave, which is always present when the stream Mach number exceeds unity, five other shock waves are associated with the flow over a sweptback wing. The three most important are the rear, forward and outboard shocks†, the last name being reserved for the single shock which occurs outboard of the intersection of the forward and rear shocks. These three shocks are clearly shown in Fig. 11a in a typical oil pattern. The tip shock, a faint inclined trace originating from close to the outboard tip is shown in Fig. 11b, and the initial tip shock, a disturbance nearly normal to the stream close to the outboard edge, is illustrated (together with a rear shock in a rather forward position) in Fig. 11c.

The effect of leading-edge modifications on these shock waves and on the associated flow separations will now be considered.

3.3.1. *The rear shock.* For a plane finite swept wing at zero incidence, the position of the maximum surface velocity is further forward at the tip and more rearward at the root compared with that appropriate to an infinite swept wing[14]. In addition the maximum velocity attained on the wing surface is higher at the tip than the root. Thus with increase in stream Mach number, supersonic flow occurs first near the tip, and subsequently spreads inboard, the associated shock wave lying obliquely across the wing.

This effect is accentuated when the wing is placed at incidence because of the high local loading over the outboard part of the wing.

In physical terms the rear shock may be regarded[3] as arising to some extent from the constraint caused by the wall (or wing centre-line) on the flow at the root. Near the leading edge the flow turns inboard because of the local increase in velocity above the stream value, and this deflection must be opposed by the wall. The resulting compression is gradual close to the wall but becomes more intense outboard (Fig. 12). It might be expected therefore that the rear shock development depends to a considerable extent on the flow conditions close to the roof.

---

* A possible explanation of this oscillation is that the changeover to completely detached leading-edge flow augments the wing lift slightly (*see* Section 3.4.1 below) and thus increases the deflection of the model. This has the effect of increasing the negative twist at the tip, thereby reducing the tip incidence and allowing the attached flow to reform. The reduced wing load then increases the effective incidence of the tip, and the flow once more separates. There would appear to be some similarity between this and two-dimensional stalling flutter.

† The nomenclature of Ref. 3 is used.

This root flow compression usually terminates the supersonic flow region close to the wing tip, thus giving rise to a single transverse shock across the wing. In certain conditions however (usually at high incidence and moderate subsonic Mach numbers) the rear shock may penetrate into the supersonic flow at the tip without reducing this to subsonic velocities*. The final compression near the tip occurs through the initial tip shock further aft (*see* Section 3.3.5 below). An example of this type of flow is given in Fig. 11c.

The dominance of the root flow suggests that the rear shock formation and movement will not primarily depend on model state (*i.e.*, leading-edge shape). Fig. 13 shows that the initial appearance of the rear shock occurs in a fairly narrow range of Mach number for a given value of C_L. This band is reduced further if the results are plotted in terms of incidence rather than lift coefficient. The rear shock appears latest in those model states where the leading edge is comparatively blunt and where the forward shock occurs earliest.

At a constant incidence the shock position across the wing seems to be almost independent of leading-edge shape. As an example the shock position for $\alpha = 5{\cdot}6$ deg has been plotted in Fig. 14, for the different model states at various stream Mach numbers, in terms of the chord of the basic sharp-edged section D. The variation between the various states is then much smaller than if the local chord had been used as the ordinate, particularly at the lower values of M_0.

Similarly, if the simple spanwise position parameter η is replaced by one involving the local chord length†, the variation is again increased. This suggests that the rear shock position is largely independent of wing aspect ratio for this series of models.

It follows therefore that the rear shock position (and hence strength) may be best altered either by changes in the thickness distribution of the wing profile near the root or by modifications to the constraint conditions at the root. For wing-body combinations of course, the latter method leads to body contouring, which is known to reduce transonic drag in a marked fashion, if correctly applied. Unpublished tests at the N.P.L. have also demonstrated the significant effect of body contouring on the rear shock, particularly over the inner part of the wing.

The spanwise and chordwise position of the rear shock, as plotted in Fig. 14, is a measure of the sweep of the shock front. This varies only slightly along the shock itself, and it is convenient to measure the mean shock sweep ($\bar{\phi}_R$) over a small spanwise region. As might be expected the shock sweep does not depend greatly on model state (Fig. 15a). The curves for states C, D and F in this Figure terminate when the rear and forward shocks intersect in the spanwise band being considered, but just before this condition there is usually a reduction in shock sweep. For state A, the intersection does not take place within the available incidence range, and the gradual decrease in shock sweep at the higher incidences occurs after flow separation takes place behind the shock.

The increase in mean shock sweep with stream Mach number is shown in Fig. 15b for state A; a reduction in shock sweep at a given value of M_0 is again associated with shock-induced separation.

In Ref. 15 there is a discussion of the value of using the measured direction of the oil-filament lines to indicate local Mach number. If it is assumed that the velocity component normal to the

---

* In extreme cases, the rear shock may intersect the wing leading edge. Extensive leading-edge separation must be absent and since the wing incidence is usually high, a drooped leading edge or an early transition to attached supersonic leading-edge flow is required. In the present tests the intersection was observed at $M_0 = 0{\cdot}875$, $\alpha = 9{\cdot}6$ deg, state A.

† For example, the overall span divided by the local chord.

leading edge is affected by the wing profile whilst the component along the edge remains unaltered, then the local surface Mach number (M_1) and the flow inclination from the stream direction (θ) are related by the equation

$$\sin(\Lambda_{L.E.} - \theta) = \sin \Lambda_{L.E.} \frac{M_0}{M_1} \left[\frac{5 + M_1^2}{5 + M_0^2}\right]^{1/2} \tag{1}$$

provided the flow is everywhere isentropic (*i.e.*, the bow wave is very weak).

This relationship is of most value in the region ahead of the forward shock (*see* Section 3.2.2 below) and is less satisfactory when used to determine the local Mach number ahead of the rear shock. This is due to the comparatively aft position of the shock, and the fairly large lateral pressure gradients that are known to exist with this type of flow and which cause the oil filament on the surface to have a somewhat different direction from the flow just outside the boundary layer. Thus no great accuracy can be expected from the analysis, which probably gives too low a value of M_1. However a comparison such as that shown in Fig. 16 between states A and C may be of value in that it suggests that the local Mach number just ahead of the shock for state C may be lower than for state A. If this is so, the chordwise pressure distributions for the two cases may be similar to those sketched at the top of the Figure.

The Mach number component (M_N) normal to the shock front is given by

$$M_N = M_1 \cos(\phi_R - \theta_R)$$

where ϕ_R and θ_R are the rear shock sweep and the filament inclination ahead of the shock. Some of the results included in Fig. 16a have been recast in this form and are given in Fig. 16b. Flow separation behind the rear shock was just detectable in the oil patterns at $\alpha = 6{\cdot}6$ deg, when M_N is about $1{\cdot}36$. Though this is in good agreement with the results of Ref. 15, where flow separation appeared to correspond to a value of M_N of $1{\cdot}39$*, this may be to some extent fortuitous in view of the difficulties in estimating M_1.

The flow separates initially where the shock is strongest (*i.e.*, on the outboard region of the wing) but inboard of this the boundary layer is greatly thickened by the shock and drifts towards the tip. Eventually this flow is influenced by the vortex formed from the separated flow and moves forward until it too separates and joins either this vortex or that originating from the tip. Fig. 17 illustrates this.

The present discussion has been mainly confined to cases for which the forward shock was absent during the development of the rear shock. The early appearance of the forward shock, as for example with states F and G (*see* below), may mean that this rapidly becomes sufficiently strong to modify the flow ahead of the rear shock and hence the strength of the rear shock itself. Moreover, in such conditions the interaction of the forward and rear shock occurs well inboard at comparatively low incidences, and the rear shock may then only exist in rather a diffuse form over the inner part of the wing. As an example, the rear shock traces around $\eta = 0{\cdot}6$ should be compared in Figs. 18a and b.

3.3.2. *The forward shock.* When the flow is locally supersonic, small pressure disturbances in the leading-edge region are propagated at the local Mach angle relative to the local flow direction. With sufficient increase in free-stream Mach number, or wing incidence, the local Mach number over the outboard portion of the leading-edge region may become sufficiently high for disturbances

* Actually, this value was obtained mainly from results for the forward shock. Less information was available for the rear shock, for which a value of $M_N = 1{\cdot}35$ seemed more appropriate.

to propagate at a greater sweep than the leading edge. This part of the wing surface is therefore effectively isolated from disturbances from the inboard region and the root, and the boundary between the two regions takes the form of a shock wave, called elsewhere [3,15] the forward shock*. In Fig. 11a the forward shock appears to originate at about 0·25 semi-span, but it may well exist for some distance inboard of this position in a position just behind the leading edge.

The first appearance of the forward shock is thus dependent on the local Mach number distribution in the leading-edge region, and thus should be influenced by modifications to the leading edge. This is shown in Fig. 19, where a large difference exists in the conditions for the first appearance of a forward shock for states A and G, for example. At a given free-stream Mach number the local supervelocities are reduced by leading-edge droop and the shock first occurs at a comparatively high C_L; as the leading edge is progressively rounded the shock appears earlier. Attached leading-edge flow is necessary for the formation of the forward shock and hence the forward-shock boundary must originate from some point on the transonic flow-attachment boundary (*see* Fig. 6a to g).

The forward shock positions for a given incidence and stream Mach number do not correlate when plotted relative to the unmodified part of the wing profile (Fig. 20), the shock being more rearward with each successive modification. A similar change is shown in Fig. 2a where the shock position is given as a fraction of the appropriate model chord. The rapid rearward movement of the shock is due mainly to its inboard motion as the wing incidence is increased and only partly to an increase in shock sweep. The rate of shock movement with incidence is similar for all model states and Fig. 21b suggests that this is not greatly altered by changes in free-stream Mach number. The rearward movement of the forward shock with M_0 at a given incidence on the other hand seems to be associated with the corresponding increase in shock sweep illustrated in Fig. 22b.

The sweep of the forward shock varies a little over that portion visible in the oil-flow patterns (*e.g.*, *see* Fig. 20) being more highly swept further outboard. As in the case of the rear shock a mean shock sweep ($\bar{\phi}_F$) has been measured over a limited part of the semi-span. This sweep is largely independent of leading-edge geometry for states C to G (Fig. 22a), but is reduced (at constant incidence) by the large droop of states A to B. The sudden increase in shock sweep shown for states D and F is due to the development of extensive regions of separated flow from the leading edge inboard of the shock (*see* Section 3.2.2 above) with a consequent change in flow conditions behind the shock. This can perhaps be regarded as an abnormal condition.

The local Mach number (M_1) ahead of the forward shock† can be estimated approximately from Equation (1) or from Fig. 23 and some typical results are shown in Fig. 25. At a given incidence, M_1 is lowest for the leading-edge state which delays the appearance of the forward shock, (*e.g.*, C) and highest for states in which the shock develops early. Changes in stream Mach number alter the general level of the local Mach number, but not apparently the rate at which this increases with incidence.

---

* There is some similarity between the two flow regions present on a swept wing of finite thickness with a subsonic leading edge, and the flow models postulated for a swept wing or flat plate with a supersonic leading edge. In the latter the dividing boundary originates from the root or wing apex and the flow ahead of the disturbance is related to that over an infinitely long yawed wing. In the former case the disturbance may turn back over the wing at any position on the leading edge and the flow in the region ahead may possibly be influenced by the lower surface.

† The estimates of M_1 are perhaps best regarded as a mean local Mach number over part of the surface ahead of the shock. Pressure-plotting tests on swept wings show that the chordwise Mach number gradient in this region is usually small (*see* below).

It was said earlier that forward shock becomes apparent when M_1 is sufficiently high as to allow a weak disturbance to propagate at a higher sweep (relative to the stream direction) than the wing leading edge. Because of the inboard turning of the streamlines by an angle θ_F, the local Mach number for this condition (M_1*) is less than 1·56, the value appropriate to flow in the stream direction ($\theta_F = 0$). The geometric condition is

$$\mu_1 - \theta_F = \frac{\pi}{2} - \Lambda_{L.E.}$$

where μ_1 is the Mach angle associated with M_1. This can be combined with Equation (1) to yield the following equation for M_1*

$$M_1^{*2} = \frac{5\lambda + 1}{1 - \lambda} \tag{2}$$

where

$$\lambda = \frac{M_0^2}{5 + M_0^2} \{\sin^2\Lambda_{L.E.}\}.$$

M_1* is plotted in Fig. 23 as a function of M_0. The increase in Mach number above the stream value is also shown and this (and hence the critical incidence) diminishes as M_0 increases, a trend shown in part by the experimental results of Fig. 19.

The theoretical values of M_1* for $M_0 = 1{\cdot}00$ and $1{\cdot}20$ are given in Fig. 25 for comparison with a linear extrapolation of the experimental curves to the incidence at which the forward shock first appears at $\eta = 0{\cdot}6$. The agreement is generally good (except for state D where the experimental value of M_1* is too low) and though this may be to some extent fortuitous, due to the uncertainties in determining M_1 and the nature of the extrapolation, this Figure does perhaps lend some confidence to the general ideas advanced about the nature of the forward shock.

One measure of shock strength is the Mach number component (M_N) normal to the shock front

$$M_N = M_1 \cos(\phi_F - \theta_F).$$

The fact that M_N must always be greater than unity gives some check on the accuracy of the present method of analysis. Only in a few cases was the estimated value of M_N between 0·95 and 1·00 and these were at the lowest incidences at which measurements could be made; the corresponding value of θ_F was the least accurate of the series.

M_N (and hence shock strength) increases with incidence and ultimately becomes sufficient to cause boundary-layer separation. This can be detected from the oil patterns†. In Fig. 26, the value of M_N has been plotted for all cases at three free-stream Mach numbers for which separation behind the forward shock was first observed; these points are linked to others at one degree smaller incidence, when separation was absent. A few other values of M_N are given for cases in which no separation was observed at the highest test incidence.

The separation condition of Ref. 15 ($M_N = 1{\cdot}39$) fits the present data quite well.

---

† Separation is considered to occur when the oil lines no longer continue through the shock front but flow along the shock. When separation is well advanced the characteristic herring-bone pattern is formed, indicating separation, reattachment and forward flow.

Estimates of M_1 may be in error due to the presence of a spanwise pressure gradient, whose effect would be to cause M_1 to be underestimated. Some indication of the gradient can be obtained by measuring the variation of the (apparent) flow inclination along the span and estimating the change in M_1. Two typical examples are shown in Fig. 27, the gradient being small for state G and much larger for state C.

Velocity changes also occur in the chordwise direction and in theory it should be possible to detect these from the changing direction of the oil filaments. In most cases analysed, the flow lines were straight, suggesting that the change in local Mach number up to the shock was small. For state G however, when the forward shock is well behind the leading edge, the flow lines curve outboard before reaching the shock, and this may be associated with a reduction in surface velocity. For example, at $\alpha = 7{\cdot}6$ deg, $\eta = 0{\cdot}5$, $M_0 = 1{\cdot}20$, the indicated value of M_1 is $2{\cdot}4$ at $x/c = 0{\cdot}2$, and $1{\cdot}95$ just ahead of the shock ($x/c = 0{\cdot}4$). The corresponding values for state F are $2{\cdot}0$ and $1{\cdot}9$ respectively, and this suggests that the pressure distribution for a moderately-rounded leading edge is smoother. A higher local Mach number near the leading edge for state G is consistent of course with the early appearance of the forward shock.

With the drooped leading edges A and B, the flow lines ahead of the forward shock continue to turn slightly inboard up to about $x/c = 0{\cdot}2$, indicating a rising velocity to that position.

3.3.3. *The outboard shock.* The outboard shock is defined as the main shock existing outboard of the intersection of the forward and rear shocks. Its strength (in terms of pressure rise) is similar to the sum of the adjacent forward and rear shocks separately, and hence for wings of moderate sweep flow separation frequently occurs behind the outboard shock.

The chordwise position of the rear shock is not greatly altered by changes in incidence at some particular value of M_0. In similar conditions the forward shock moves inboard rapidly, and the intersection point will move along the relatively unchanged rear shock position. Thus the spanwise extent of the outboard shock may be regarded as determined by the forward shock (and hence is influenced by leading-edge changes); the chordwise position of the inboard end of the shock is related to the rear shock position and is much less affected by model state. Because the positions of both shocks change with M_0, the region of the wing influenced by the outboard shock alters in a complex manner. For example, at constant incidence but increasing Mach number, the spanwise position of the intersection point (η_i) moves toward the tip (Fig. 28a) but the shock itself becomes more rearward. At constant stream Mach number, the value of η_i usually diminishes as α increases (Fig. 28b) and there is little change in the mean chordwise position.

At subsonic speeds however, when the rear shock lies close to the leading edge, its slight rearward movement with increasing incidence is sufficient to cause the intersection point to move rapidly outboard until this movement is restrained and finally reversed by the inboard motion of the forward shock. An example of this is shown in Fig. 28b for state C at $M_0 = 0{\cdot}95$.

Though the position of the inboard end of the outboard shock depends on that of the rear shock, the mean position of the outboard shock correlates less well when plotted in terms of the unmodified part of the wing profile (Fig. 29a). The forward movement with increasing incidence is most marked at the highest values of M_0; a slight rearward movement is sometimes apparent at lower incidences and stream Mach numbers when the flow separation to the rear of the shock is less marked. The rearward movement of the shock with increasing M_0 is shown in Fig. 29b, the rate being independent of leading-edge shape.

The mean sweep of the outboard shock ($\bar{\phi}_0$) does not vary greatly with model state (Fig. 30a) or incidence, but there is a steady increase in sweep with increasing M_0 (Fig. 30b). The outboard shock sweep is similar to that of the rear shock; in general it seems that $\bar{\phi}_R$ is slightly greater than $\bar{\phi}_0$ for the drooped states, the converse being true when the leading edge is rounded. The delay in the appearance of the outboard shock for states A, B and C enables the rear shock to achieve its maximum sweep angle at a given stream Mach number.

The parameter ϕ_0 is the shock sweep relative to the free-stream direction. Relative to the oncoming, inwardly-deflected flow over the wing surface the effective shock sweep is $\phi_0 - \theta$; this is appreciably smaller than ϕ_0 as is shown in Fig. 30b, and generally tends to decrease with increasing incidence. It is important therefore to recognise that the effective sweep of an outboard shock may be very small, despite its geometric position on the wing planform.

For all cases tested, the geometric sweep of the outboard shock was less than the leading-edge sweep (50 deg), and in certain conditions (usually when the wing incidence is high and the stream Mach number close to unity) there is a possibility of the outboard shock intersecting the leading edge.Before this occurs however the flow separates from the leading edge outboard of the shock as in Fig. 31. The boundaries of this tip separation are given in Figs. 6c to g; the exact flow mechanism is not understood at present but must involve the presence of the tip shock itself. Certainly tip separation seems to be critically dependent on the position of the outboard shock and occurs when the shock approaches within about $0{\cdot}1c$ of the leading edge.

The local Mach number ahead of the outboard shock can also be determined approximately from the oil-filament direction, and for most model states this increases with both Mach number and incidence. With states F and G, a reduction in the value of M_1 may occur when the shock moves sufficiently rearward with changes in α or M_0 for the chordwise reduction in local Mach number to become predominant. An example is shown in Fig. 33.

The value of the Mach number component normal to the shock front can be obtained simply and some results are plotted in Fig. 34. Only in one case (state G, $M_0 = 1{\cdot}05$, $\alpha = 1{\cdot}6$ deg) was separation behind the shock thought to be absent. For this condition the outboard shock had only just formed and existed over the last 5 per cent of the semi-span*; thus an accurate estimate of M_N is not easy, but it would seem to be about $1{\cdot}31$.

Most of the values of M_N are greater than $1{\cdot}39$, the tentative critical condition put forward in Ref. 15, for separation behind the forward shock† but some points below this value were found at $M_0 = 0{\cdot}9$ and $1{\cdot}0$. In these cases the shock is unfortunately near the leading edge and θ difficult to measure. Since reliable data corresponding to flow attachment behind the outboard shock is lacking (a usual occurrence for wings of moderate sweepback), the results do not enable a decision to be made about the value of applying the two-dimensional criterion ($M_N \simeq 1{\cdot}24$) to the comparatively unswept outboard shock.

The separated flow behind the outboard shock rolls into a vortex, and initially this lies just behind, and parallel to, the shock. With increase in incidence however the vortex becomes more swept until a maximum sweep angle of 60 deg is reached, beyond which little further change occurs (Fig. 35). Fig. 31 shows an example of a well-developed vortex behind the outboard shock, fed by fluid

* The outboard shock was thus partly in the region influenced by the tip shock. The marginal nature of this possible exception to the general rule may well be significant.

† But *see* first footnote in Section 3.3.2.

separating from the rear of the shock and from the leading and side edges; in Fig. 32 the main contribution is from the flow separated by the outboard shock.

The vortex sweep seems to be largely independent of stream Mach number and model state, and hence presumably of shock-wave strength. The general variation with incidence is, in fact, similar to that exhibited by the vortex formed from the leading-edge separation at subsonic speeds (*see* Fig. 35). In this case, when the vortex is well-developed, the dominant parameter is probably the leading-edge sweep, and it may be that at transonic speeds the sweep of this outboard vortex also depends mainly on the sweep of the line of separation. This is of course the outboard shock, whose sweep changes only slowly with stream Mach number, and model state (Fig. 30).

The oil patterns often show very clearly the inboard end of the reattachment line of the outboard vortex (*e.g.*, Fig. 31) and this is almost always directly downstream from the inboard end of the outboard shock. Flow separating from the latter point reattaches at the former, but the flow further inboard, after passing through the rear shock, appears to drift both forwards and towards the tip (under the separated flow) until it too separates close to the outboard shock and joins the outboard vortex.

Some of the photographs similar to Fig. 31 suggest that the forward shock may still persist behind the outboard shock, for the fluid moving under the shear layer detached by the outboard shock, suffers a change in direction along a line which is a continuation of the well-defined forward shock trace. On the other hand, if the outboard shock is assumed to be normal to the plane of the wing in this case, the effective shock sweep $(\phi_0 - \theta)$ is sufficiently low to reduce the oncoming flow to subsonic velocities (about $M = 0{\cdot}84$). This may be however too simple a model of the flow through the outboard shock, since separation occurs to the rear. It might then be supposed that normal shock conditions are not applicable and supersonic flow velocities can persist.

3.3.4. *Tip shock and vortex.* The tip shock may be regarded as a disturbance associated with the presence of the wing tip which propagates inboard over the wing surface*. Though its trace can often be detected from the deviation of the oil filaments, its most noticeable effect is to modify the sweep of the rear (or outboard) shock, outboard of the intersection of this and the tip shock (Fig. 11a for example).

The tip-shock trace is often not very clearly defined, which suggests that it is comparatively weak. It is most noticeable with model states D to G and is less apparent when the nose of the section is drooped. The trace becomes stronger as the free-stream Mach number increases.

The inclination (μ_T) of the tip-shock trace to the local filament direction just upstream (*see* Fig. 36) can be used to check the local surface Mach number deduced (as described earlier) from the filament direction. The tip shock is assumed to be very weak and to propagate at the local Mach angle.

The results of such a comparison are given in Fig. 37 and the agreement obtained is considered to be satisfactory if allowance is made for the approximations involved.

The trace of the rear or outboard shock is further modified when it intersects the tip vortex, a characteristic kink being obtained (Fig. 36). The angle of the vortex (ξ), measured between the stream direction and the reattachment line, seems to depend, at a given incidence and Mach number,

* This tip shock, being cone-like in form, also propagates outboard from the tip, but this region is of little interest in the present context.

on the model state (Fig. 36), being lower for the drooped profiles. The difference between the shape of the curves for states D and F is noteworthy, but is so far unexplained*.

With the drooped sections, the tip vortex appears to originate at some distance from the leading edge of the tip section. This may be because the surface-flow inclination is small close to the leading edge on both the upper and lower surfaces and not until the local velocities have changed appreciably from the free-stream value (but in opposite directions on the upper and lower surfaces) can true side-edge separation and reattachment take place.

This rearward origin of the tip vortex seems to coincide with a similar displacement of the tip shock and it seems reasonable to suppose that the latter can be regarded primarily as a conical shock from the vortex itself rather than from the tip leading edge. Such a shock would be fairly weak, and this justifies the assumption made in deriving Fig. 37. For example if the half-angle of the equivalent tip-vortex cone is 10 deg, and the local Mach number is 2·0, the shock angle should be about 31 deg, compared with the Mach angle of 30 deg.

At zero lift, when the tip vortex does not occur, the tip shock should be very weak, the disturbance then being due solely to the tip thickness. It is certainly not absent, as its trace can be seen in a few oil patterns for some of the undrooped states.

3.3.5. *The initial tip shock.* As will be seen from Fig. 38, this shock only appears for a limited range of lift and stream Mach number, disappearing when the rear shock increases in strength or moves rearward. Optical methods show that the shock is very nearly normal to the plane of the wing, and may extend to considerable distances from the model surface. It probably arises because of boundary conditions imposed by the outboard tip edge, with the consequent reduction in isobar sweep in that region. Though the flow constraint is somewhat different at the root, there is some resemblance between the rear shock and the initial tip shock; both arise from modifications to the ideal flow over a long yawed wing. The initial tip shock is much weaker and extends for a shorter distance over the adjacent wing surface.

The Mach number range in which the shock appears does not vary greatly with model surface though it should be pointed out that the boundaries shown in Fig. 38 are less certain than those for the other types of shock wave. The effect of nose droop is to increase the value of C_L at which, for given M_0, the shock first appears.

When the initial tip shock is close to the leading edge of the tip section (*i.e.*, at stream Mach numbers between 0·90 and 0·95) its position in terms of the local model chord is roughly independent of model state. When the shock moves rearward, as it rapidly does as M_0 increases, there is a tendency for the shock position to be related more to the unmodified part of the wing profile, in a similar manner to the rear shock. For example, the two lines labelled N in Fig. 39 are at $0{\cdot}40c_E$ and $0{\cdot}48c_A$ respectively; when plotted in terms of the chord (c_D) of the 'basic' wing section D, the values are $0{\cdot}40_5c_D$ and $0{\cdot}39_4c_D$.

The initial tip shock almost always lies normal to the oncoming flow over the wing surface. Since the direction of this may vary somewhat, the initial tip shock may be swept slightly backward or forward relative to the free stream and the wing root, as illustrated in Fig. 40. In some cases where there is a spanwise change in local flow direction ahead of the shock, it may be curved slightly.

---

* It may be relevant that the surface Mach numbers at a given incidence are high for state F and much lower for state D.

The flow lines suffer no deflection in passing through this normal shock, and boundary-layer separation to the rear was never observed. The shock seems to be fairly weak, with the estimated local Mach number just upstream never greater than 1·2.

In some cases, the initial tip shock exists despite the presence of leading-edge separation and reattachment on the surface ahead. The shock trace is finally obliterated by the growth and movement of the vortex. Generally however the disappearance of the initial tip shock is due to an increase in the strength of the rear shock existing in the flow upstream (Fig. 11c).

3.4. *Wing Forces.* In preceding paragraphs the changes in flow pattern associated with changes in stream Mach number, incidence and model state have been discussed in some detail. It is now pertinent to consider how the overall wing lift and drag are affected.

3.4.1. *Lift-curve slope and lift.* In Figs. 41a, b and c, the lift curves for the various model states are compared at stream Mach numbers of 0·7, 1·0 and 1·2. At the lowest speed, the most noticeable feature is the increase in lift-curve slope at the higher incidences. This is associated mainly with the growth of the low-pressure region lying under the vortex, and thus occurs at lift coefficients above those at which leading-edge separation was first observed. The effect is most marked therefore with the sharp-edged section D, and least apparent for the drooped sections A and B. Leading-edge separation occurs at almost the same lift for states A and B, but the vortex development is slower with the smaller leading-edge radius (A), and this explains the difference in the shape of the two lift curves.

An increase in lift-curve slope near zero incidence is apparent for state A and to a lesser degree for state B. This is associated with the formation of a vortex from leading-edge separation on the lower surface at positive wing incidences, a phenomenon restricted to the drooped wing sections. This lower-surface vortex is very well defined at $\alpha = -0{\cdot}4$ deg for state A (Fig. 42a); with state B the reattachment line is closer to the leading edge and the vortex shows a tendency to break into several segments. By reducing the extent of the droop (state C), the lower surface vortex can be almost eliminated at this incidence.

A similar reduction in the strength of the vortex (accompanied by a progressive increase in the number of vortex segments) is obtained with state A by increasing the wing incidence (Fig. 42d). By $\alpha = 6$ deg, the lower-surface flow is free from vortex traces. Upper-surface separation for this state occurs around $\alpha = 8$ deg however, so that the incidence range with no leading-edge separation is comparatively limited. Above $\alpha = 2$ deg, however the lower-surface vortices appear to have little effect on the wing lift.

The flow patterns for the lower surface show little change with increase in free-stream Mach number (*cf.*, Fig. 42a and e), but the associated change in lift-curve slope is reduced and is absent at $M_0 = 1{\cdot}20$.

At $M_0 = 1{\cdot}00$, the formation on the upper surface of a leading-edge vortex within the incidence range tested was restricted to states D and E. A more important feature is the development of a vortex from the separated flow behind the outboard shock (as in Fig. 31) whose effect on the wing lift should be rather similar to that of the conventional subsonic part-span vortex. There is in fact some correlation between the formation of the outboard vortex and a small increase in lift-curve slope for states C to G. With the drooped states A and B, the outboard shock has not formed, and only just formed, respectively at the highest test incidence. The slight increase in $\partial C_L/\partial\alpha$ at incidences above 7 deg is probably due in these cases to the vortex formed from the separated flow behind the rear shock, which was first observed near $\alpha = 6$ deg.

At $M_0 = 1 \cdot 20$, the outboard shock for a given lift is more rearward, and the vortex formed influences less of the wing surfaces. The change in lift-curve slope is therefore smaller.

For any particular wing state, the variation of $\partial C_L/\partial \alpha$ with M_0 is relatively small (Fig. 43). Moreover the lift-curve slope does not vary greatly with model state; however the type of comparison is complicated by the change in wing aspect ratio with model state (Table 2).

Fig. 41 shows that in addition to changes in lift-curve slope, there is a shift in the lift curve with change of model state so that a given lift is obtained at somewhat different incidences.

For the drooped sections (A, B, C), a change in zero-lift incidence might be expected, though this effect is overshadowed by that due to the lower-surface vortex, which is stronger for state A than for state C. At moderate incidences, where this vortex influence is negligible, there is still a change of about $0 \cdot 3$ deg between states A and B for a given lift.

The no-lift incidence (α_0) should be zero for states D to G, but for state E α_0 varies between $0 \cdot 2$ deg and $0 \cdot 3$ deg over the Mach number range (Fig. 44). Despite checks made during the tests, this behaviour has not been explained satisfactorily*, and it is possible that a similar incidence error applies to state B also. This error is masked at subsonic speeds in Fig. 44 by the influence on lift slope of the lower-surface vortex. When this effect diminishes at high Mach number, the curves for states A and B diverge.

It must be pointed out that the twisting of wing by the aerodynamic loading (Section 2.3.1) reduces the lift-curve slope at the higher incidences and Mach numbers, but this effect is very similar for all model states, and does not modify the comparison of results.

At moderate incidences the variation of C_L with M_0 is small and similar for all model states. As an example, typical curves at $\alpha = 5 \cdot 6$ deg are shown in Figs. 5a to g, and are labelled with a 'b'. The peak value of C_L is reached near $M_0 = 1 \cdot 10$.

At $\alpha = 8 \cdot 6$ deg, for state D, there is a marked fall in lift between stream Mach numbers of $1 \cdot 00$ and $1 \cdot 05$ (curve 'c_1', Fig. 5d). This is due to the change in flow from complete leading-edge separation at the lower Mach number to attached flow over the outer portion of the wing, a flow pattern discussed in Section 3.2 and illustrated in Fig. 10. The lift reduction is caused by the diminution of the vortex influence once partial leading-edge attachment has occurred. The complete leading-edge separation boundary (curve 'a') and the partial (inboard) separation boundary ('d') are also plotted in Fig. 5d, and illustrate the relationship between the flow changes and the wing lift. At a lower incidence ($7 \cdot 6$ deg), the lift reduction is still present but it is smaller, probably because the vortex influence at the lower Mach number is less (curve 'c_2', Fig. 5d).

A similar but smaller effect is found when the sharp leading edge is slightly rounded (Fig. 5e) but for state F, the lift change is not apparent.

3.4.2. *Drag.* The variation of C_D with C_L for the seven wing states is shown in Figs. 5a to g. From these it is possible to plot the variation with Mach number of the drag coefficient at constant lift coefficient, and also the minimum drag coefficient. Some results are given in Fig. 45a and b.

---

* The balance readings for state E could be repeated with considerable accuracy, and the geometric incidence was set, and checked, in a similar fashion to that used for the other states. It was therefore supposed that the wing in state E was slightly twisted (either due to aerodynamic overloading or due to distortion during machining the modified leading edge). The measured twist was too small to account for the observed error in α_0, however.

The minimum value of C_D (C_{D0}) occurs at zero lift for states D to G but at a small positive C_L for the drooped sections*. C_{D0} is highest for the states with the largest droop, possibly due to the presence of the lower-surface vortex. There is little difference in C_{D0} for states D, E and F, but the large leading-edge radius for state G (and perhaps the associated increase in wing thickness/chord ratio) causes a marked increase in C_{D0}. A similar relationship between the drag coefficients of the wing states is obtained at $C_L = 0{\cdot}1$, but at $C_L = 0{\cdot}2$, the drag of the sharper sections (D and E) has risen considerably relative to the other, doubtless due to the onset of leading-edge separation. At $C_L = 0{\cdot}4$ and at subsonic Mach numbers, there is a wide variation in C_D, the lowest values being for states A and B which are about 70 per cent of those for states D and E. It is interesting to note that the slight leading-edge rounding between D and E causes an increase in drag.

The variation with Mach number shown in Fig. 45 is not large and it is difficult to assess the influence of leading-edge shape on drag-rise Mach number particularly as the wing thickness and aspect ratio alters with each modification. At $C_L = 0{\cdot}1$, only state G has an appreciably earlier drag rise than the rest, which are very similar. This may be due to the formation of the initial tip shock at a lower value of M_0 for this state, though the present data are too approximate to enable an estimate to be made of the relative contributions of the rear shock and initial tip shock to the drag rise.

There is a significant rise in drag for the drooped sections as M_0 increases so that by $M_0 = 1{\cdot}15$ the drag of all wing states is nearly the same.

The superiority of the drooped sections at all but the highest Mach numbers can be illustrated in another way by considering the variation of the downstream axial force, C_X (which is measured directly on the balance) with C_L at different Mach numbers. At small incidences, the wing drag may be written as

$$C_D \simeq C_X + C_L\alpha .$$

Thus if C_X decreases as C_L and α increase, the lift-dependent drag will be below the value obtained when the resultant force acts normal to the plane of the wing. The variation of C_X with C_L is thus a measure of the forward inclination of the force vector†. The theoretical limit for this variation is of course that corresponding to elliptic spanwise loading.

The results for four representative model states are shown in Fig. 46; these correspond to a long droop (A), a short droop (C), a sharp leading edge (D) and a moderately rounded leading edge (F). At $M_0 = 0{\cdot}8$, C_X decreases rapidly for state A, but with the sharp-edged section, the reduction is much less pronounced. In the absence of shock waves, the failure to maintain the fall on C_X appropriate to low lift-dependent drag is usually due to leading-edge separation. The curves for $M_0 = 0{\cdot}8$ in Fig. 46 have been marked to show when this was first observed from the oil patterns, and there is some relationship between these points and those parts of the curves where dC_X/dC_L ceases to increase with C_L, except perhaps for the wing state with the largest droop (A).

At the two higher Mach numbers ($1{\cdot}0$ and $1{\cdot}2$) similar sets of curves are obtained, but the variation in C_X with model state at a given lift is smaller, particularly at $M_0 = 1{\cdot}2$. This is consistent with the trend shown at $C_L = 0{\cdot}4$ in Fig. 45. The small rates of decrease of C_X with C_L are now more due to the development of extensive shock systems, rather than to leading-edge separation which is comparatively limited at these Mach numbers.

---

* About $C_L = 0{\cdot}07$ for states A and B, and $0{\cdot}02$ for state C. There is a slight reduction in these values as the stream Mach number increases.

† Or of what has been loosely called 'the degree of leading-edge suction'.

Though Fig. 46 illustrates the superiority of the drooped sections with respect to lift-dependent drag, the magnitude of this improvement is reduced by the variation in aspect ratio from state to state. Since the aspect ratio of the complete wing in state A is 2·71, and that of F is 3·38, it is reasonable to suppose that at constant aspect ratio the differences in performance of these two states would be more marked. It is possible to avoid this difficulty to some extent by making a more conventional analysis of the lift-dependent drag, and using the factor κ in the expression

$$C_D - C_{D0} = \frac{\kappa(C_L - C_{L0})^2}{\pi A} \tag{3}$$

as a measure of the behaviour of the various states. A is the wing aspect ratio and C_{L0} is the lift coefficient at minimum drag coefficient. Doubts about the interpretation of κ arise when the lift curve is non-linear, but the use of this factor is nevertheless convenient.

The balance data are at intervals too large in incidence to enable an accurate determination of κ below $C_L = 0{\cdot}3$. Most of the curves of $C_D - C_{D0}$ against C_L^2 for states D to G are in fact linear up to and beyond this point, and hence the values shown in Fig. 47 for this lift coefficient are still appropriate at smaller C_L's. For comparison, some values of κ at $C_L = 0{\cdot}5$ are also given.

State A has a low value of κ which is little different for a wide range of lift, but which increases steadily as the stream Mach number rises above unity. A curve of similar shape, but at higher values of κ is obtained for the smaller droop (C), but with this state, κ is much larger at the higher C_L. The two curves for state F (moderate leading-edge radius) are rather similar to those for state C, but the actual values of κ are considerably bigger. With the sharp leading edge, κ is almost constant over the entire Mach number range, and varies little with C_L.

It is interesting to note that for state A, leading-edge separation is absent at $C_L = 0{\cdot}3$, but has developed appreciably by $C_L = 0{\cdot}5$. Despite this, the value of κ changes little between the two cases. This is probably because the increase in drag associated with the separation (and which would normally increase κ) is accompanied by an increase in non-linear lift due to the vortex. The latter effect on its own would tend to reduce the parameter κ of Equation (3), which is essentially based on a linear lift curve. Thus the two opposite trends may well give rise to only a small change in κ.

For the other states shown in Fig. 47 leading-edge separation occurs below a lift coefficient of 0·3, and the above-mentioned difficulties associated with the production of non-linear lift are present. Despite this the Figure is valuable in illustrating the significant drag reductions likely to be associated with the drooped leading edges.

It is perhaps of interest to note that two-dimensional aerofoil sections having a blunt leading edge (like state G) always fail to maintain the suction peak close to leading edge, as sonic conditions are approached in this region. This would correspond to a slow drag rise even before critical conditions are reached or an increase in lift-dependent drag with incidence at moderate subsonic Mach numbers. This behaviour may be analogous to some of the results shown in Fig. 45b ($C_L = 0{\cdot}4$) and Fig. 46.

3.4.3. *Lift/drag ratio.* The ratio of wing lift to drag is plotted for each state in Figs. 5a to g, and the maximum values achieved are plotted in Fig. 48. At moderate subsonic speeds there is a wide variation in $(L/D)_{\max}$, the highest value being achieved with the drooped section A and the lowest with state E. This range is reduced markedly as the stream Mach number rises above 1·0 and by $M_0 = 1{\cdot}2$, there is little change with leading-edge shape, except for the very large nose radius (G).

The maximum value of L/D is of course the reciprocal of the minimum slope line from the origin to the drag polar (*see* inset of Fig. 48), and this is sensitive to small changes in the curve in this region. All states (except D and E) have a characteristic kink on the C_D vs. C_L curve in a C_L range between 0·15 and 0·20, and this persists in most cases up to $M_0 = 1{\cdot}05$. The oil patterns show no corresponding change in flow in the critical region. The balance results reveal that the normal force increases steadily with incidence, but that the kink is always due to a change in the shape of the axial-force curve, the reason for which is unknown*.

This kink is exaggerated when the L/D curves are plotted, and gives rise to the characteristic shape of curve for states B and G for example, and by this means contributes to the large fall in $(L/D)_{\max}$ caused by rounding off the leading edge of state A to form state B. This change is at first sight a little unexpected.

The theoretical variation of $(L/D)_{\max}$ for state A (assuming that the lift-dependent drag is proportional to $C_L{}^2$ and that $\kappa = 1$) is also shown in Fig. 48. It is comparatively close to the experimental curve at subsonic Mach number, a wider discrepancy occurring at the highest test speeds.

4. *Some Remarks on the Design of Sweptback Wings.* The results analysed in the preceding pages are perhaps of some value in relation to the general problems of swept-wing design. These of course vary with the type of aerodynamic characteristics required, and with the Mach number range which is of interest.

The present tests show that at moderate subsonic speeds, in the absence of shock waves, the simple type of droop used for states A to C is beneficial in delaying leading-edge separation and hence in reducing lift-dependent drag at the higher C_L's. The minimum drag of the wing is slightly higher for an undrooped section and care is required in the design of the under surface of the droop in order to reduce or eliminate the lower-surface vortex. It seems unlikely that the onset of leading-edge separation for drooped sections of the present type will be at a higher lift than for a very blunt leading edge in the landing condition, but the latter section shows a very marked deterioration as the Mach number increases. The present droops may be regarded as a means of achieving the benefits of small leading-edge radius at high Mach number, without detriment to the low-speed performance.

At cruising conditions, the appearance of shock waves (without accompanying boundary-layer separation) determines the beginning of the drag rise; the shock waves involved are the rear shock and the initial tip shock, both of which are thought to be primarily associated with conditions at the inboard and outboard extremities of the wing. The initial tip shock seems to appear before the rear shock for the undrooped sections, though in view of the difficulties of much of this type of assessment, it is perhaps more satisfactory to regard both shocks as appearing at about the same stream Mach number.

If the initial tip shock is caused by the loss of isobar sweep at the tip, it may be possible to delay its occurrence by suitable planform design in that region (*i.e.*, by the curved tip advocated by Dr. Weber) or by a judicious change in wing twist or section. Section changes would need to be rather different from the leading-edge modifications of the present tests which have very little effect on the initial tip shock.

---

* The most obvious explanation of a change in transition position seems unlikely in view of the constant check on this by means of the oil patterns and sublimation patterns. Results from N.A.C.A. tests sometimes reveal similar kinks in the drag polars, as well as the characteristic distortion of the L/D curve.

The rear shock is more important however, since it may ultimately become sufficiently strong to eliminate the initial tip shock, and also to cause flow separation. The spanwise position and stream Mach number for the formation of a true shock, as opposed to a diffuse recompression region, can probably be controlled by altering the shape of the wing-root junction and hence relaxing the condition that the root flow must be parallel to the stream. This type of modification is of course achieved by the waisted wing-body intersections resulting from area-rule, or root-design, treatments. The expansion zone from the forward part of the indentation modifies the root compression system. Considerable gains in drag-rise Mach number have been achieved this way.

It might be possible to achieve similar benefits by means of section changes alone in the root region, for example by moving the maximum thickness position further forward to offset the usual rearward loading shift. Such methods may prove to be insufficiently powerful to accomplish what is required however. The present tests suggest that the rear shock position (and perhaps strength) is largely unaffected by leading-edge modifications.

The formation of a rear shock over the outboard part of the wing may be delayed by suitable wing twist (to unload the outer section), or section changes*, but it is possible that if the local flow is supersonic the root disturbance will continue to propagate outboard. Certainly a reduction in local Mach number ahead of the rear shock delays the onset of shock-induced separation. Though it seems preferable to influence the rear shock by means of a compensating root expansion, experimental data suggest that its effect may sometimes be limited to the inboard half of the wing at transonic speeds, and that the beneficial effects may also be restricted to a limited range of stream Mach number. Thus for a high aspect-ratio wing of fixed general planform and thickness, the use of the part-span bodies developed by Whitcomb[16] would seem to be indicated; amongst their several virtues would seem to be that of interfering with the rear-shock development.

The forward shock is obviously strongly influenced by the section shape, particularly in the leading-edge region. Its appearance is probably determined by the attainment of a specific local Mach number near the leading edge, and this occurs at the lowest stream Mach number when the nose radius is large. When the leading edge is drooped, the appearance of the forward shock is considerably delayed. The occurrence of a forward shock may not be important in itself, since its strength may well be small compared with that of the rear shock; however its appearance is a precursor to the formation of the strong outboard shock with its attendant separation, and therefore some delay is welcome. The limiting delay is however dependent on the conditions under which separation occurs behind the rear shock on its own and delay beyond this point is of little benefit. Indeed the presence of a forward shock on the surface ahead of a strong rear shock, when intersection is avoided, will reduce appreciably the local Mach number upstream of that shock and hence may delay the associated separation. There is therefore a critical design condition in which the rear shock is shielded by the forward shock; the most significant gains are likely to be achieved near $M_0 = 1$. This design philosophy involves the exploitation of the fundamental nature of the three-dimensional flow and hence is the opposite of that which attempts to secure yawed-wing flow over the entire wing. It would seem that lower drags should result from the latter approach, although the former may be easier to obtain when the wing aspect ratio is small.

---

* Such changes would require either the formation of expansion region to counteract the compression of the rear shock, or more practically perhaps, a profile design which reduces the local Mach number ahead of the rear shock and hence decreases its strength.

As far as flow separation is concerned, the drooped sections are not the most satisfactory at all Mach numbers. In Fig. 49, the boundaries corresponding to the onset of separation have been plotted to illustrate this. At $M_0 = 1{\cdot}05$, for example, separation occurs at a lower lift (behind the rear shock) for state A than for state D (behind the outboard shock).

In Ref. 17 some attempt was made to influence the position of the forward shock by body waisting. The effect was much smaller than can be achieved by section modifications of the type discussed in this Report. Provided the problem of rear shock separation discussed earlier can be overcome, the greatest benefits in delaying the forward shock (or more particularly, its intersection with the rear shock) would seem to come from some form of progressive droop which increases outboard. Prevention of the formation of a true rear shock (as opposed to diffuse compression system) by methods such as body waisting does not automatically reduce the need to delay the forward shock. In supplementary experiments to those reported in Ref. 17 it was found that a strong outboard shock tends to form even when the forward shock intersects the root compression zone*; a well-marked rear shock did not seem to be necessary.

Once the outboard shock has formed, its chordwise position will depend mainly on the rear shock (and hence it would seem on the inboard part of the wing) and its spanwise extent by the forward shock (and thus on the wing profile). Though the local Mach number ahead of the shock can be reduced by section design, the very existence of a forward shock for leading-edge sweeps of about 50 deg seems to ensure that the local Mach number is high enough for separation to occur behind the outboard shock. This could be prevented presumably by increasing the effective sweep of the shock but it is not obvious how this can be achieved.

The problem of the outboard shock would seem to be more severe for wings of comparatively high aspect ratio, since the intersection of the forward and rear shocks is likely to occur earlier than for a corresponding wing of low aspect ratio. If the wing is sufficiently long the outboard shock might ultimately approach the leading edge and cause tip separation in the manner of Fig. 31a. It is more likely however that as the root influence on the outboard shock direction diminishes with spanwise distance the shock may increase in sweep and become parallel to the leading edge, like the shock on the hypothetical yawed wing.

In this connection, it would seem more advantageous to obtain yawed-wing flow by delaying (or eliminating) the forward shock, rather than by encouraging an earlier appearance of the forward shock and thus restricting the root influence to a limited part of the wing area. In the former case there seems to be more likelihood of dealing successfully with flow separation to the rear of the main shock front since the local Mach numbers will not be so high as in the latter case. If this cannot be done, a wing entirely dominated by root flow and, as was discussed earlier, in which the pressure recovery is judiciously balanced between the forward and rear shocks to prevent separation might be the best solution.

The present tests were made on untapered wings and these show that extensive regions of separated flow can exist behind the rear and outboard shocks at transonic speeds. These regions probably influence the wing pitching moment considerably and contribute to the buffeting problem, and since their extent changes with flow conditions, some reduction in effect seems desirable. This can be achieved by tapering the wing so that the rear shock lies closer to the trailing edge. Some

---

* This is rather similar to the formation of a strong outboard shock with state G outboard of the intersection of a strong forward shock and a rather diffuse rear shock.

loss in isobar sweep will result, together with a decrease in rear shock sweep and it is to be expected that the wing drag may rise, even though separation has been suppressed. The loss in wing lift at transonic speeds will be generally small. Ref. 15 shows that the loading is almost zero behind rear shock when there is no well-defined rear vortex. If the trailing edge is less swept so that the shock is at the edge, then supersonic-type flow can take place around the corner, and high loadings be sustained to the rear of the section.

A change in leading-edge sweep is far more significant. If the sweep is reduced, the root constraint is less severe and the rear shock has more similarity with the shock on a two-dimensional aerofoil. The forward shock will appear earlier, and the wing area influenced by the root region will be comparatively limited in extent. The tip shock however will probably become more significant and ultimately, for a straight wing at a suitable incidence and Mach number, the root and tip zones of influence will be comparable in extent, a single unswept shock lying between them. Separated flow may no longer roll into the well-defined vortices observed with the present wing.

If the leading-edge sweep is higher than about 65 deg, there may be a simplification of the flow pattern, in that the forward shock may occur only at the limits of the incidence range when the local Mach numbers become sufficiently high. With such large sweeps however there is the possibility of the rear shock intersecting the leading edge and causing separated flow along the edge outboard. With a sufficiently high sweep, leading-edge separation may well dominate the flow in the transonic region, since the flow attachment may occur at a much higher stream Mach number.

5. *Concluding Remarks.* The present tests have given some indication of the influence of leading-edge modifications on the flow over a moderately-swept wing at transonic speeds, and the possible influence of this information on the design of swept wings has been discussed in a rather speculative manner in Section 4.

More information in two directions would seem to be required. Firstly, knowledge of the effects of such devices as body waisting, wing twist, etc., on the flow patterns of a swept wing is lacking. In view of the complicated nature of the flow it seems unlikely that this can come from other than wind-tunnel tests. Secondly more information must be obtained about the relationship between two-dimensional aerofoil and three-dimensional wing flows in order to establish the value of data obtained from aerofoil tests.

The simple nature of the present experiment has its own inherent disadvantage in that the quantitative nature of the wing flow is largely unknown. This can be overcome to some extent by the approximate analysis devised for oil-flow photographs, but at best this is rather unsatisfactory. It is hoped therefore to make pressure-plotting models corresponding to states A, D and F to obtain further information, and at the same time to test the corresponding two-dimensional sections. In addition, tests are in progress at the N.P.L. to help specifically with the problems raised in the second paragraph of this section.

Some confirmation is available from the present tests of the condition for shock-induced separation of a turbulent boundary layer under the influence of the swept shocks in the wing surface; this condition (that the Mach number component normal to the shock front shall be greater than about 1·39) is put forward in a tentative manner in Ref. 15. The value of such a confirmation should not be overestimated however, and the puzzling features of such a separation condition (*e.g.*, its apparent independence of shock pressure ratio and its inconsistency with the comparatively well-established conditions for the comparable phenomenon on aerofoils[9]) remain unresolved. It may be that this

apparent difference between the behaviour of swept and unswept shocks is mainly attributable to the flow conditions immediately downstream which tend to be rather dissimilar. Again the fact that one shock is cone-like and the other normal may be important. Obviously more work is required.

6. *Acknowledgements.* The authors wish to acknowledge the assistance given by Miss B. M. Davis with the experimental work and with the reduction of the observations. Mr. W. Haywood made the model and carried out the successive modifications.

Finally, acknowledgement must be made to Dr. I. M. Hall and Mr. H. H. Pearcey for their help during frequent discussions on the results contained in this Report.

REFERENCES

No.	*Author*	*Title, etc.*
1	L. H. Tanner	Curves suitable for families of aerofoils with variable maximum thickness position, nose radius, camber and nose droop. A.R.C. C.P. 358. February, 1957.
2	I. M. Hall	The operation of the N.P.L. 18-in. × 14-in. Wind Tunnel in the transonic speed range. A.R.C. C.P. 338. January, 1957.
3	I. M. Hall and E. W. E. Rogers	The flow pattern on a tapered swept-back wing at Mach numbers between 0·6 and 1·6. A.R.C. R. & M. 3271. Part I. November, 1957.
4	E. C. Maskell	Flow separation in three dimensions. A.R.C. 18,063. November, 1955.
5	W. F. Lindsey and E. J. Landrum	Compilation of information on the transonic attachment of flows at the leading-edges of airfoils. N.A.C.A. Tech. Note 4204. February, 1958.
6	B. D. Henshall and R. F. Cash ..	An experimental investigation of leading-edge flow-separation from a 4 per cent thick two-dimensional biconvex aerofoil. A.R.C. R. & M. 3091. February, 1957.
7	H. J. Walker and W. C. Maillard	A correlation of airfoil section data with the aerodynamic loads measured on a 45 deg sweptback wing at subsonic Mach numbers. N.A.C.A. Research Memo. A55C08 TIL/4684. May, 1955.
8	G. P. Wood and P. B. Gooderum	A factor affecting transonic leading-edge flow separation. N.A.C.A. Tech. Note 3804. October, 1956.
9	H. H. Pearcey	Some effects of shock-induced separation of turbulent boundary layers on transonic flow past aerofoils. Symposium on Boundary-Layer Effects in Aerodynamics. Paper 9. National Physical Laboratory. 1955.
10	D. W. Holder and R. F. Cash ..	Experiments with a two-dimensional aerofoil designed to be free from turbulent boundary-layer separation at small angles of incidence for all Mach numbers. A.R.C. R. & M. 3100. August, 1957.
11	H. H. Pearcey	The occurrence and development of boundary-layer separations at high incidences and high speeds. A.R.C. R. & M. 3109. September, 1955.
12	J. B. Scott-Wilson	An experimental investigation of the transonic flow over an unswept wing of aspect ratio 3·5, taper ratio 0·5, with a 4 per cent biconvex section. A.R.C. R. & M. 3209. November, 1955.
13	H. Behrbohm	Einige Ergebnisse aus der Tragflächenforschung in Schweden. Proc. 2nd. European Aeronautical Congress. 1956.

REFERENCES—*continued*

No.	*Author*	*Title, etc.*
14	L. W. Hunton	Effects of finite span on the section characteristics of two 45 deg sweptback wings of aspect ratio 6. N.A.C.A. Tech. Note 3008. September, 1953.
15	I. M. Hall and E. W. E. Rogers	Experiments on a tapered sweptback wing of Warren 12 planform at Mach numbers between 0·6 and 1·6. A.R.C. R. & M. 3271. Part II. July, 1960.
16	R. T. Whitcomb	Special bodies added on a wing to reduce shock-induced boundary-layer separation at high subsonic speeds. N.A.C.A. Tech. Note 4293. June, 1958.
17	R. C. Lock and E. W. E. Rogers	Some preliminary experimental results on the effect of asymmetric body waisting on the drag due to lift of a sweptback wing at transonic speeds. N.P.L./Aero/328. 1957.
18	H. H. Pearcey	A method for the prediction of the onset of buffeting and other separation effects from wind-tunnel tests on rigid models. A.R.C. 20,631. September, 1958.
19	E. W. E. Rogers and I. M. Hall	An investigation of transonic speeds of the performance of various distributed roughness bands used to cause boundary-layer transition near the leading edge of a cropped delta half-wing. A.R.C. C.P. 481. May, 1959.

APPENDIX

Comparison of Flow Patterns for Sweptforward and Sweptback Configurations

When the model was in state D, with a sharp leading edge, some oil patterns were obtained with the wing in a reversed condition, so that it represented part of a sweptforward configuration. The comparison with the results of the sweptback wing can only be approximate since the wing profile is not symmetrical about mid-chord (*see* Fig. 2a). Moreover the wing twist under aerodynamic loading tends to decrease the tip incidence on a sweptback wing but to increase this when the wing is sweptforward. Nevertheless in view of the present interest in sweptforward planforms and the relative scarcity of data on the likely flow patterns, some results are included in the present text.

At $M_0 = 0{\cdot}80$, there is little difference in the incidence at which leading-edge separation first occurs but with the sweptforward wing the vortex (which now runs inboard) has a slightly higher sweep, since it is forced to turn back over the wing surface by the wall. This increase in vortex sweep is maintained for a limited range of incidence, but by $\alpha = 9{\cdot}6$ deg, the vortex sweep is almost identical in both the planforms (Fig. 50a and b). A marked difference occurs in the shape of the two secondary separation lines, near the tip and root respectively.

The onset of leading-edge separation is unchanged for the sweptforward wing by raising the Mach number to $1{\cdot}10$, but at $M_0 = 1{\cdot}20$ and $\alpha = 3{\cdot}6$ deg, a forward shock may exist over the inboard part of the wing*, indicating attached leading-edge flow at this condition. A vortex lies immediately behind this shock, and is associated with a leading-edge separation outboard (Fig. 50e). This photograph also shows a shock (corresponding to the rear shock) along most of the span.

By $\alpha = 5{\cdot}6$ deg, at $M_0 = 1{\cdot}20$, the flow is again separated along the whole leading edge. Fig. 50d is an oil pattern at $\alpha = 7{\cdot}6$ deg showing a well-marked part-span vortex, and secondary separation line as well as a small tip vortex. The 'equivalent' rear shock is between the part-span vortex and the tip, close to the trailing edge. For comparison the sweptback wing pattern is shown at $\alpha = 8{\cdot}6$ deg in Fig. 50c. This discrepancy in wing incidence represents an attempt to allow for wing-twist effects in the two cases.

No measurements of the wing forces were made with the model in a sweptforward condition.

* Though the interpretation is not easy, the trace in question has more the appearance of being due to a shock than to a secondary separation line.

TABLE 1

Profile Ordinates

	State A		State B		State C		State D
$\frac{x}{c_n}$	$\left(\frac{y}{c_n}\right)_{US}$	$\left(\frac{y}{c_n}\right)_{LS}$	$\left(\frac{y}{c_n}\right)_{US}$	$\left(\frac{y}{c_n}\right)_{LS}$	$\left(\frac{y}{c_n}\right)_{US}$	$\left(\frac{y}{c_n}\right)_{LS}$	$\left(\frac{y}{c_n}\right)$
−0·180	−0·06746	−0·06746					
−0·179	−0·06525	−0·06904					
−0·175	−0·06229	−0·06948					
−0·160			−0·06124	−0·06124			
−0·159			−0·05828	−0·06359			
−0·156			−0·05517	−0·06429			
−0·150	−0·05072	−0·06575	−0·05143	−0·06503			
−0·130			−0·04243	−0·06239			
−0·125	−0·04036						
−0·100	−0·03083	−0·05752	−0·03083	−0·05752			
−0·075	−0·02206		−0·02206				
−0·060					−0·02466	−0·02466	
−0·059					−0·02264	−0·02713	
−0·056					−0·01881	−0·02883	
−0·050	−0·01400	−0·04938	−0·01400	−0·04938	−0·01543	−0·02973	
−0·040					−0·01154	−0·02958	
−0·030					−0·00832	−0·02888	
−0·025	−0·00666	−0·04537	−0·00666	−0·04537			
−0·020					−0·00552	−0·02801	
−0·010					−0·00264	−0·02709	
0	0	−0·04151	0	−0·04151	0	−0·02618	0
0·0375	↑	−0·03628	↑	−0·03628	↑	−0·02332	
0·040							0·00936
0·075		−0·03252		−0·03252		−0·02263	
0·080							0·01724
0·120							0·02374
0·125		−0·03108		−0·03108		−0·02601	
0·160							0·02897
0·175		−0·03308		−0·03308		−0·03101	
0·200							0·03304
0·225		−0·03599		−0·03599		−0·03517	
0·250	ϕ		ϕ		ϕ		0·03672
0·275		−0·03836		−0·03836		−0·03803	
0·300							0·03892
0·325		−0·03973		−0·03973		−0·03959	
0·350							0·03992
0·375		−0·04000		−0·04000		−0·04000	0·04000
0·410		↑		↑		↑	0·03970
0·425							0·03942
0·480							0·03784
0·560							0·03407
0·650		ϕ		ϕ		ϕ	0·02838
0·780							0·01842
1·00	↓	↓	↓	↓	↓	↓	0

c_n is chord normal to leading edge of basic section D.

y is measured from chord line of section D towards upper surface.

x is measured from leading edge of section D towards trailing edge.

ϕ denotes profile is identical with section D.

TABLE 1—*continued*

	State D	State E	State F	State G
$\frac{x}{c_n}$	$\frac{y}{c_n}$	$\frac{y}{c_n}$	$\frac{y}{c_n}$	$\frac{y}{c_n}$
0	0			
0·0080		0		
0·0083		0·00104		
0·0090		0·00174		
0·0100		0·00225		
0·0120		0·00291		
0·0150		0·00368		
0·0200		0·00488		
0·0300		0·00717		
0·0400	0·00936	0·00936		
0·0543		↑	0	
0·0550			0·00280	
0·0573			0·00574	
0·0620			0·00905	
0·0690			0·01223	
0·0800	0·01724		0·01569	
0·0960			0·01936	
0·1200	0·02374		0·02374	
0·1400			↑	0
0·1408				0·00408
0·1433				0·00810
0·147				0·01162
0·153		ϕ		0·01557
0·160	0·02897			
0·163				0·02015
0·177				0·02462
0·196				0·02884
0·200	0·03304		ϕ	
0·222				0·03277
0·250	0·03672			
0·258				0·03624
0·300	0·03892			0·03857
0·350	0·03992			↑
0·410	0·03970			
0·480	0·03784			
0·560	0·03407			ϕ
0·650	0·02838			
0·780	0·01842			
1·000	0	↓	↓	↓

All profiles are symmetric.

TABLE 2

Details of Wing and Profile Parameters for Each State

State		A	B	C	D	E	F	G
Thickness/chord ratio (per cent)	along stream (t/c_s)	4·36	4·43	4·85	5·14	5·18	5·44	5·97
	normal to leading edge (t/c_n)	6·78	6·90	7·55	8·00	8·07	8·46	9·30
Leading-edge radius/chord (per cent)	in terms of local chord	—	—	—	0	0·20	0·59	1·16
	in terms of chord of state D	0·20	0·38	0·38	0	0·20	0·56	1·00
Droop parameters (in terms of chord of state D, *see* Fig. 2b)	$-\frac{m}{c_D}$	0·18	0·16	0·06	0	—	—	—
	$-\frac{n}{c_D}$	0·067	0·061	0·024	0	—	—	—
Aspect ratio of complete wing		2·71	2·76	3·02	3·20	3·23	3·38	3·72

State	Chord length (inches)	
	c_s (along stream)	c_n (normal to leading edge)
A	5·90	3·79
B	5·80	3·73
C	5·30	3·41
D	5·00	3·21
E	4·96	3·19
F	4·73	3·04
G	4·30	2·77

Wing aspect ratio is given in Table 2.

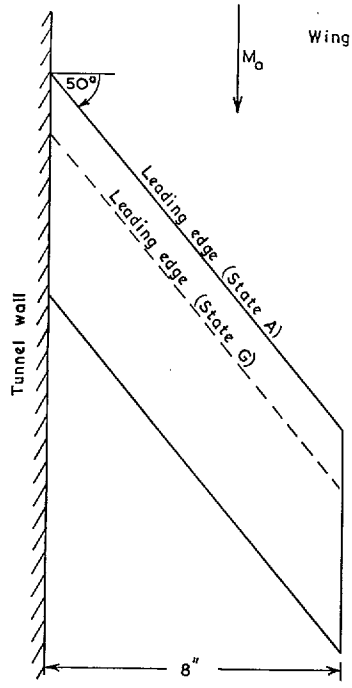

FIG. 1. Wing planform.

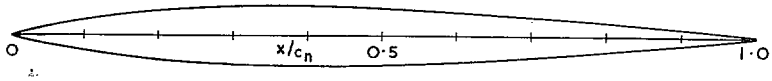

(a) Profile of basic sharp-nosed section (D) along chord normal to leading edge (c_n)

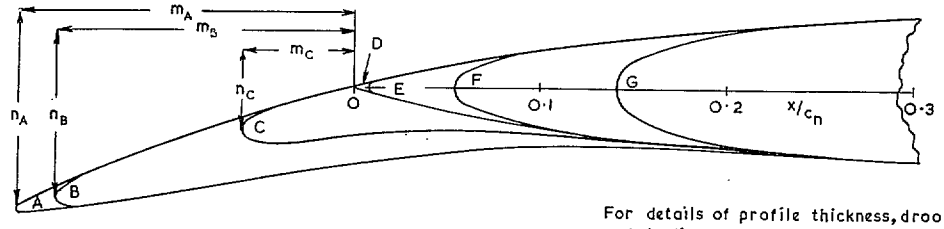

For details of profile thickness, droop, and leading edge radius, see Table 2. Profile ordinates are given in Table 1.

(b) Variation of nose shape with model state in terms of chord normal to leading edge (c_n)

FIG. 2. Details of the seven model states.

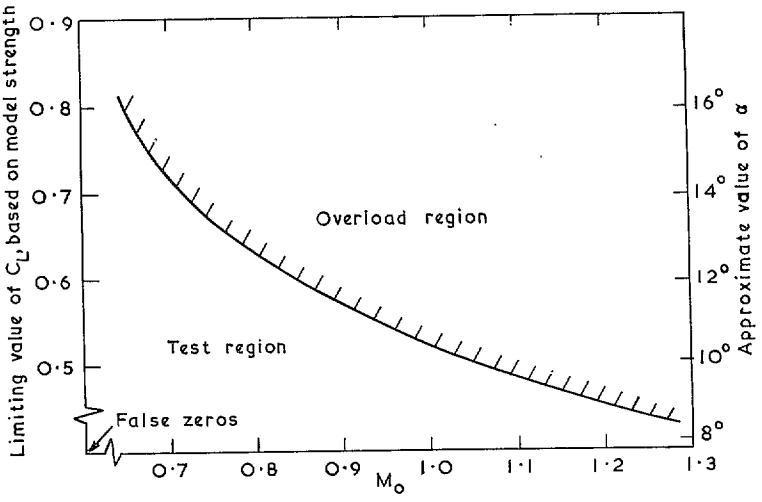

FIG. 3. Approximate loading boundary used for all models.

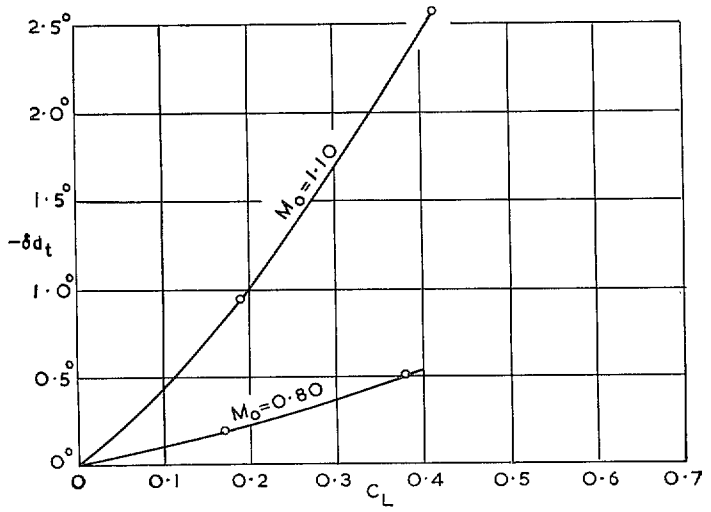

FIG. 4. Measured changes in tip incidence due to aeroelastic effects. (State G).

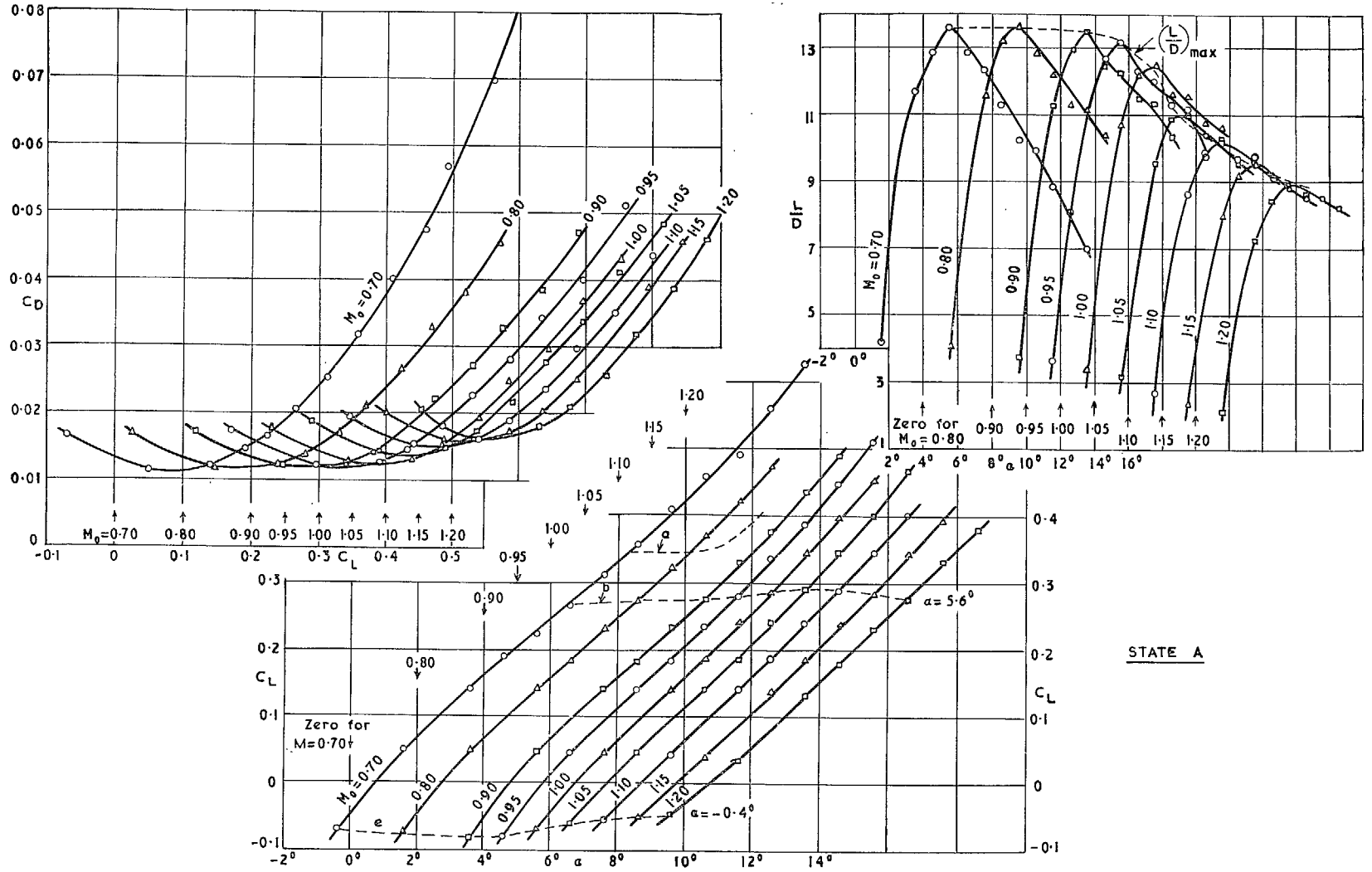

FIG. 5a. Lift and drag characteristics of wing in state A.

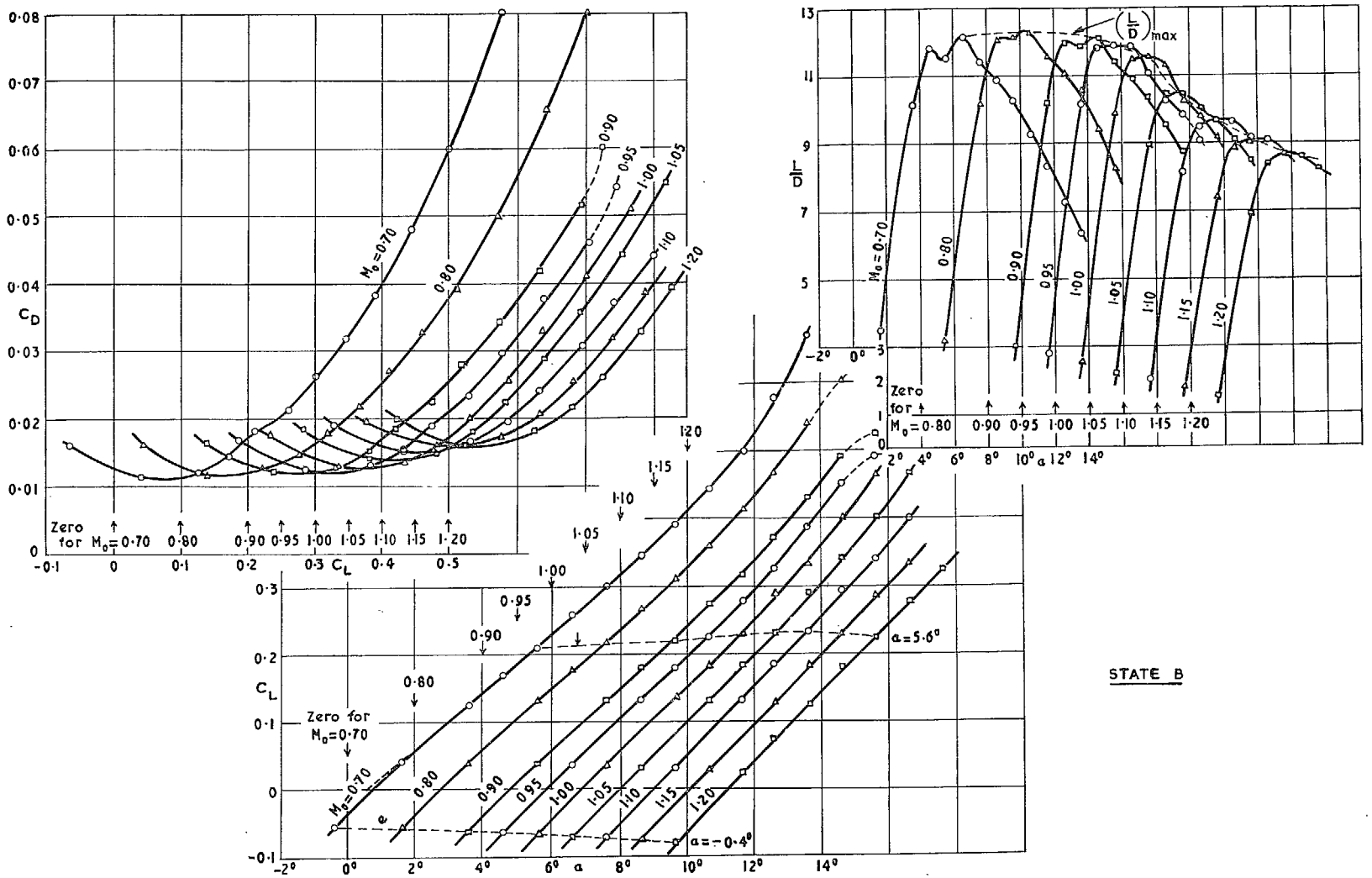

FIG. 5b. Lift and drag characteristics of wing in state B.

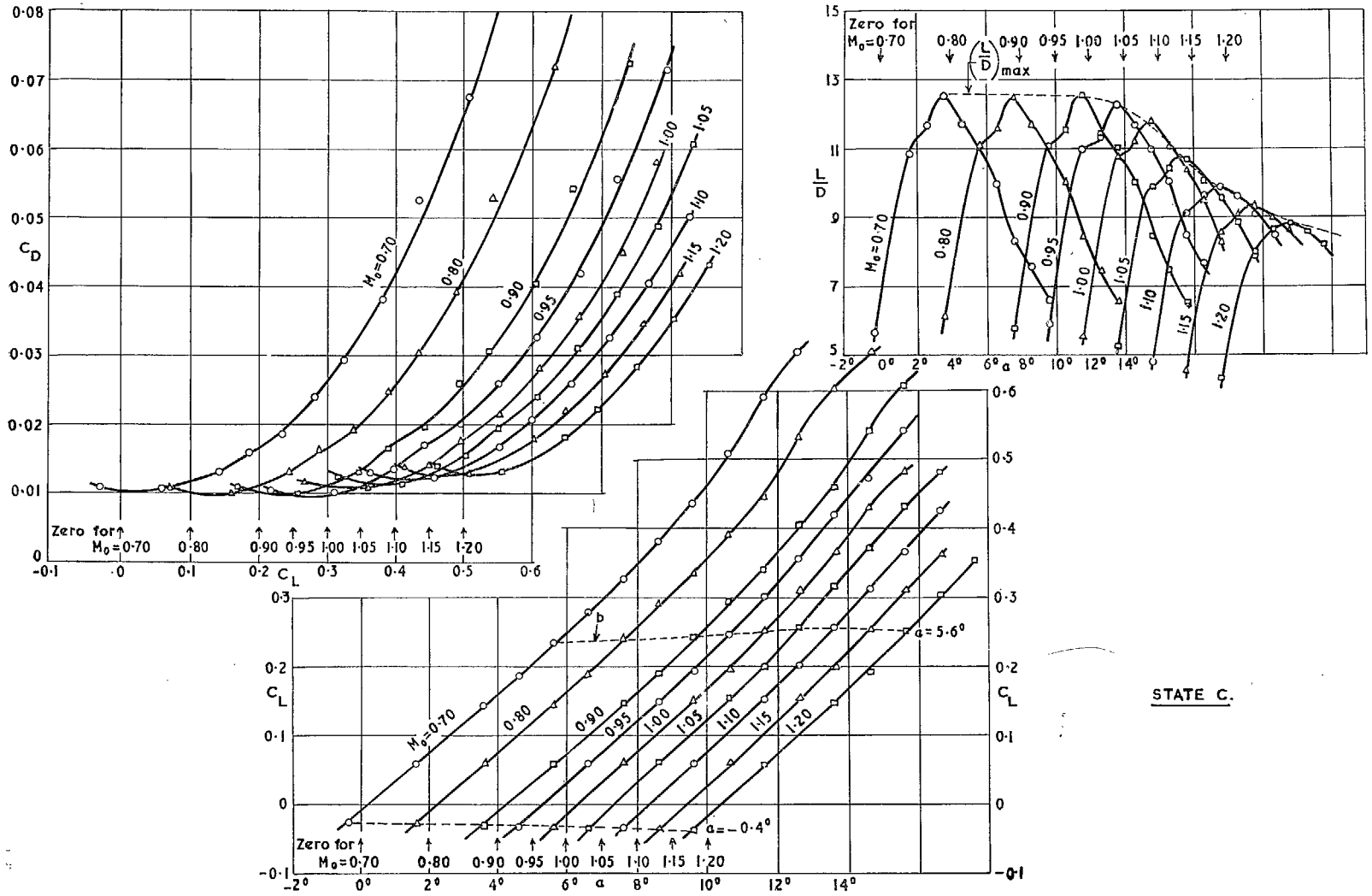

FIG. 5c. Lift and drag characteristics of wing in state C.

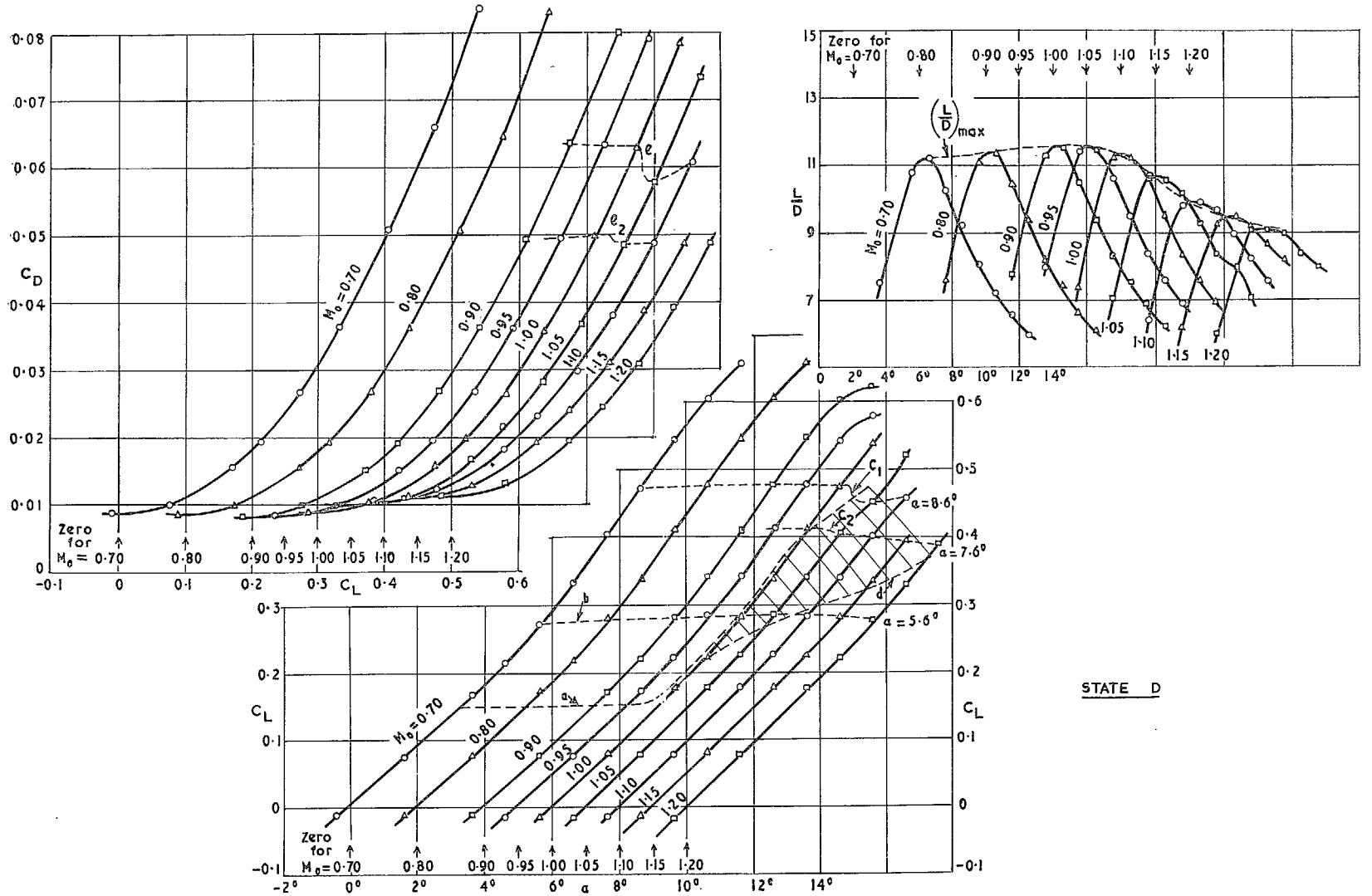

FIG. 5d. Lift and drag characteristics of wing in state D.

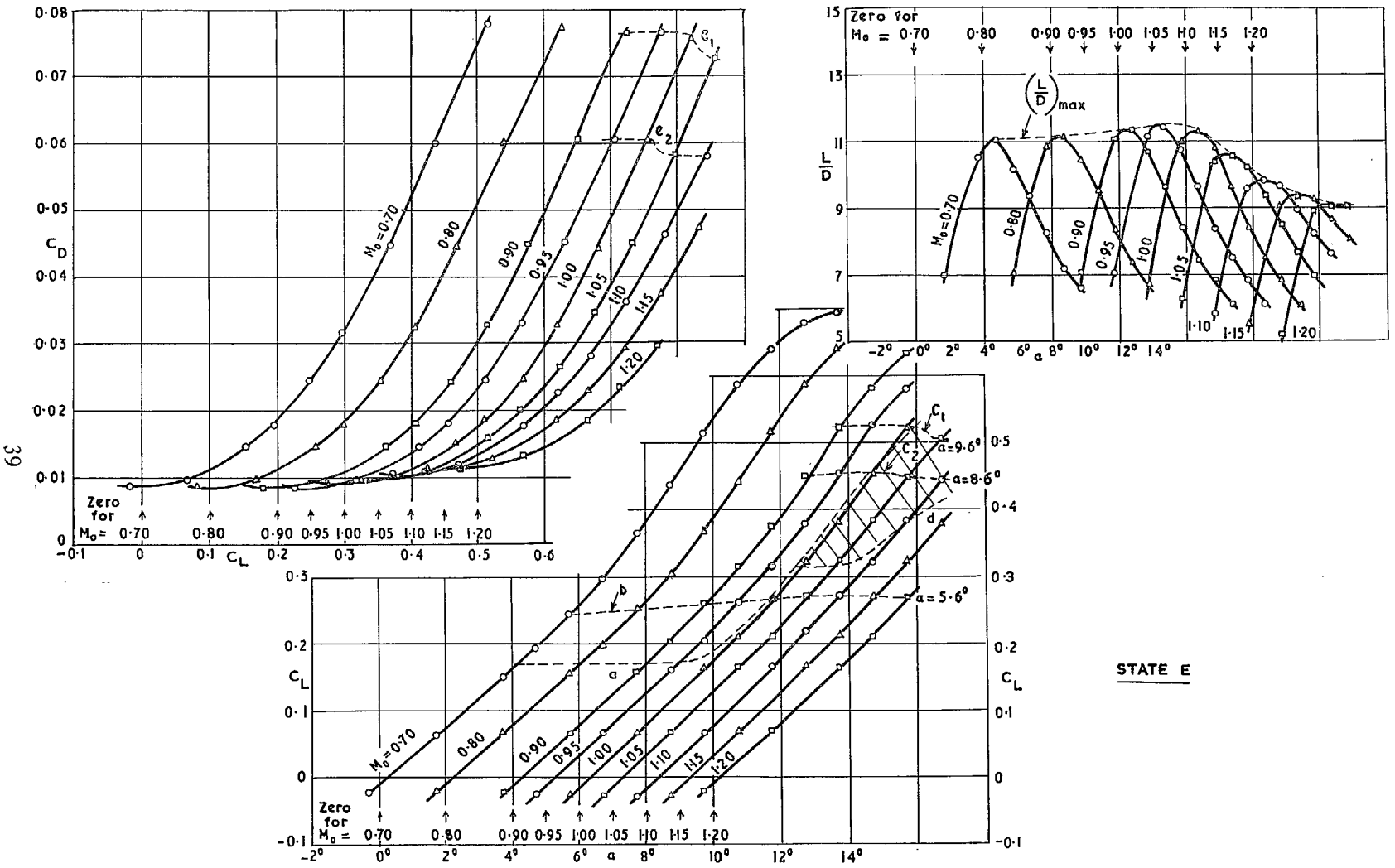

FIG. 5e. Lift and drag characteristics of wing in state E.

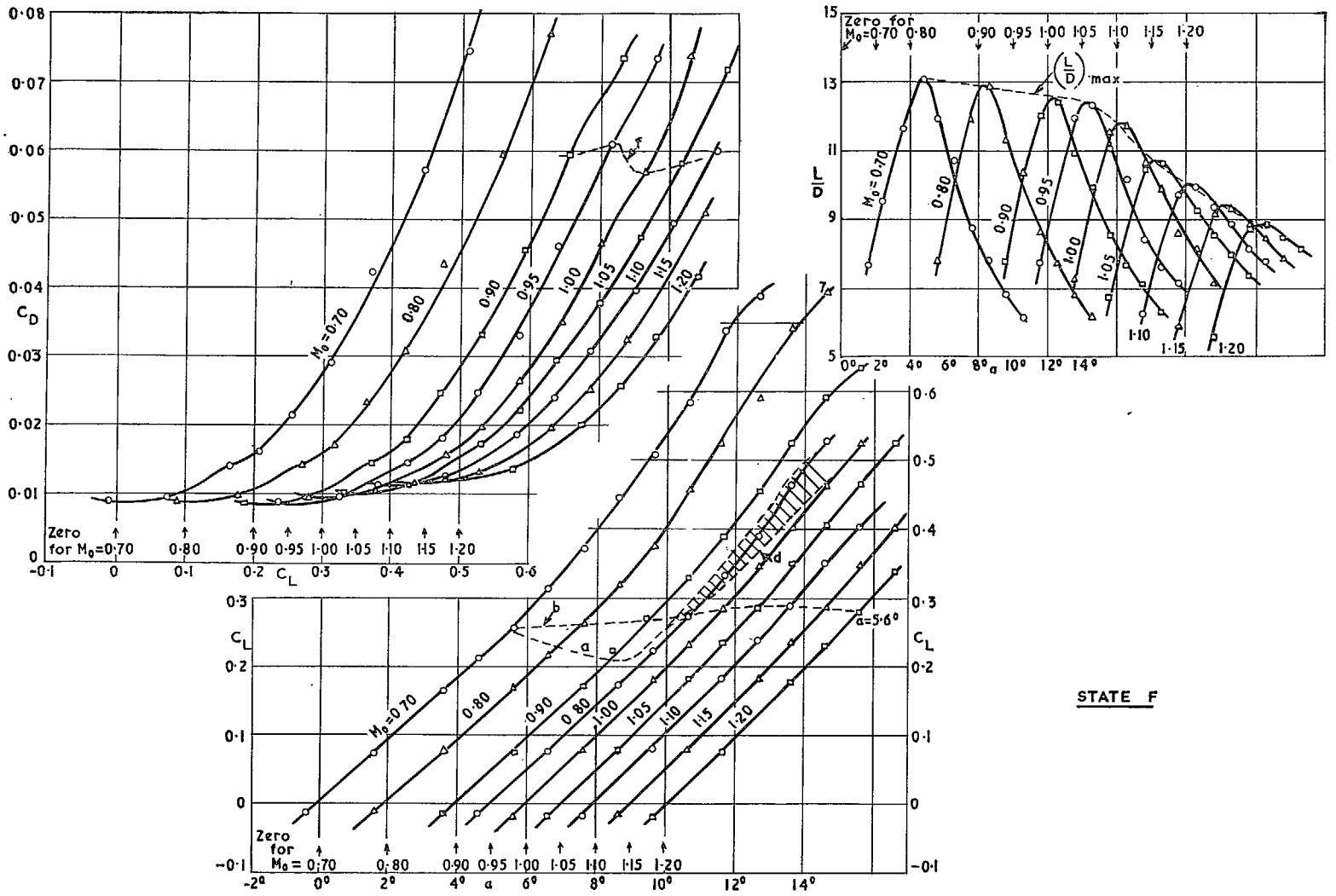

FIG. 5f. Lift and drag characteristics of wing in state F.

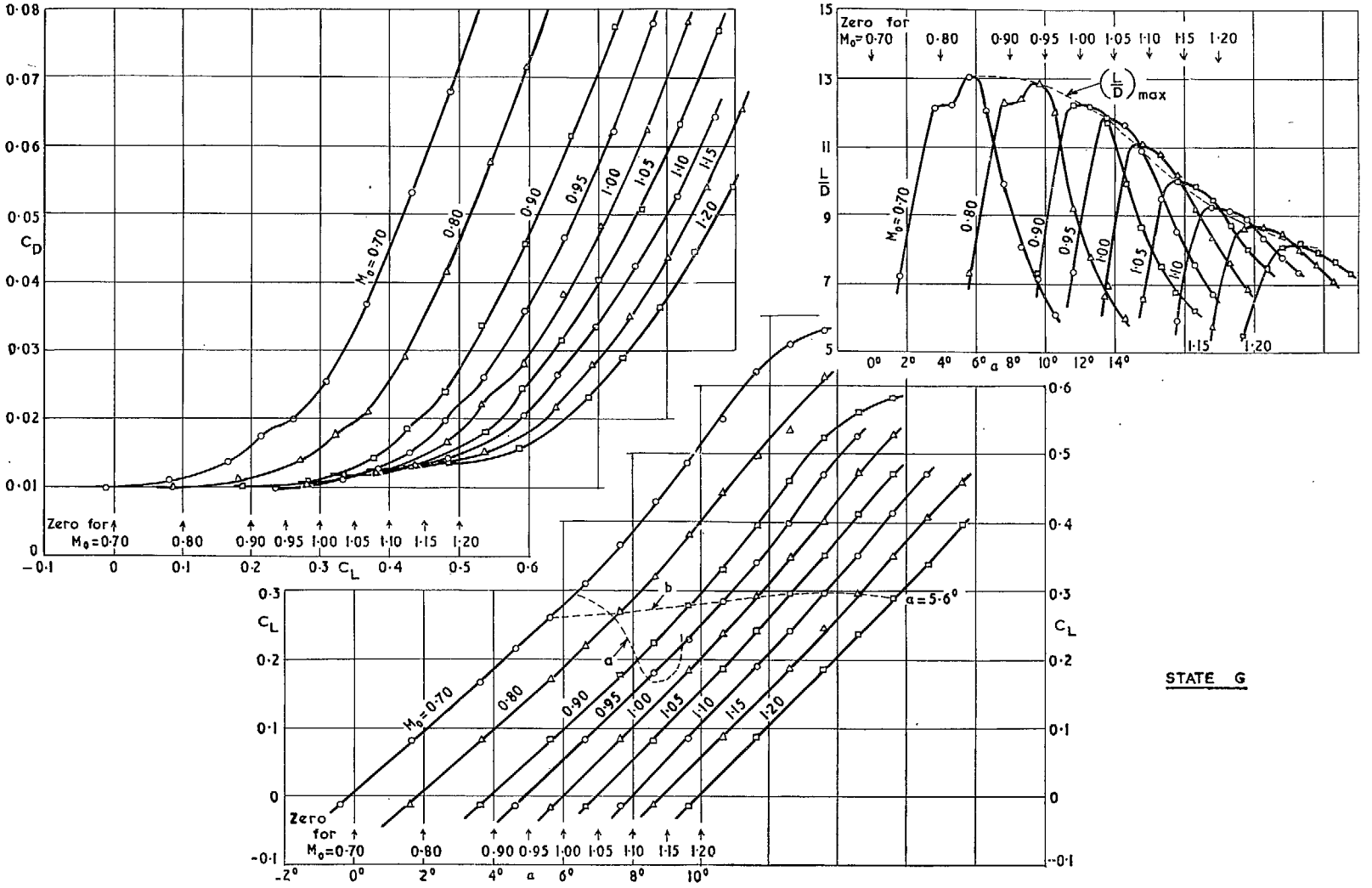

FIG. 5g. Lift and drag characteristics of wing in state G.

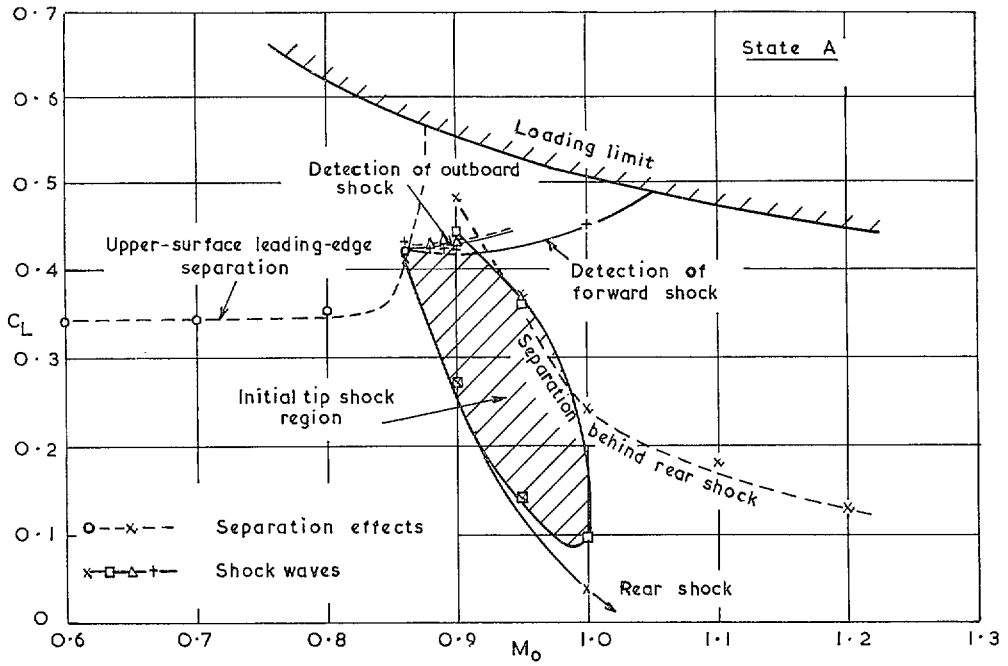

FIG. 6a. Flow characteristics of wing in state A.

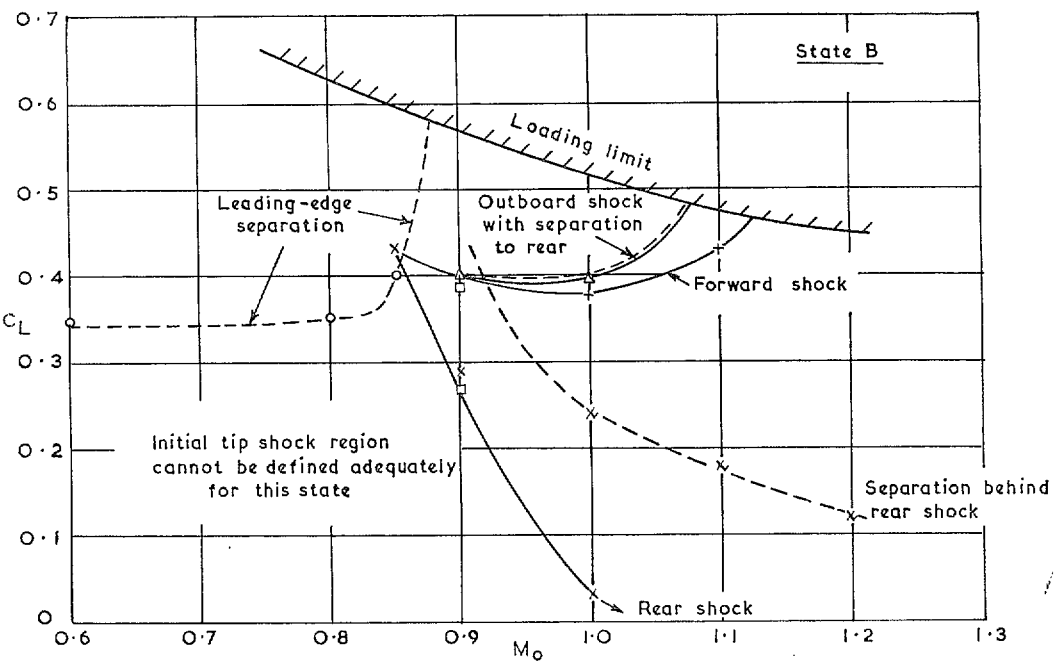

FIG. 6b. Flow characteristics of wing in state B.

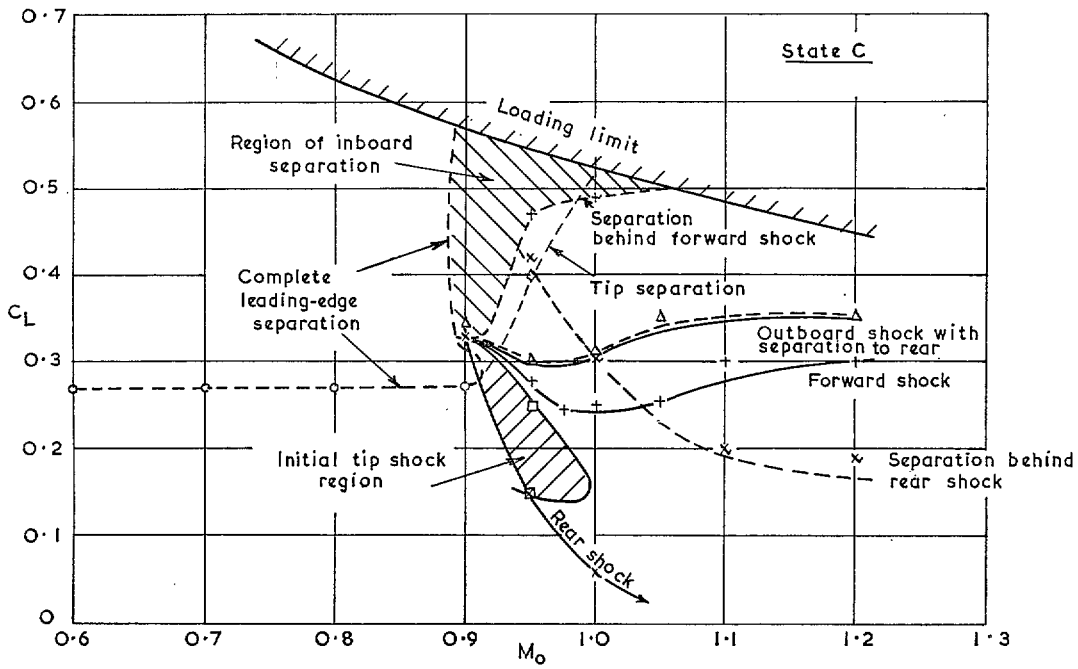

FIG. 6c. Flow characteristics of wing in state C.

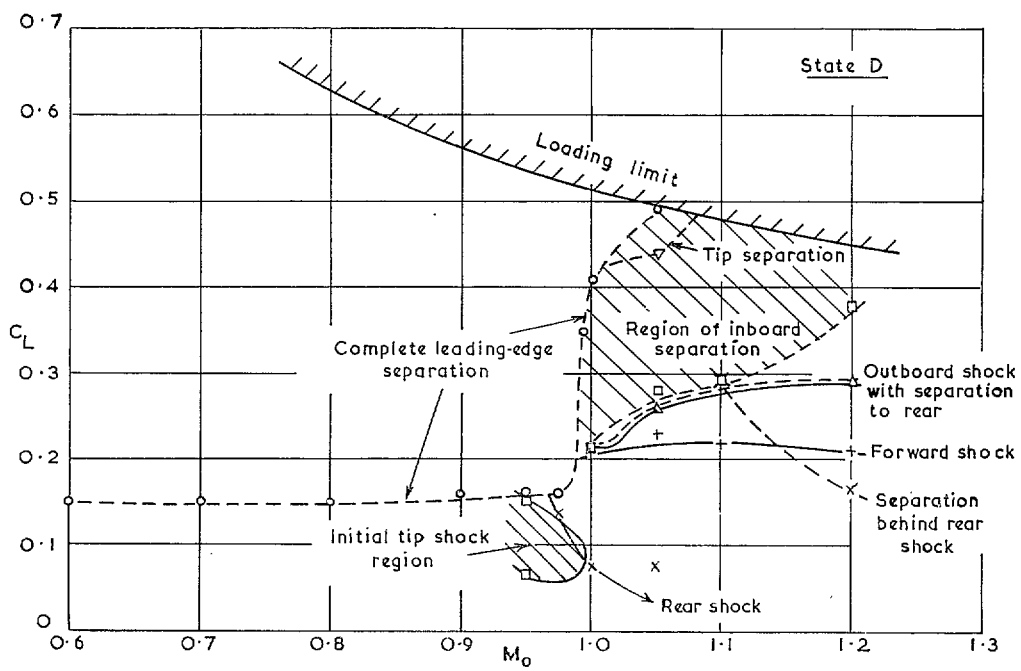

FIG. 6d. Flow characteristics of wing in state D.

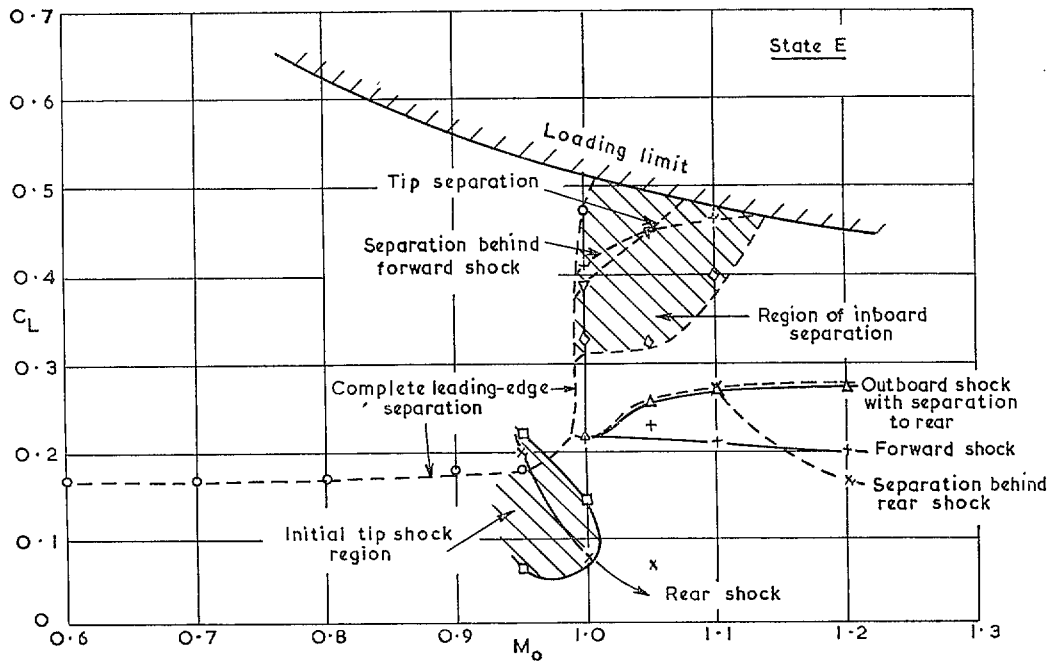

FIG. 6e. Flow characteristics of wing in state E.

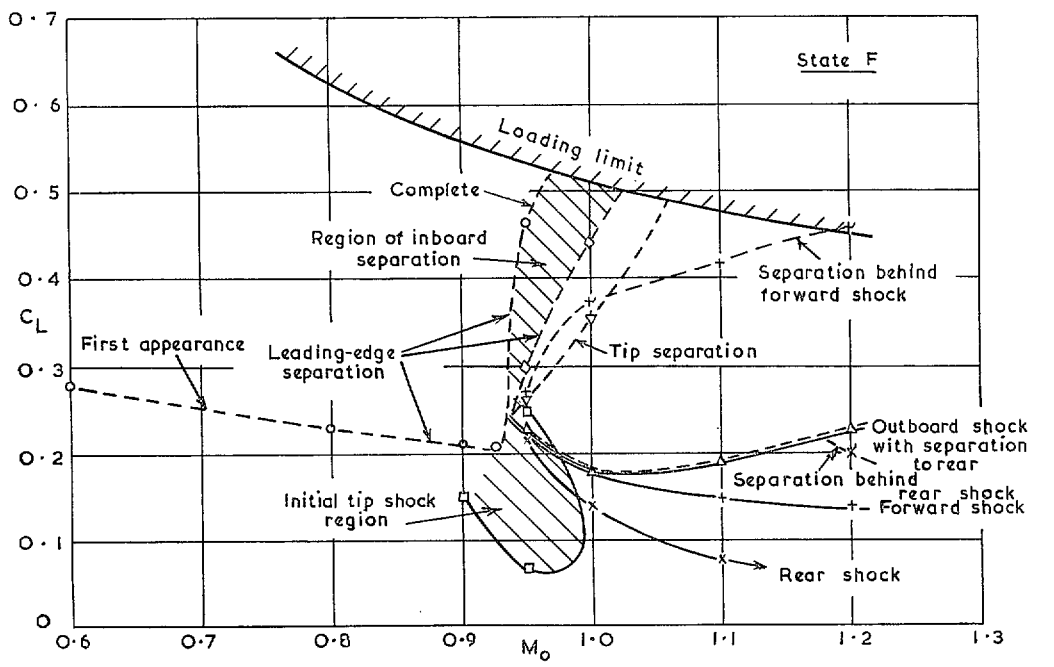

FIG. 6f. Flow characteristics of wing in state F.

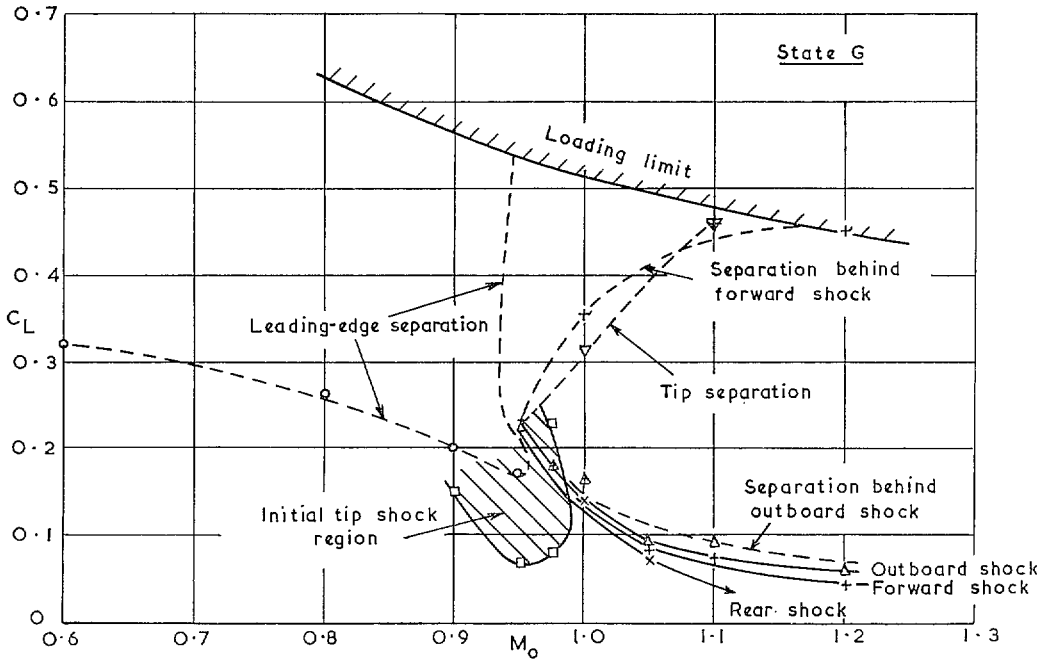

FIG. 6g. Flow characteristics of wing in state G.

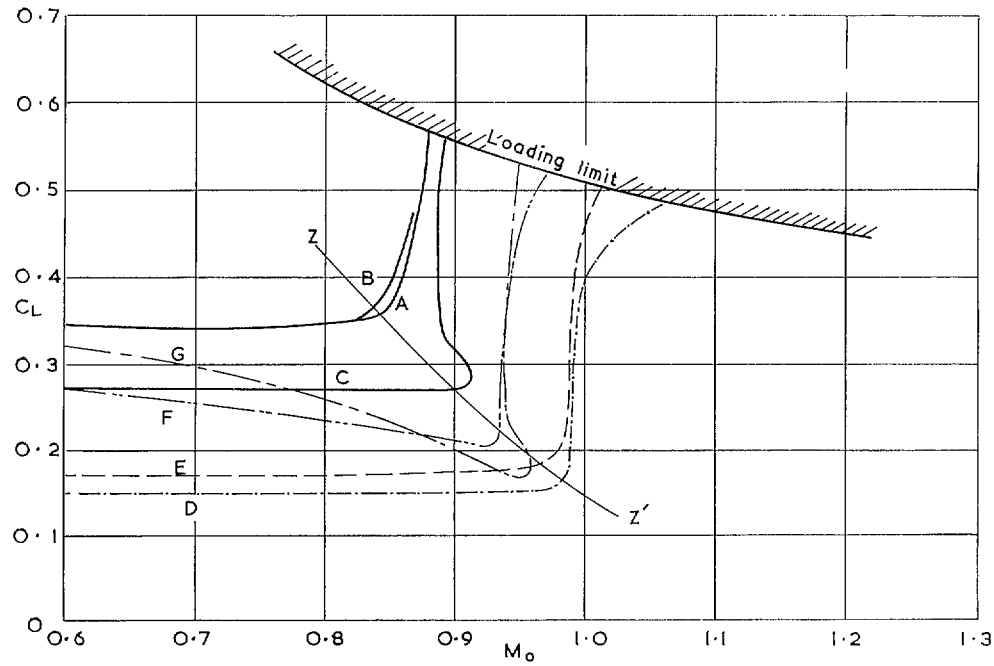

FIG. 7a. Summary of leading-edge separation boundaries for various model states.

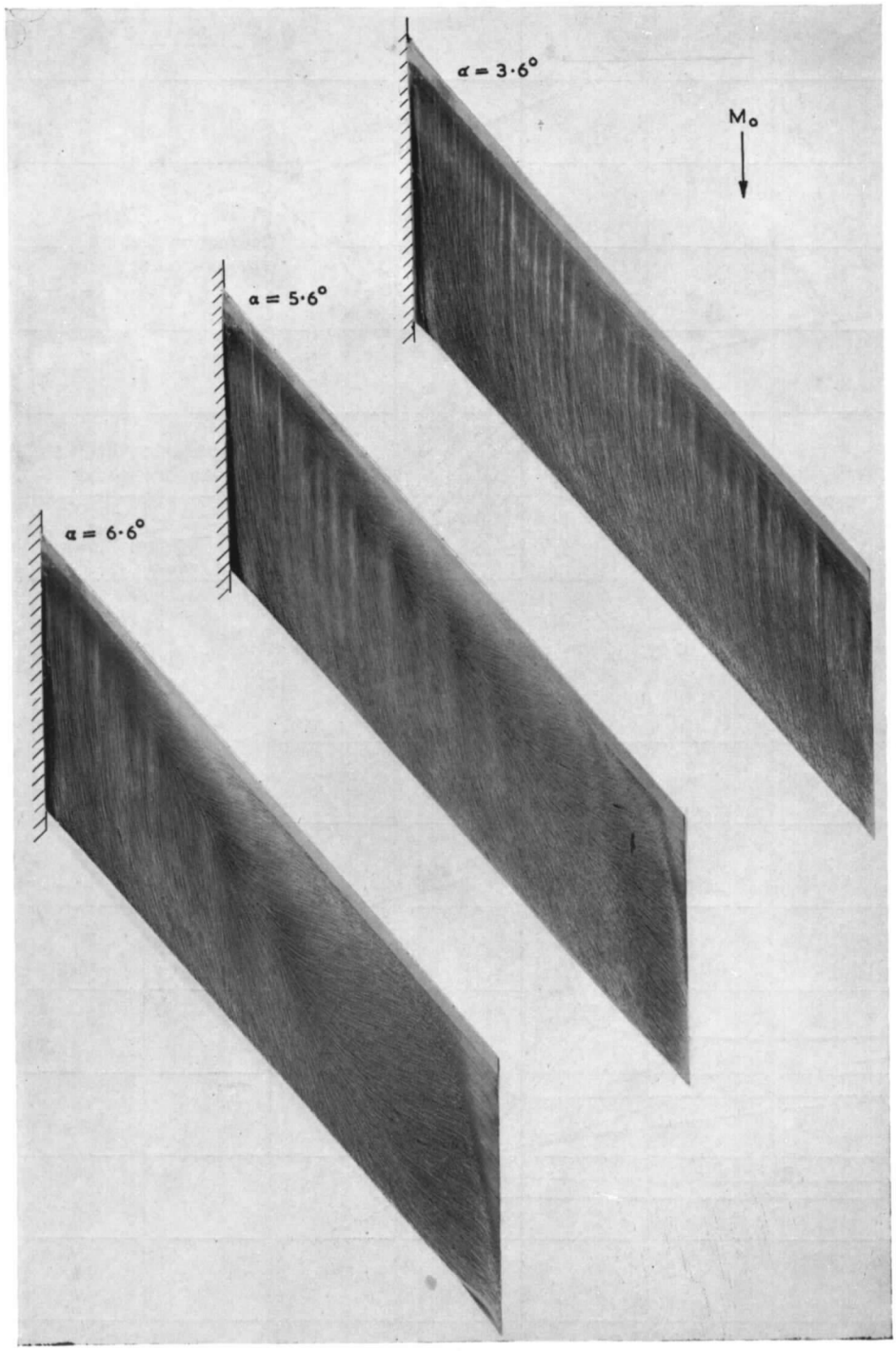

FIG. 7b. Development of leading-edge separation with incidence for sharp-edged wing (D) at $M_0 = 0{\cdot}80$.

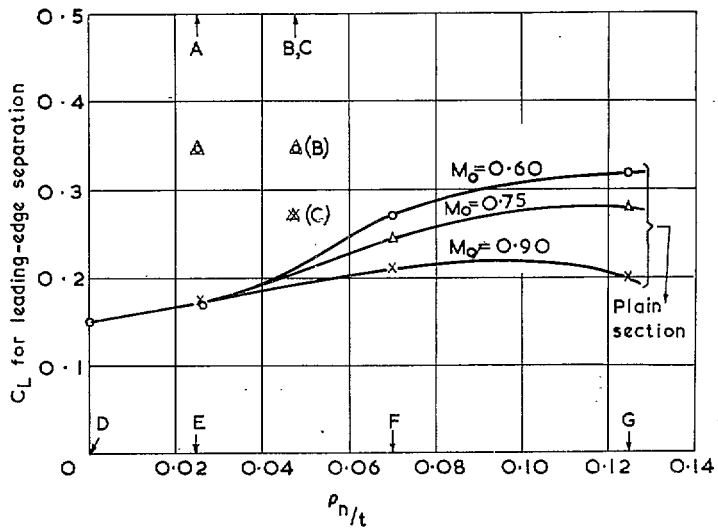

FIG. 8a. Variation of separation lift coefficient with leading-edge radius.

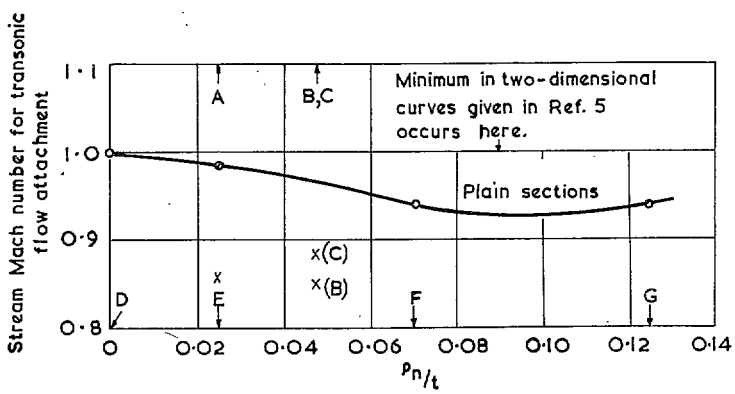

FIG. 8b. Possible variation of leading-edge attachment Mach number with leading-edge radius at $C_L = 0{\cdot}4$.

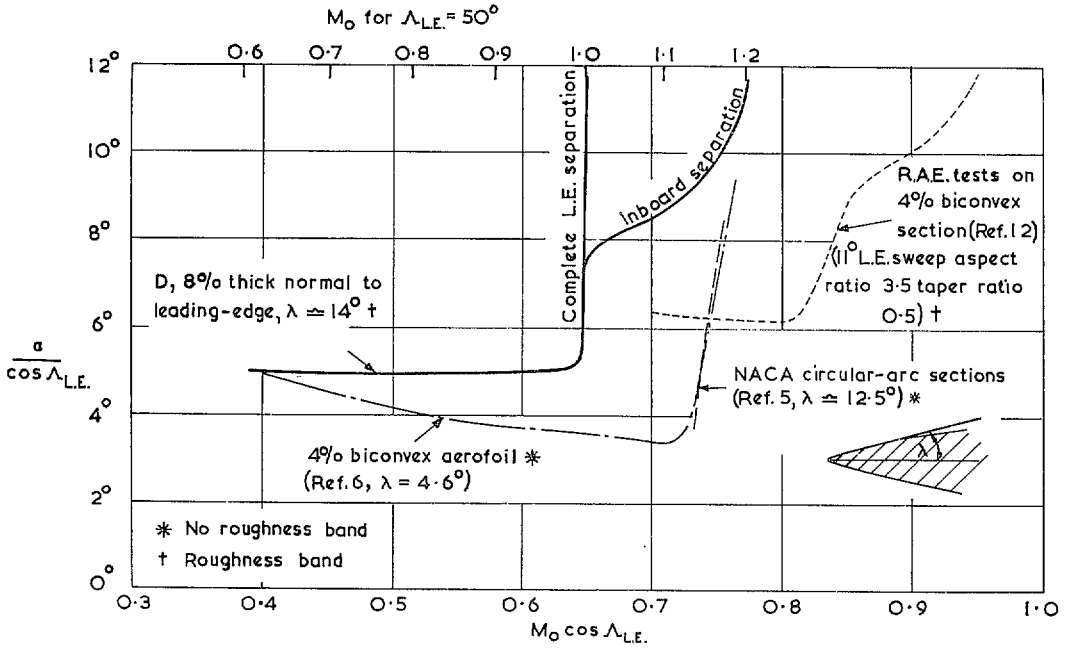

FIG. 9a. Separation boundaries for sharp-edged sections. Two-dimensional tests* on present basic profile indicated that transonic flow attachment occurred near $M_0 = 0{\cdot}7$ at incidences above 4 deg.

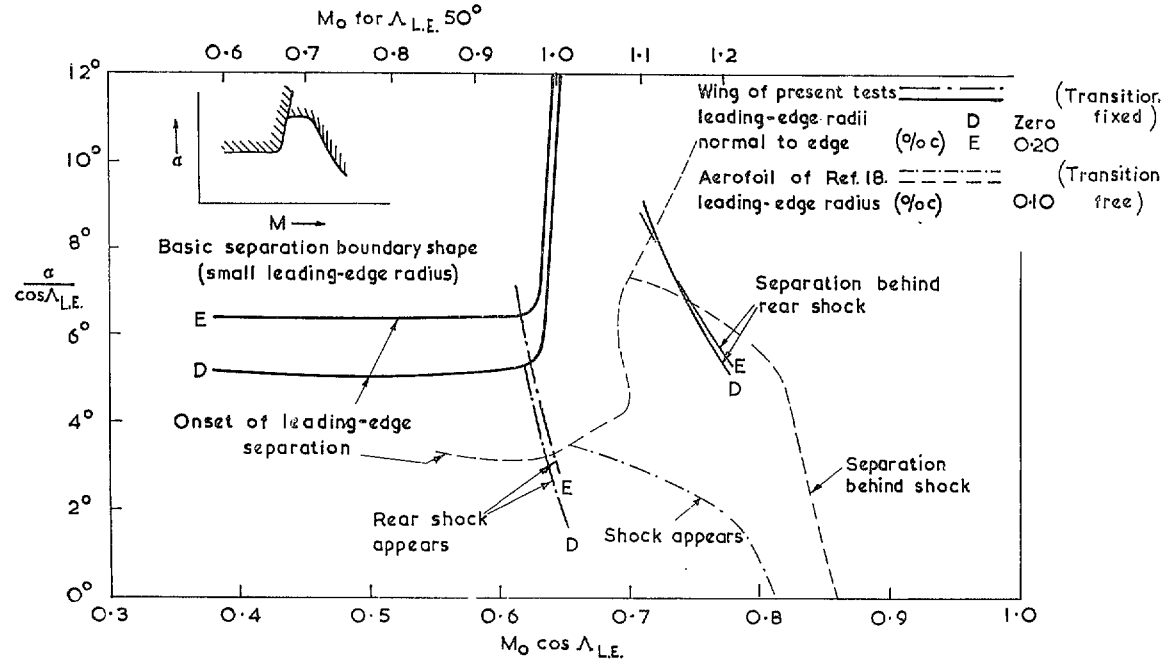

FIG. 9b. Comparison of three- and two-dimensional boundaries obtained from present tests and from aerofoil intermediate in profile between states D and E.

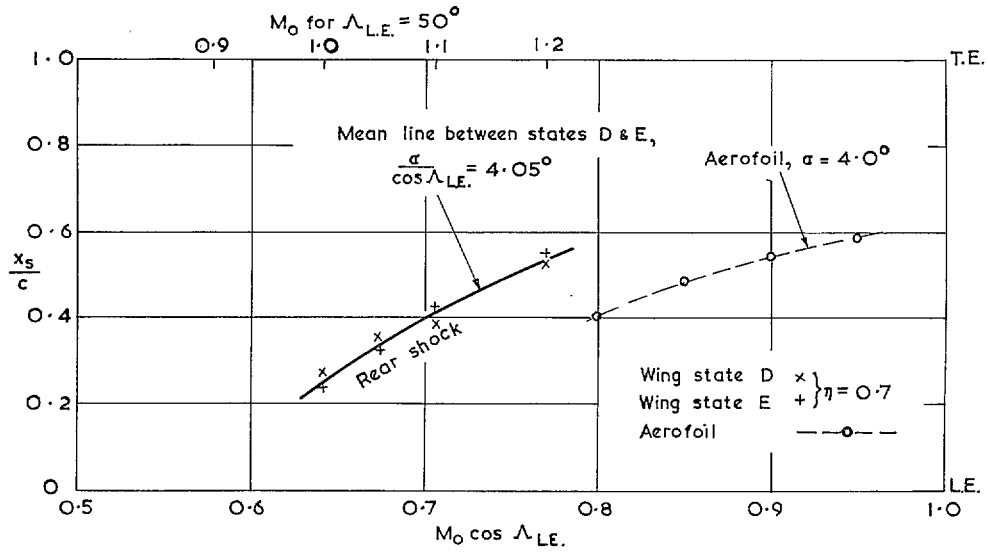

FIG. 9c. Comparison of shock position for wing in states D and E and related intermediate aerofoil.

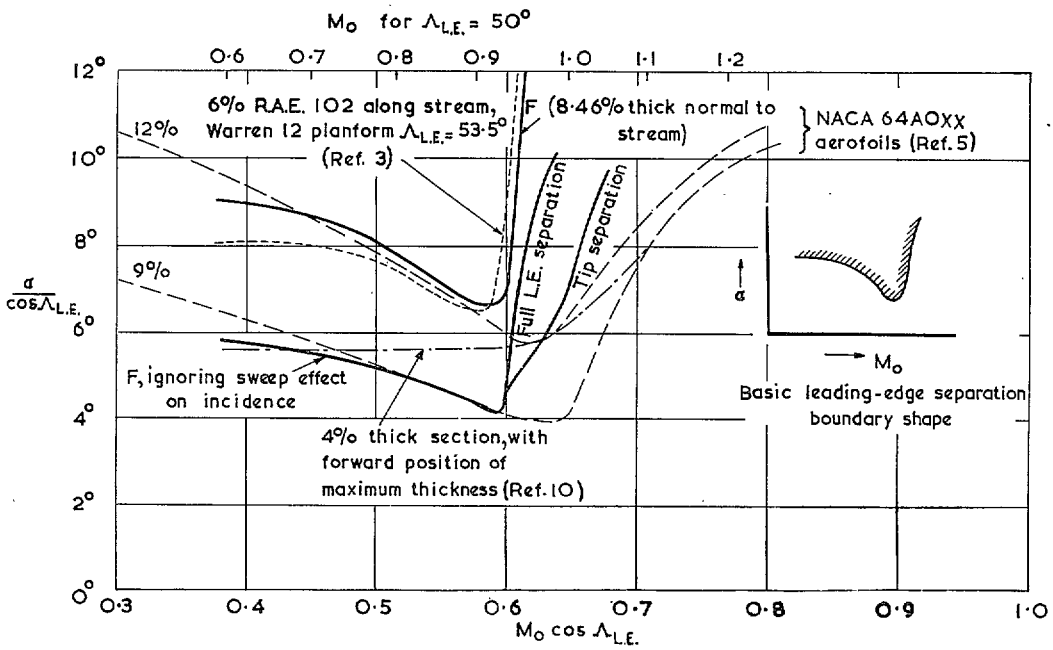

FIG. 9d. Separation boundaries for sections with moderately rounded leading edges.

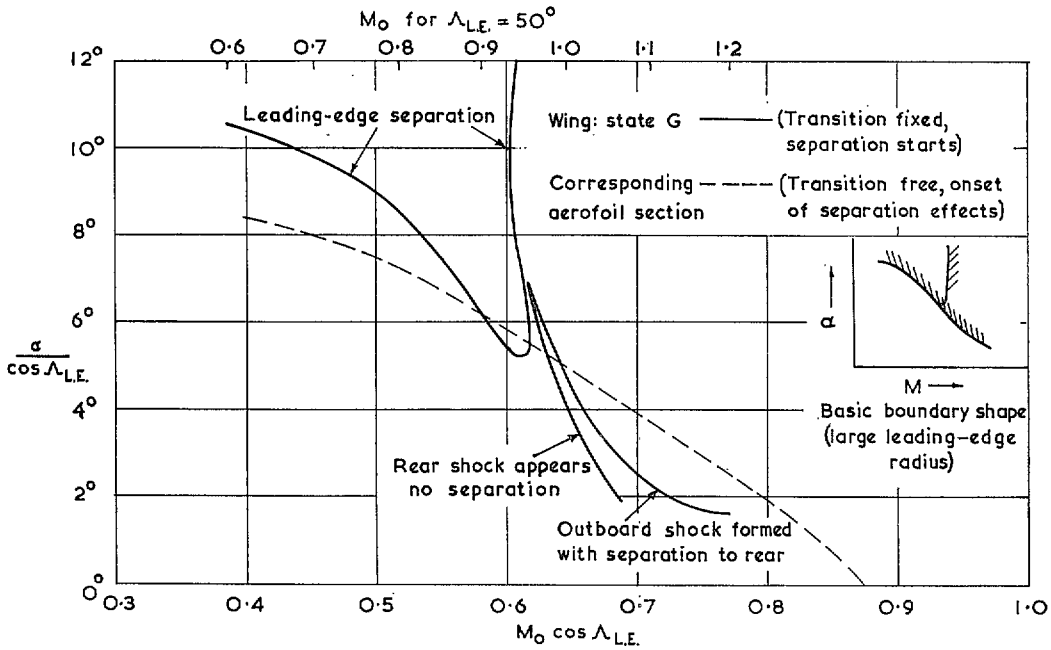

FIG. 9e. Comparison of flow boundaries for wing in state G and corresponding aerofoil section.

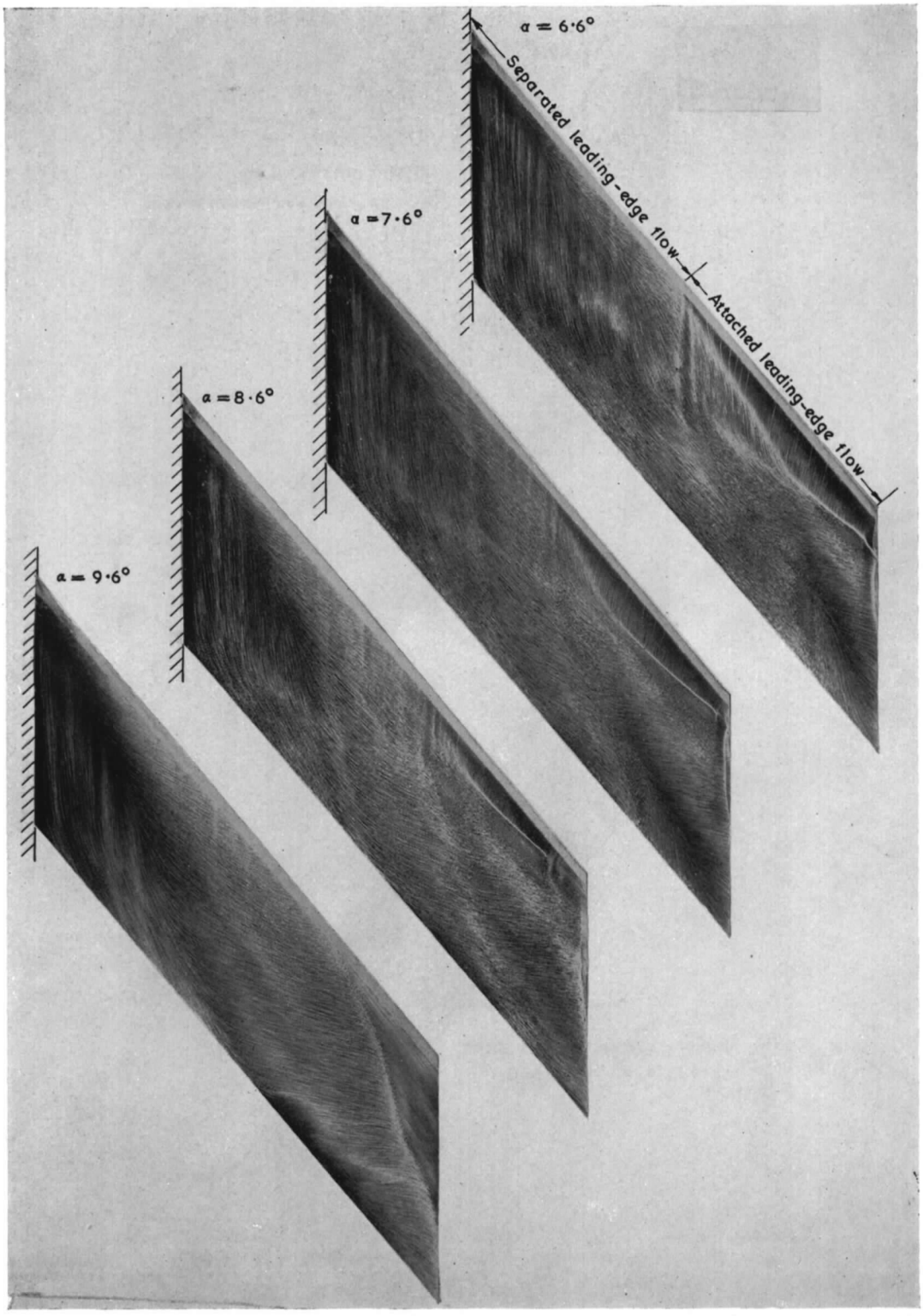

FIG. 10. Flow breakdown for state D at $M_0 = 1 \cdot 05$, showing region of outboard attached flow.

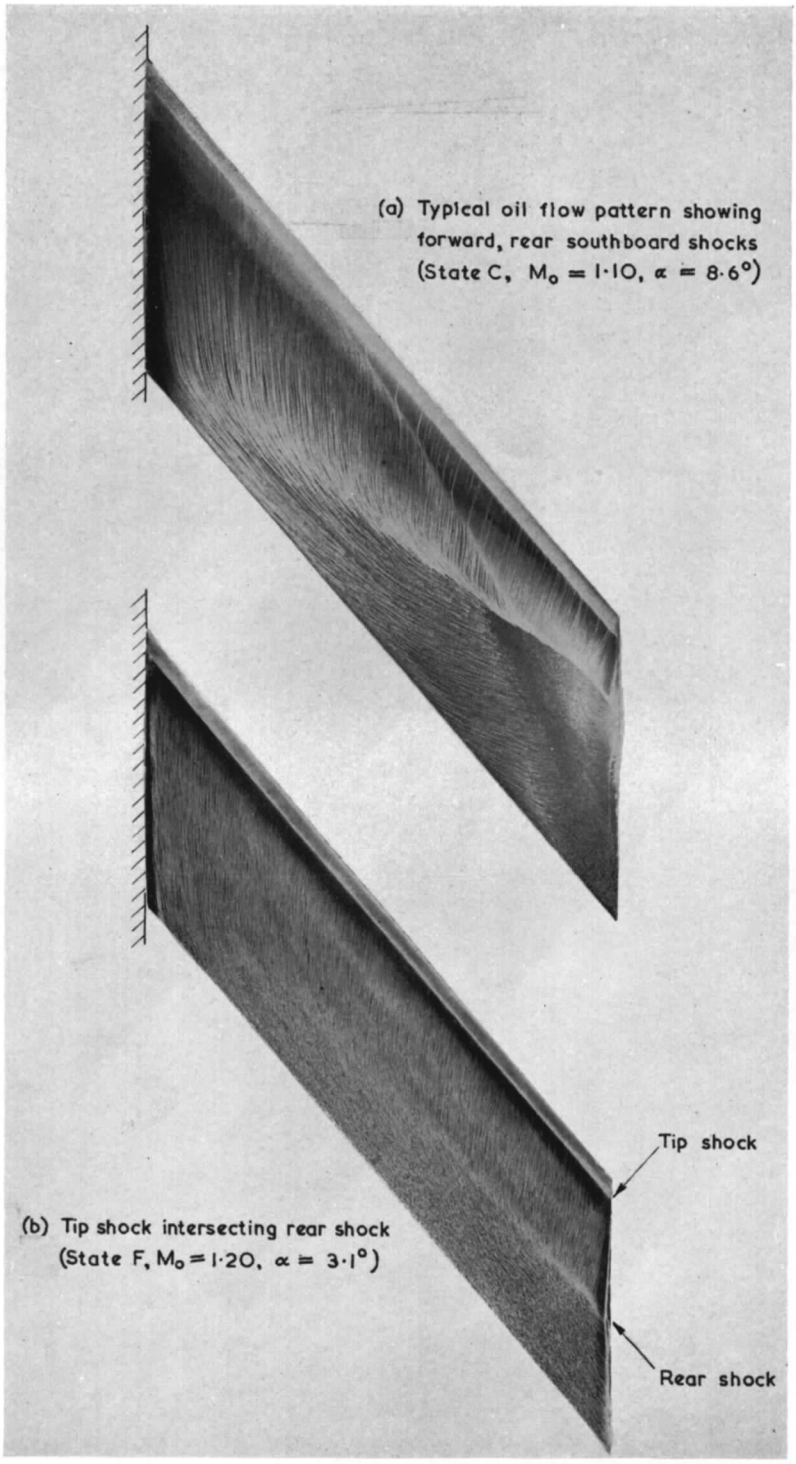

FIGS. 11a and b.

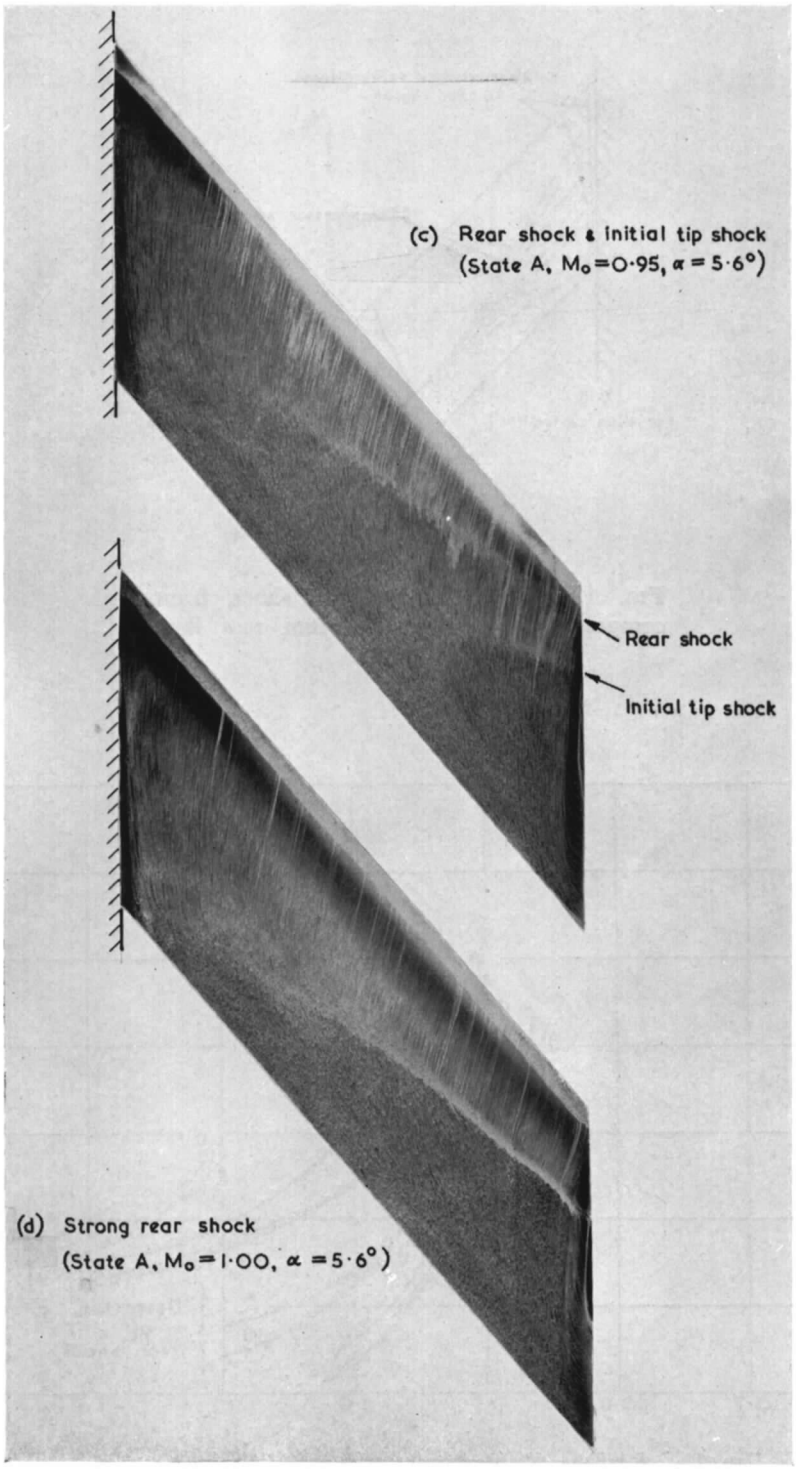

FIGS. 11c and d.

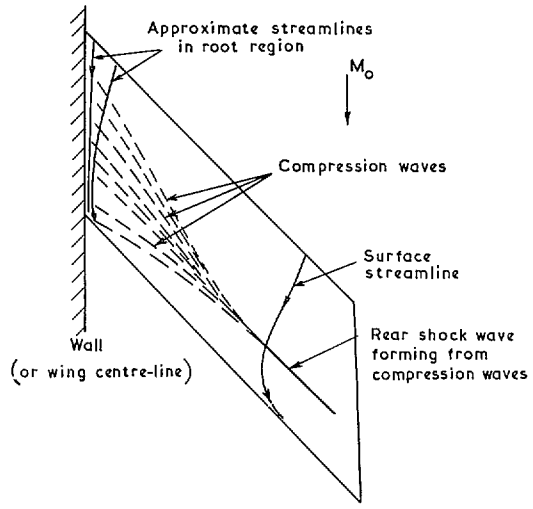

FIG. 12. Formation of rear shock from compression waves arising from root flow conditions.

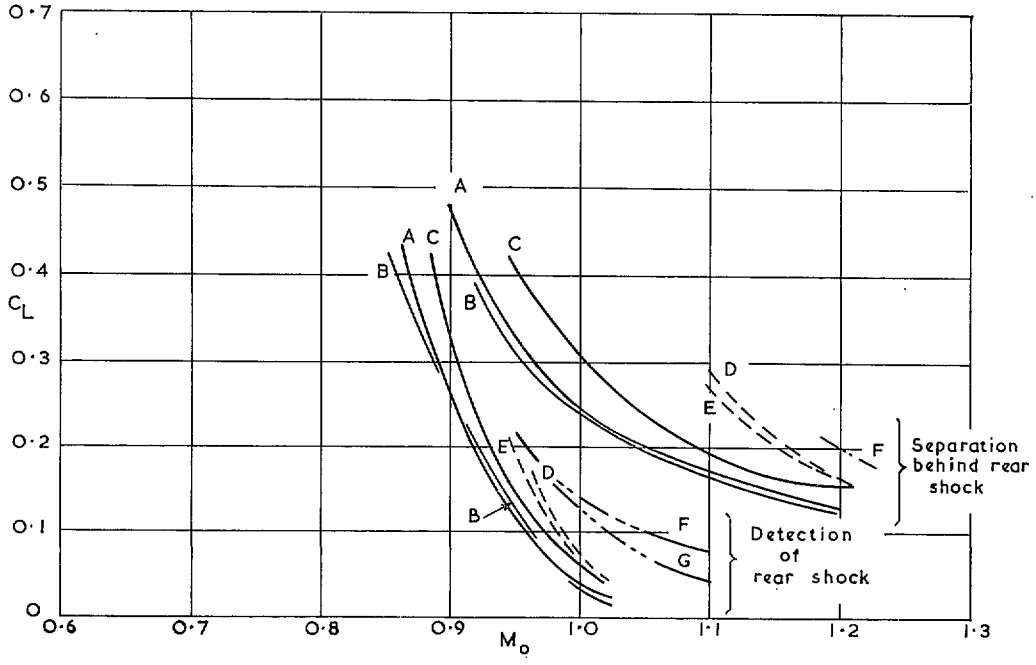

FIG. 13. Rear shock characteristics deduced from oil patterns.

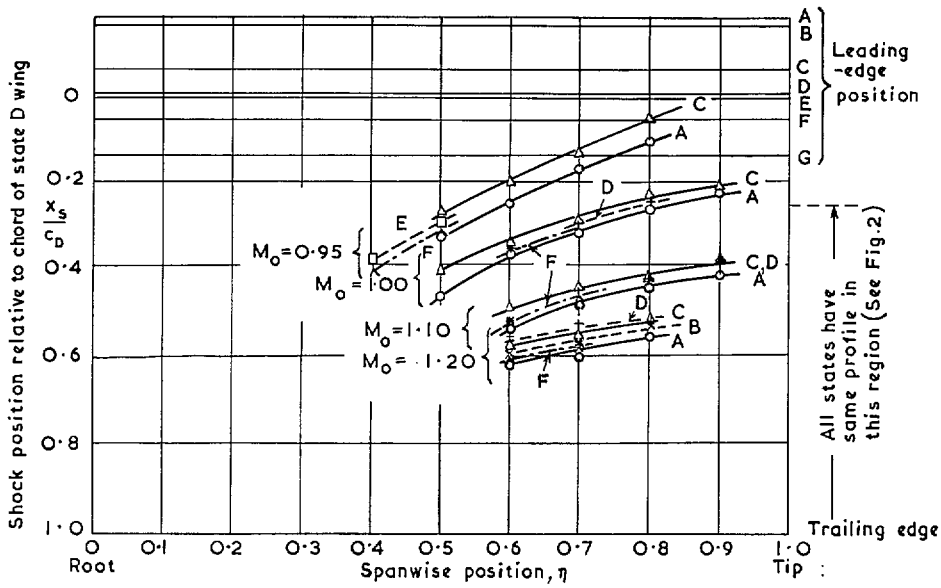

FIG. 14. Rear shock position at $\alpha = 5{\cdot}6$ deg for various free-stream Mach numbers.

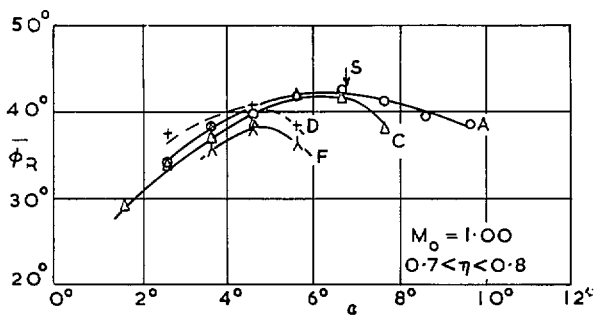

(a) Effect of model state on mean sweep of rear shock.

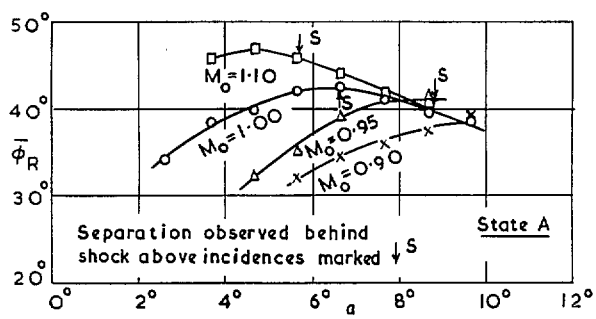

(b) Effect of stream Mach number on mean sweep of rear shock.

FIG. 15. Mean sweep of rear shock.

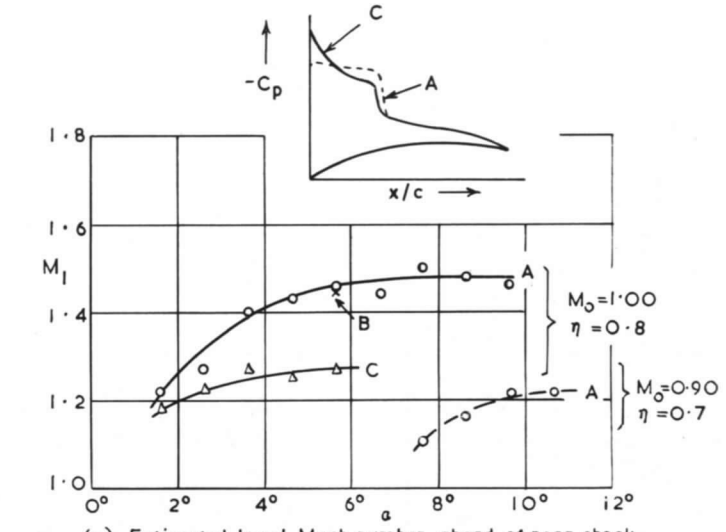

(a) Estimated local Mach number ahead of rear shock

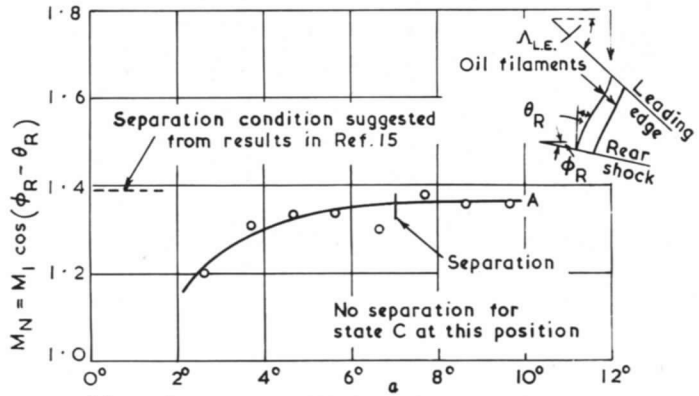

(b) Estimated local Mach number normal to rear shock

FIG. 16. Flow ahead of rear shock for wing states with droop.

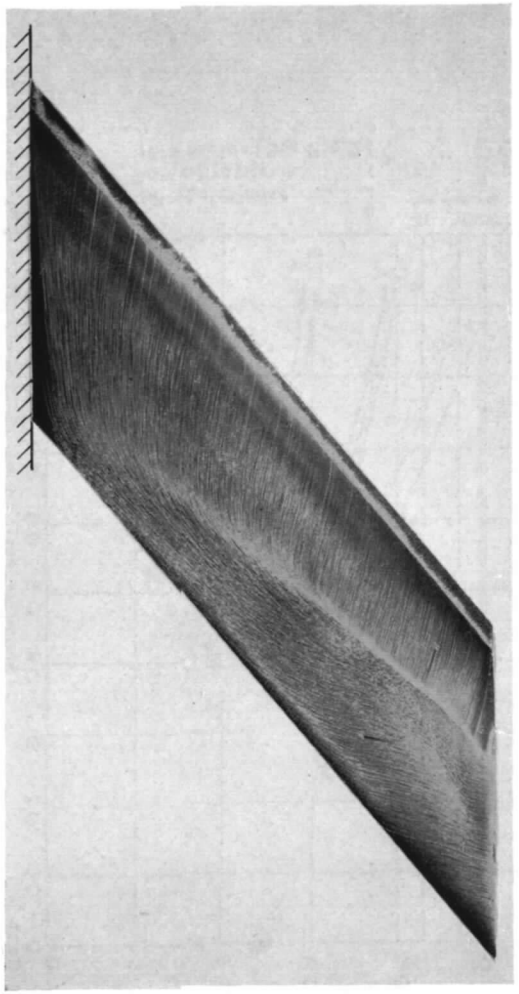

FIG. 17. Rear shock with separation outboard of about $\eta = 0{\cdot}6$, showing boundary-layer drift in trailing-edge region. (State B, $M_0 = 1{\cdot}10$, $\alpha = 8{\cdot}6$ deg).

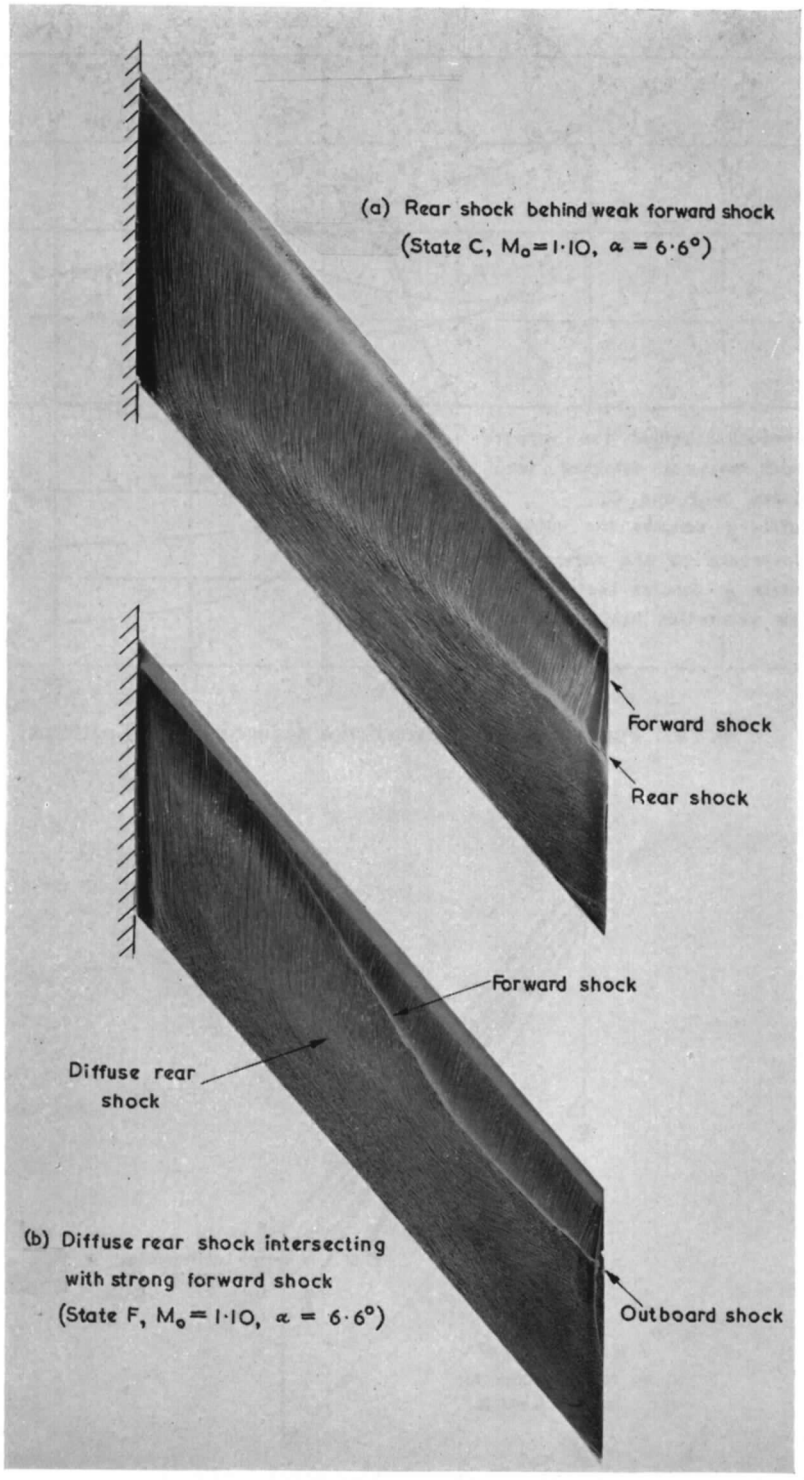

FIGS. 18a and b.

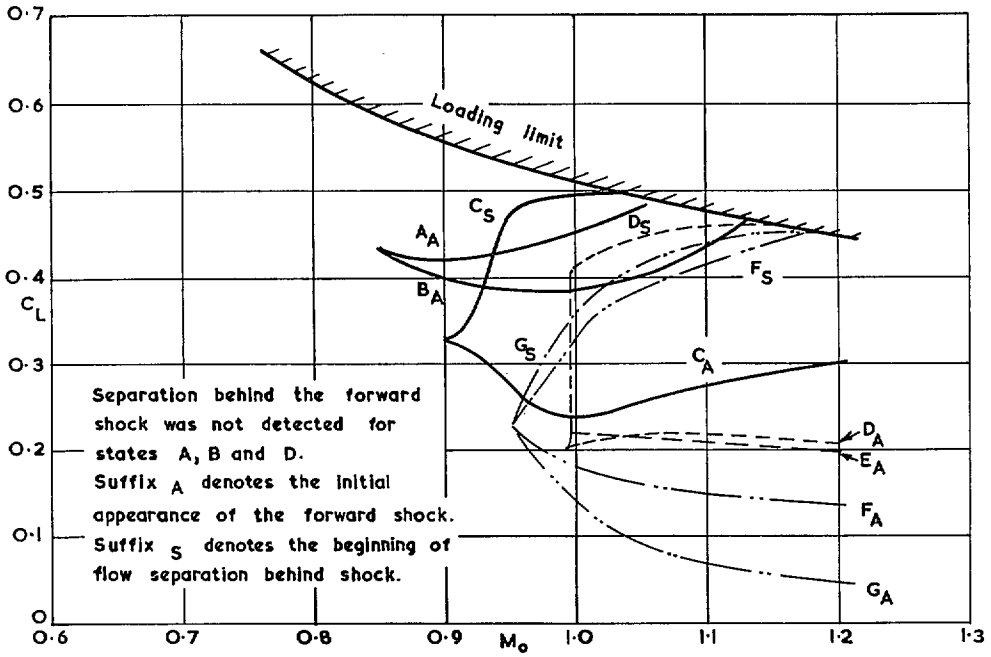

FIG. 19. Forward shock characteristics deduced from oil patterns.

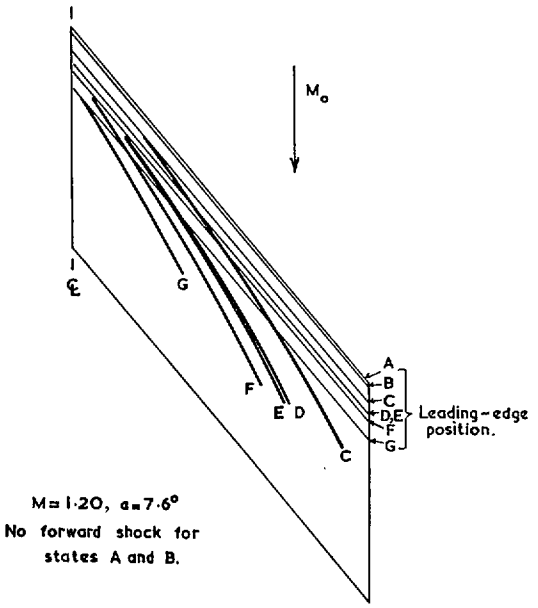

FIG. 20. Typical forward shock positions.

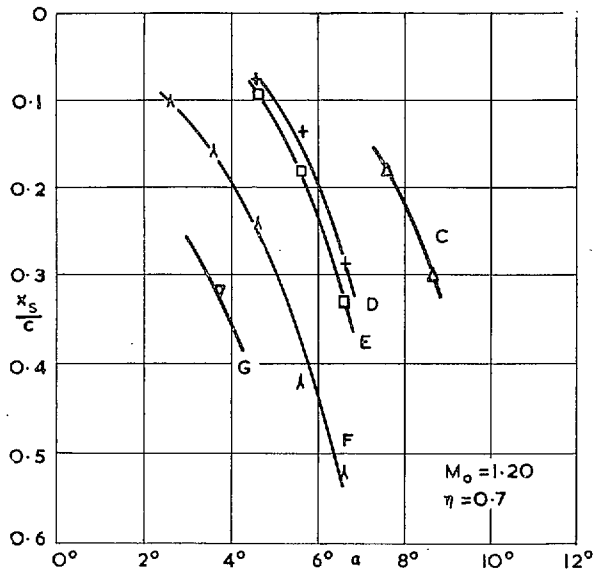

FIG. 21a. Effect of model state on forward shock position.

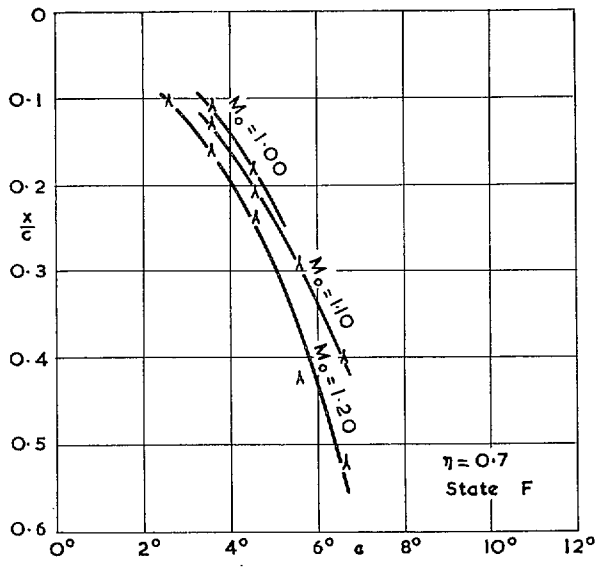

FIG. 21b. Effect of stream Mach number on forward shock position.

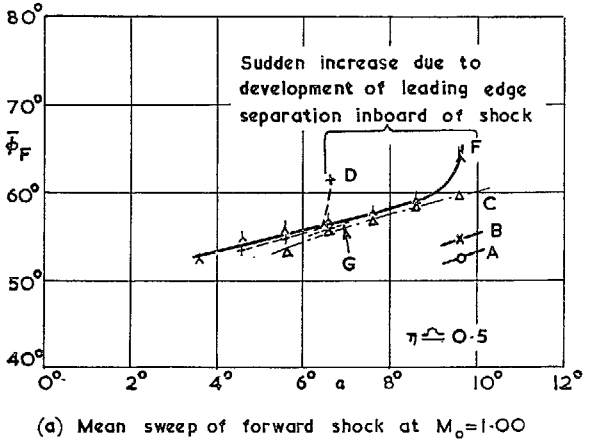

FIG. 22a. Mean sweep of forward shock at $M_0 = 1{\cdot}00$.

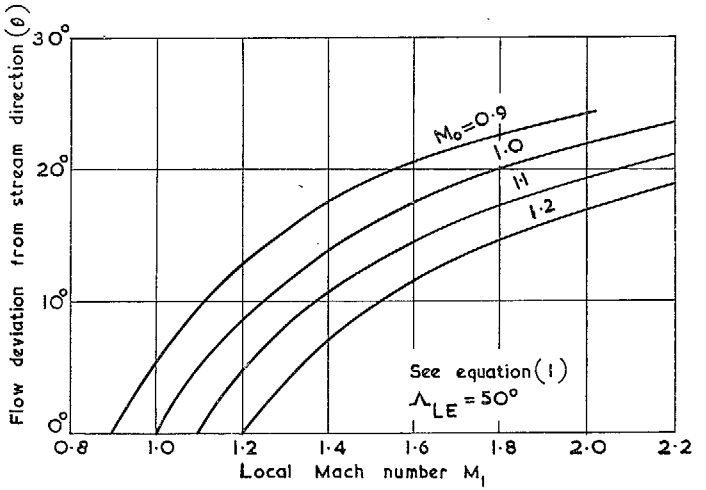

FIG. 23. Variation of flow deflection angle with local Mach number.

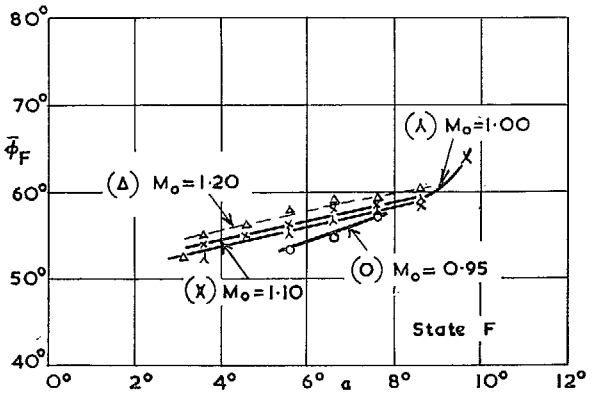

FIG. 22b. Effect of stream Mach number on mean sweep of forward shock.

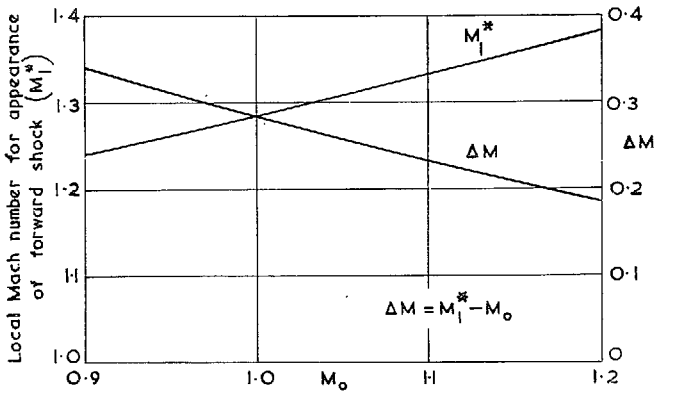

FIG. 24. Theoretical estimate of first appearance of weak forward shock.

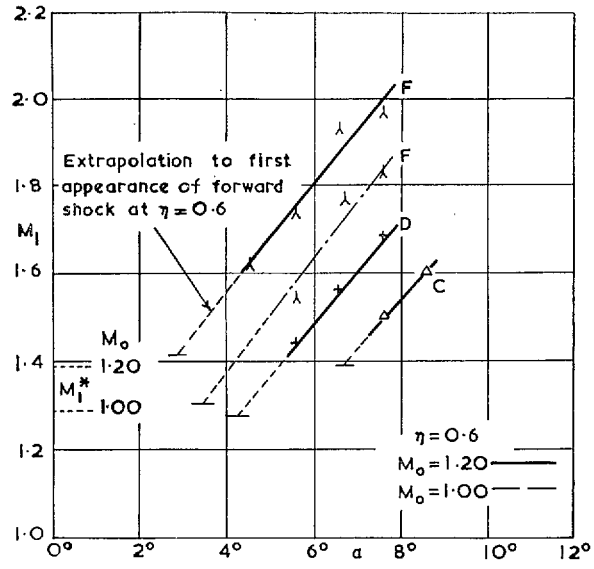

FIG. 25. Effect of leading-edge changes on local Mach number ahead of forward shock.

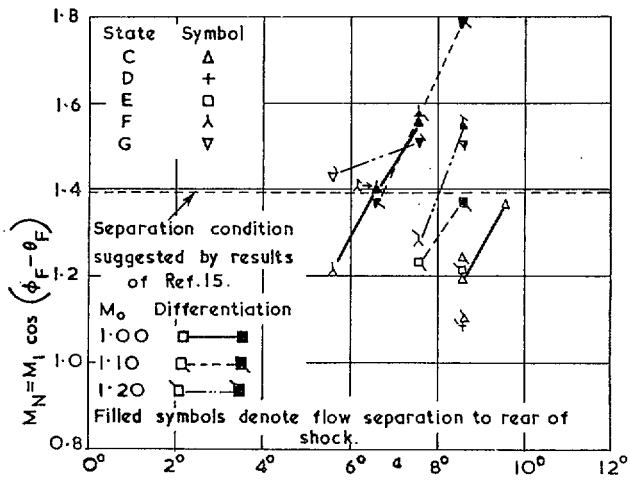

FIG. 26. Assessment of conditions for flow separation to rear of forward shock. (Results for $0·4 \leqslant \eta \leqslant 0·6$).

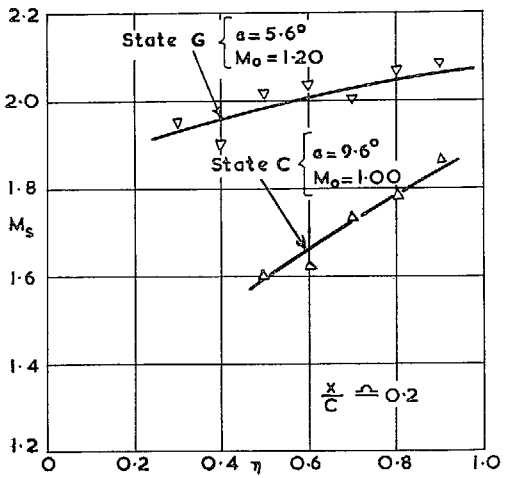

FIG. 27. Typical spanwise variation in local Mach number in region ahead of forward and outboard shocks.

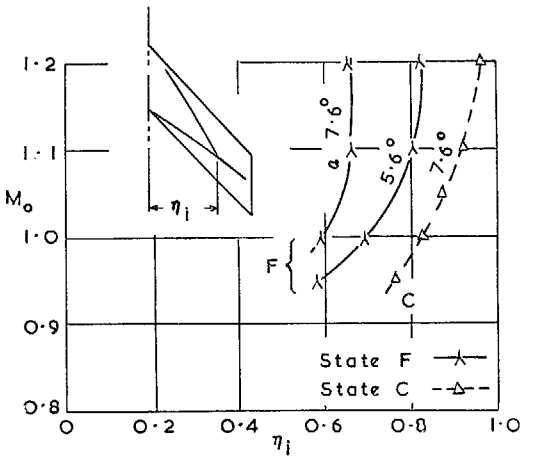

FIG. 28a. Effect of stream Mach number on inboard limit of outboard shock.

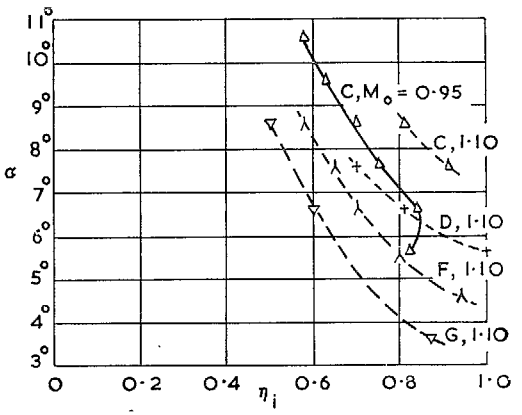

FIG. 28b. Effect of incidence and model state on inboard limit of outboard shock.

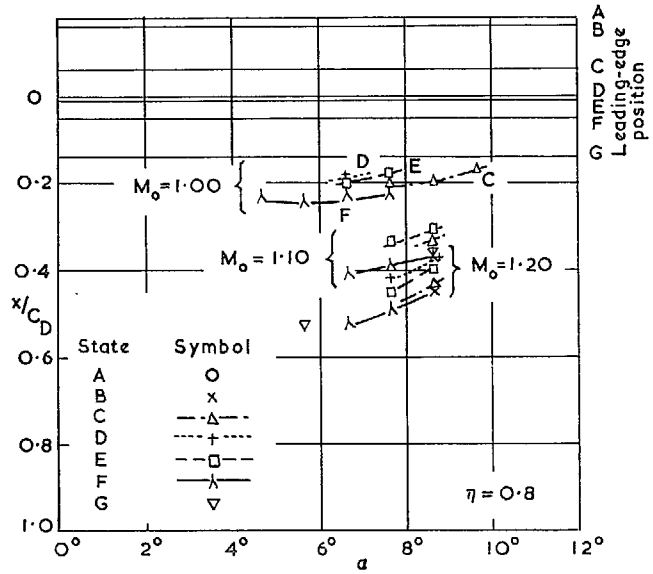

FIG. 29a. Outboard shock position, in terms of unmodified section of profile.

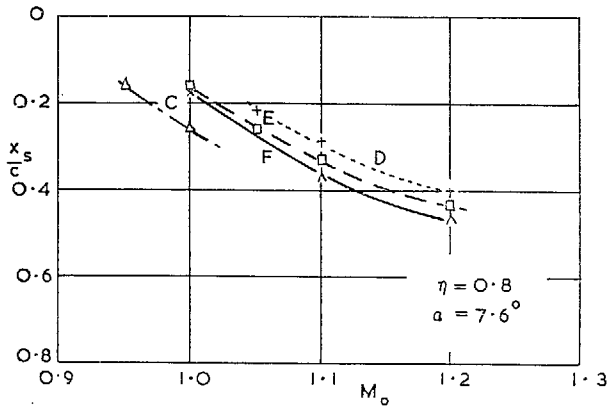

FIG. 29b. Variation in outboard shock position with Mach number.

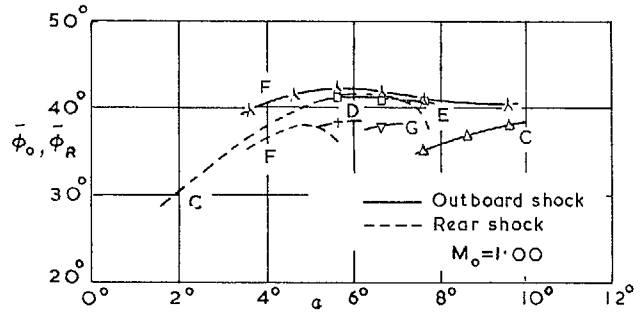

FIG. 30a. Effect of model state on mean sweep of outboard shock.

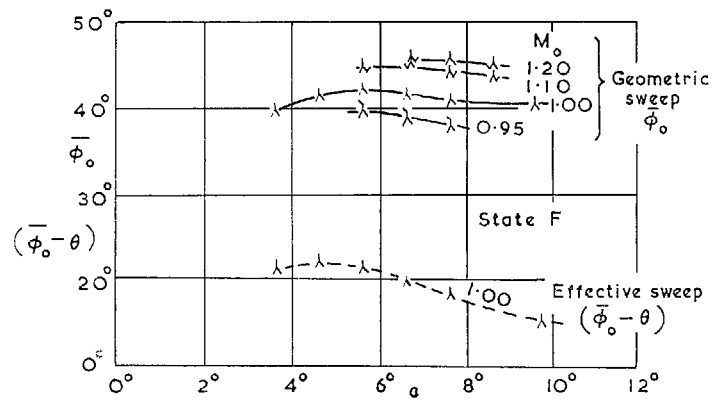

FIG. 30b. Effect of wing incidence on geometric and effective sweep of outboard shock.

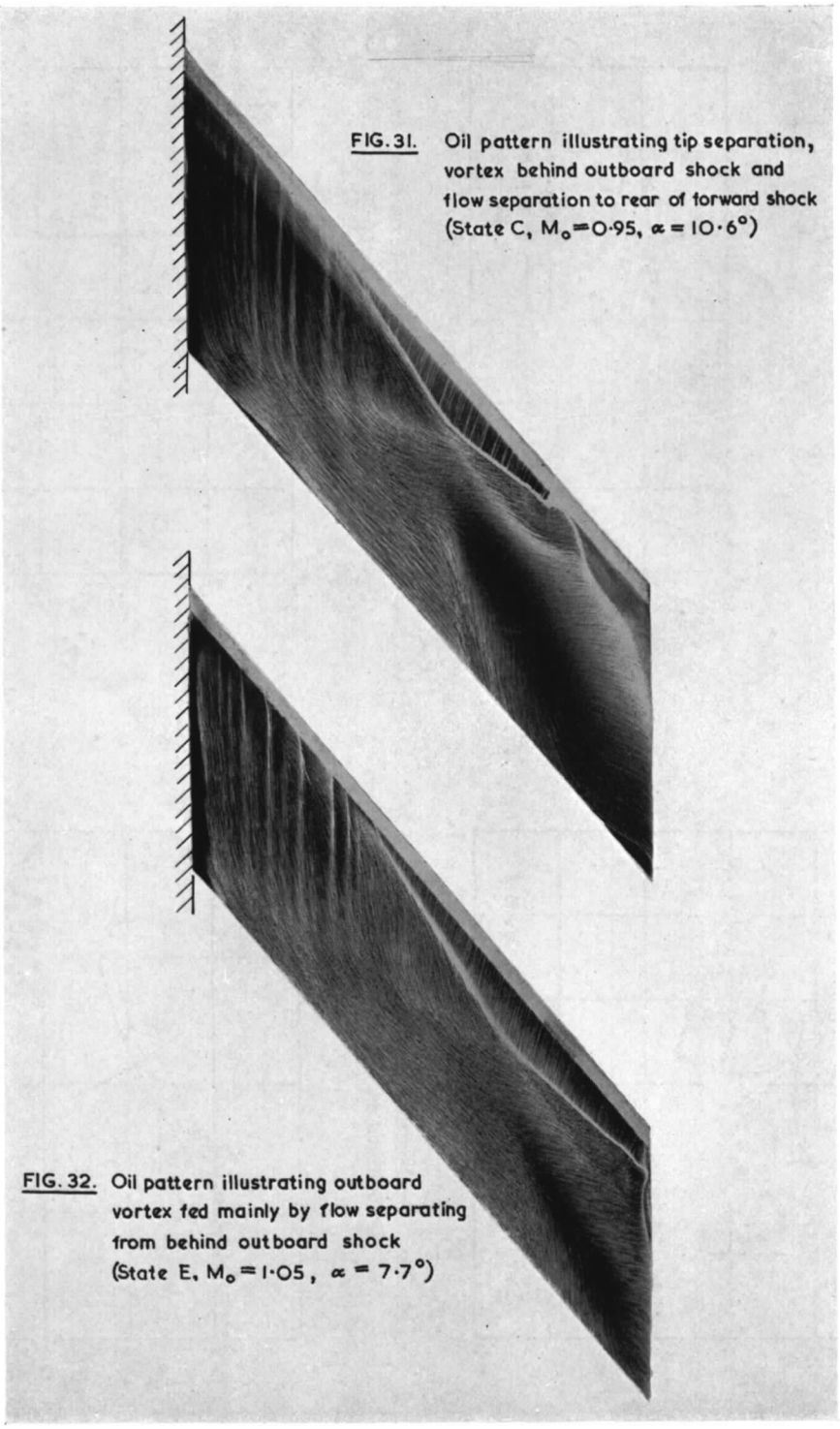

FIG. 31. Oil pattern illustrating tip separation, vortex behind outboard shock and flow separation to rear of forward shock (State C, $M_o = 0{\cdot}95$, $\alpha = 10{\cdot}6°$)

FIG. 32. Oil pattern illustrating outboard vortex fed mainly by flow separating from behind outboard shock (State E, $M_o = 1{\cdot}05$, $\alpha = 7{\cdot}7°$)

FIGS. 31 and 32.

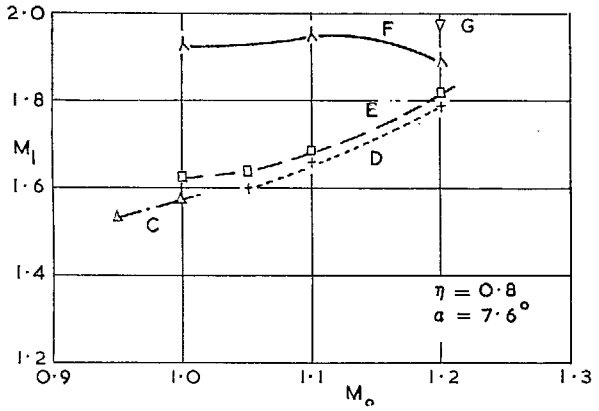

FIG. 33. Effect of model state on local Mach number ahead of the outboard shock.

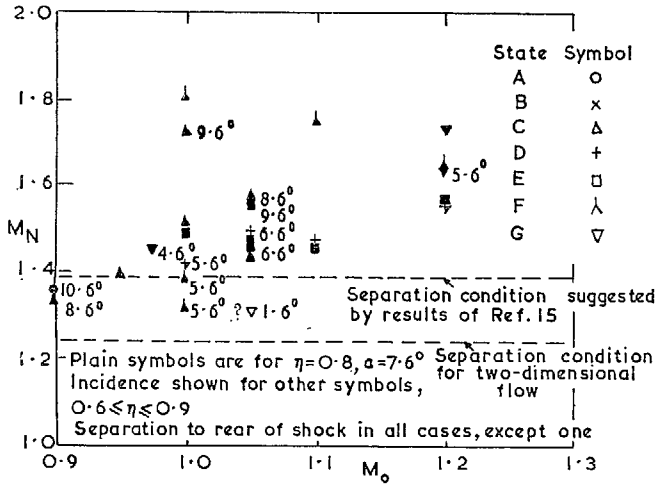

FIG. 34. Mach number component normal to the outboard shock.

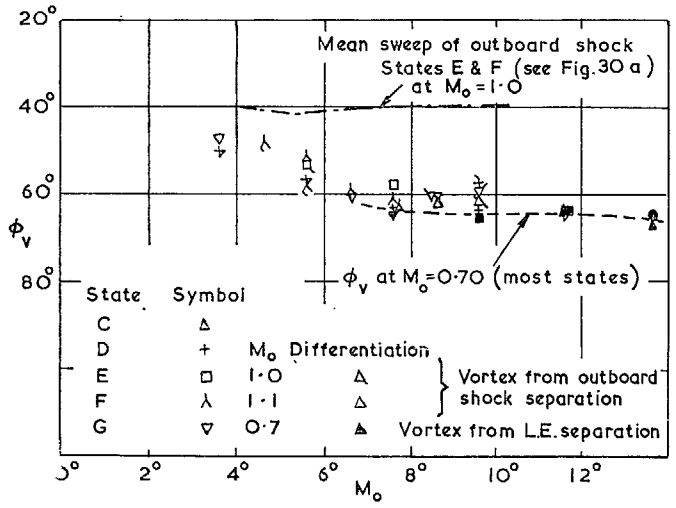

FIG. 35. Comparison of vortex sweep at subsonic and transonic speeds.

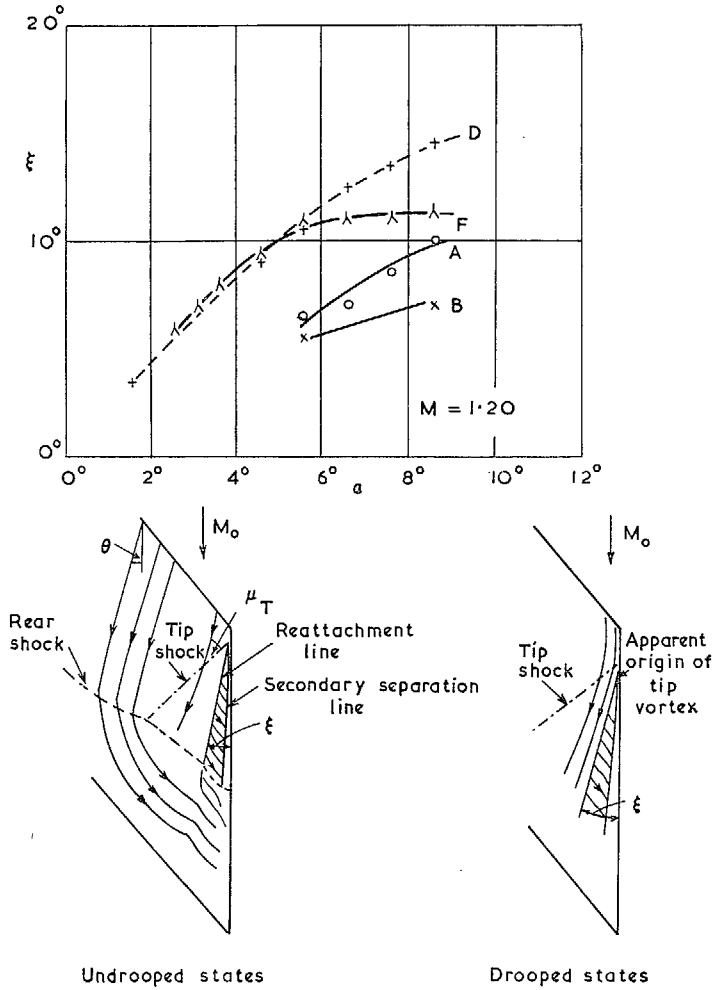

FIG. 36. Tip shock and vortex characteristics.

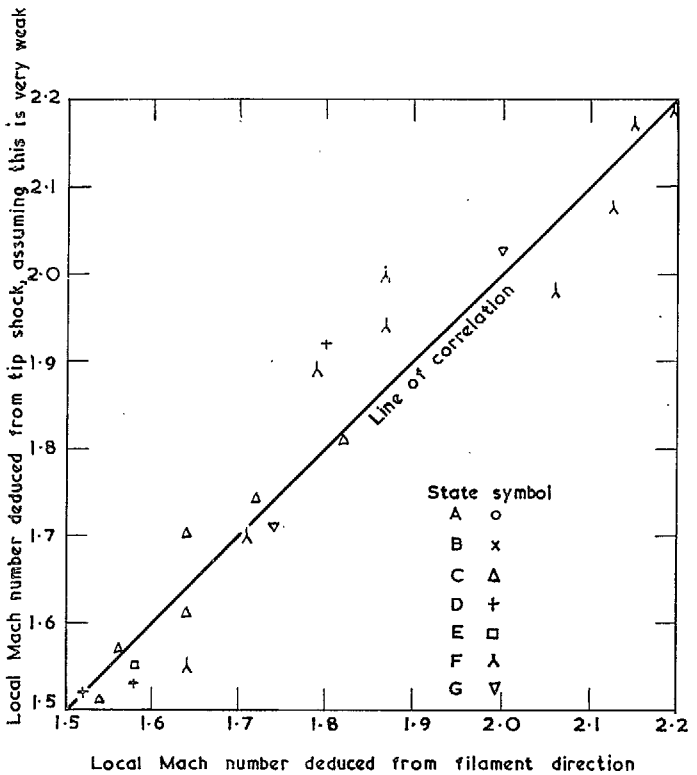

FIG. 37. Comparison of two methods of deducing local Mach number from oil-flow patterns.

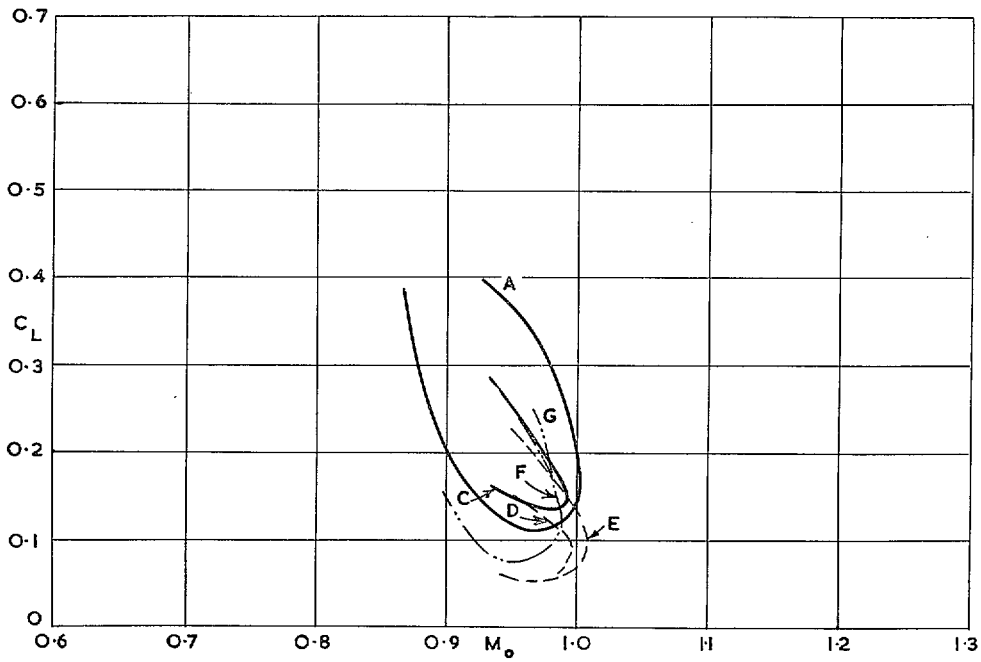

FIG. 38. Boundaries for existence of initial tip shock.

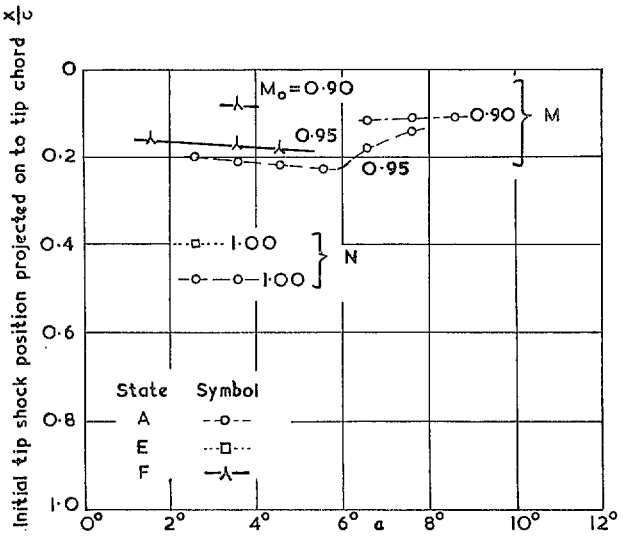

FIG. 39 Effect of Mach number and incidence on initial tip-shock position.

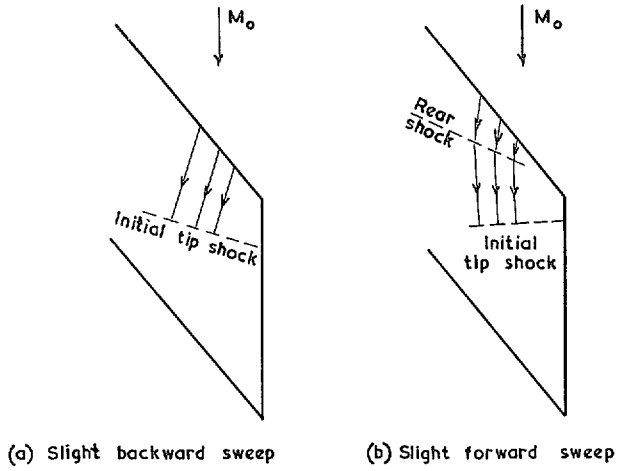

FIG. 40. Effect of upstream flow direction on sweep of initial tip shock.

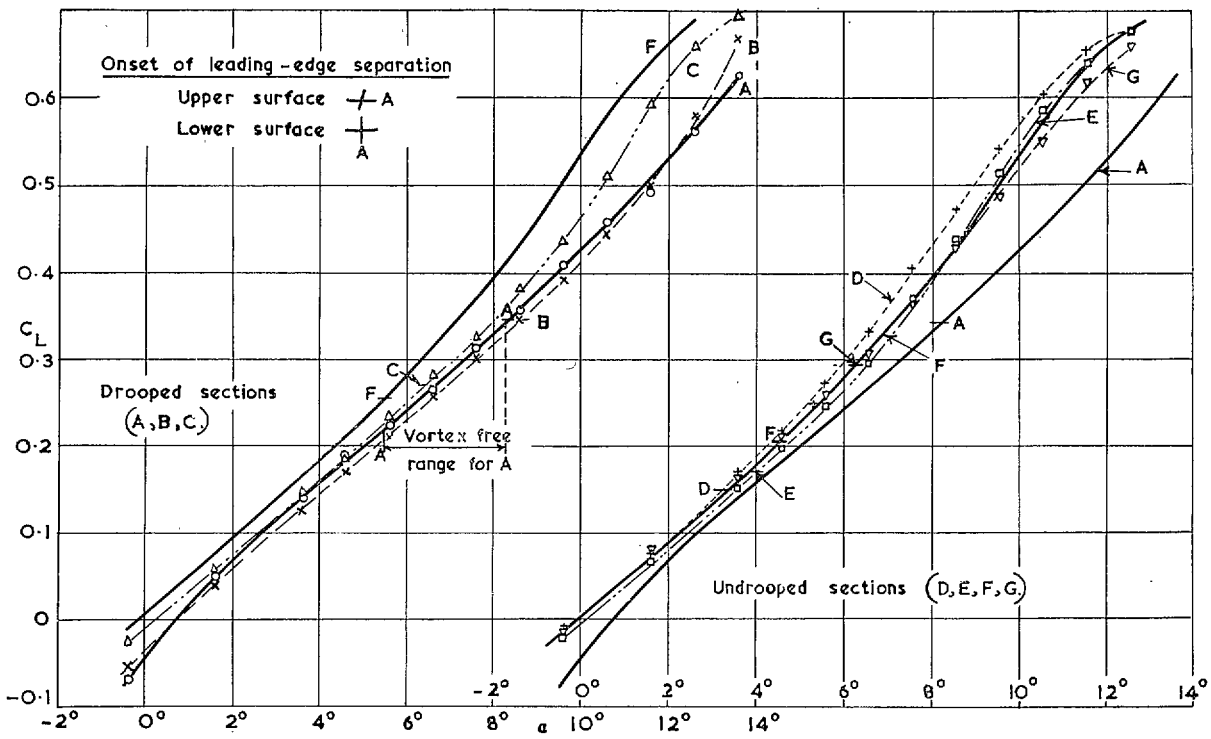

FIG. 41a. Comparison of lift curves at $M_0 = 0{\cdot}70$.

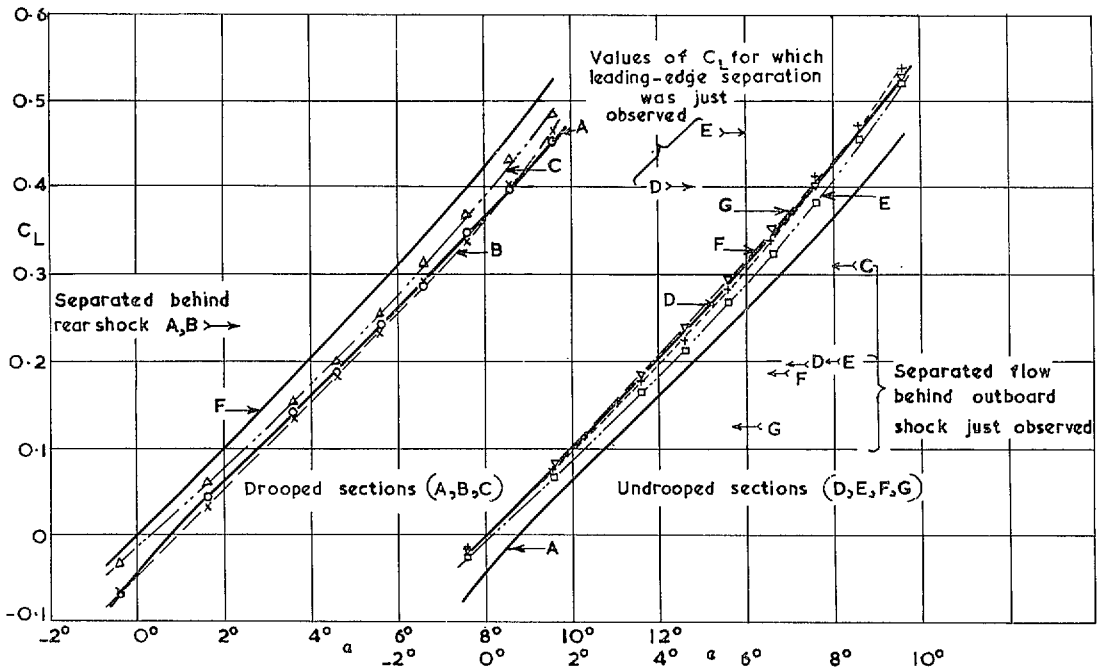

FIG. 41b. Comparison of lift curves at $M_0 = 1{\cdot}00$.

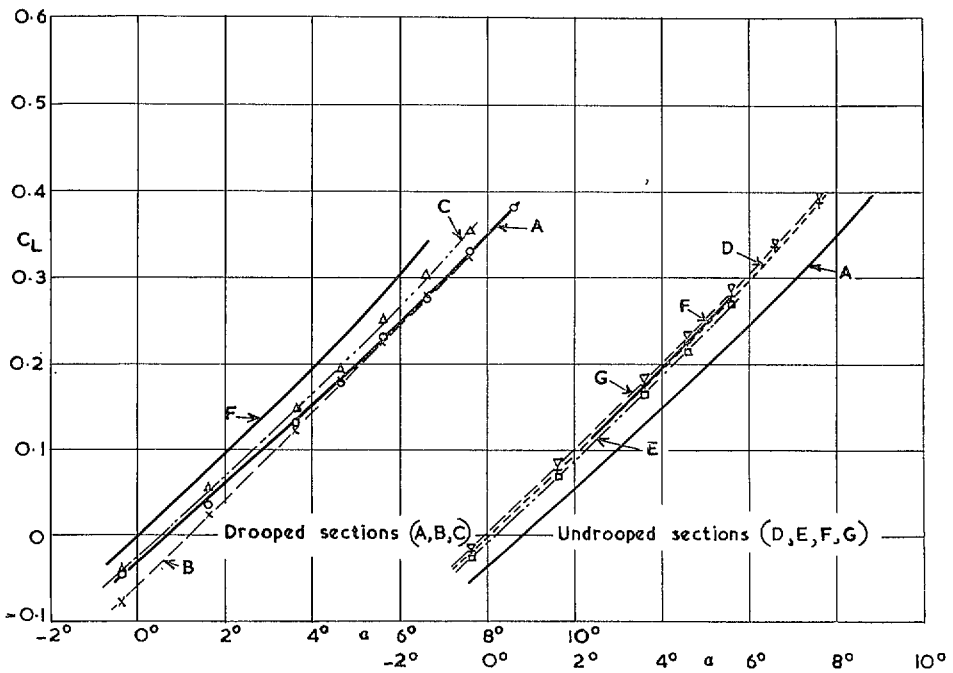

FIG. 41c. Comparison of lift curves at $M_0 = 1{\cdot}20$.

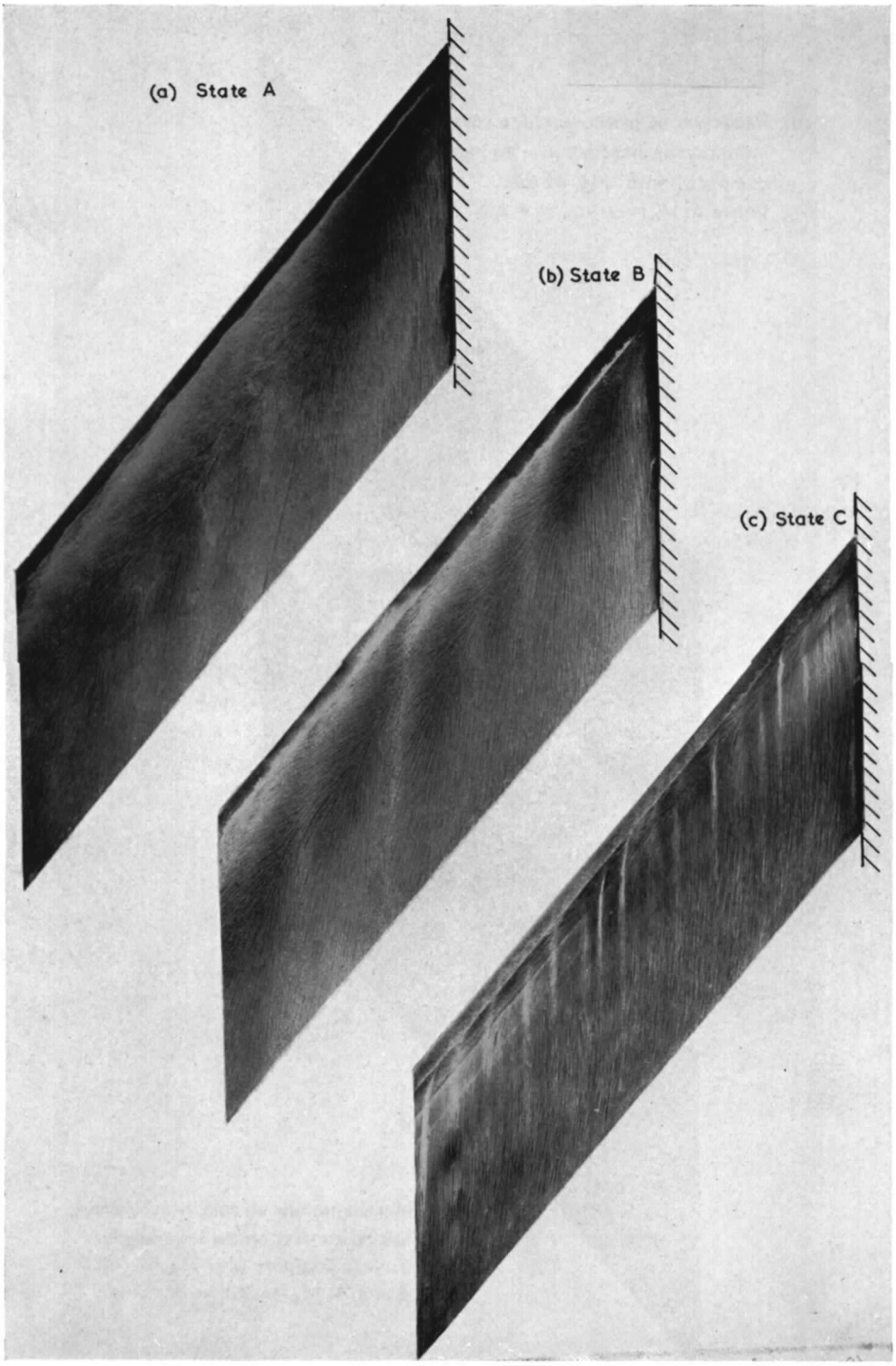

FIG. 42a to c. Effect of nose droop on lower-surface vortex ($M_0 = 0{\cdot}8$, $\alpha = -0{\cdot}4$ deg).

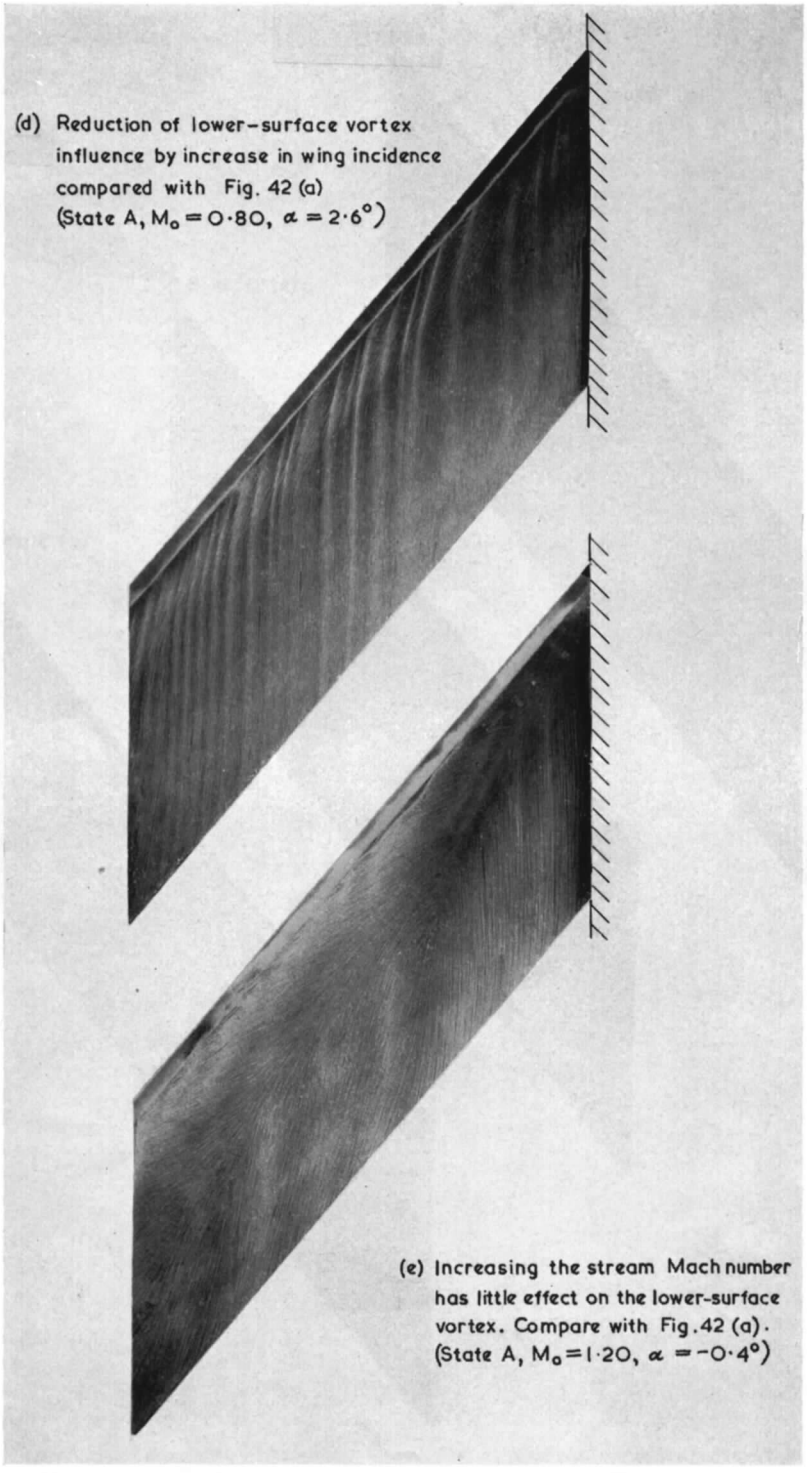

FIGS. 42d and 42e.

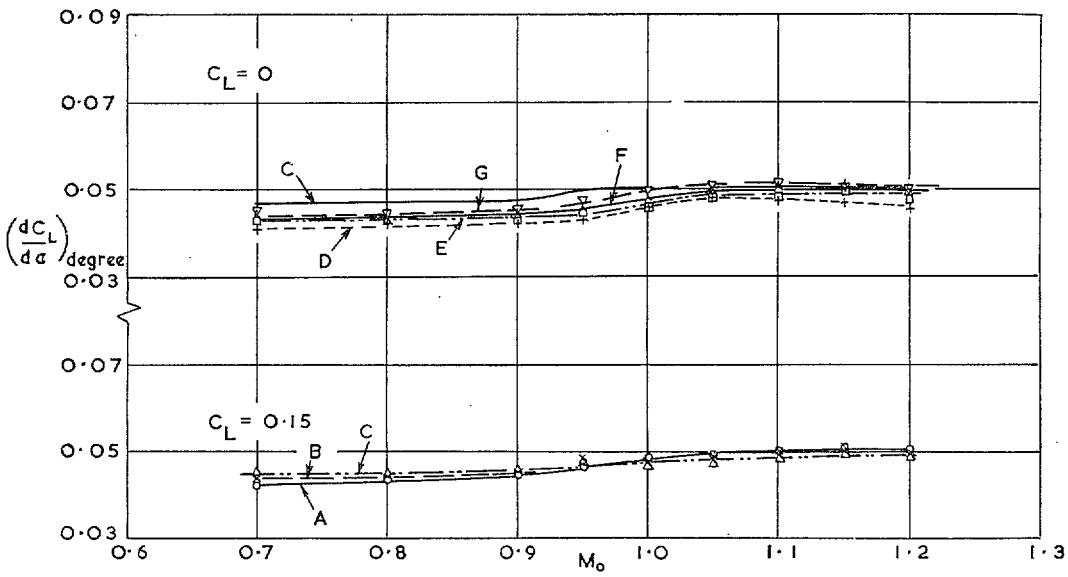

FIG. 43. Variation of lift-curve slope with Mach number.

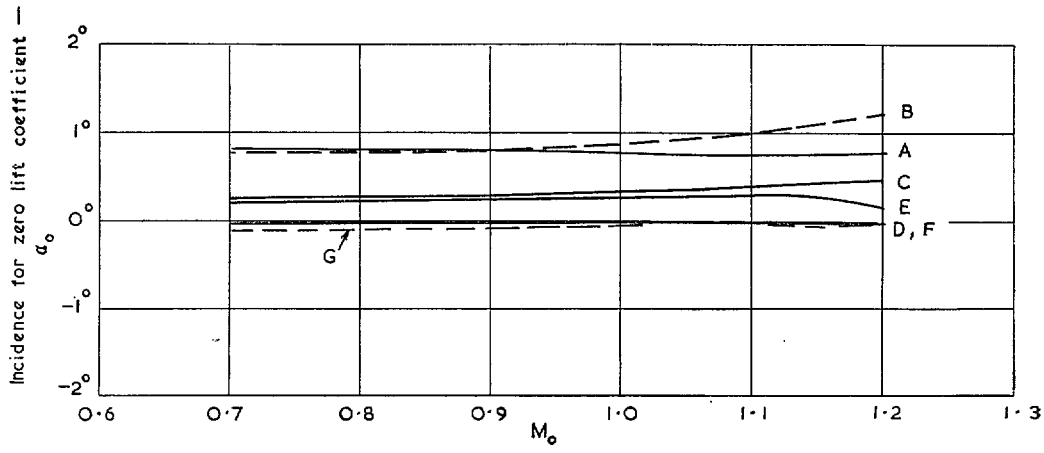

FIG. 44. Variation of zero-lift incidence with free-stream Mach number.

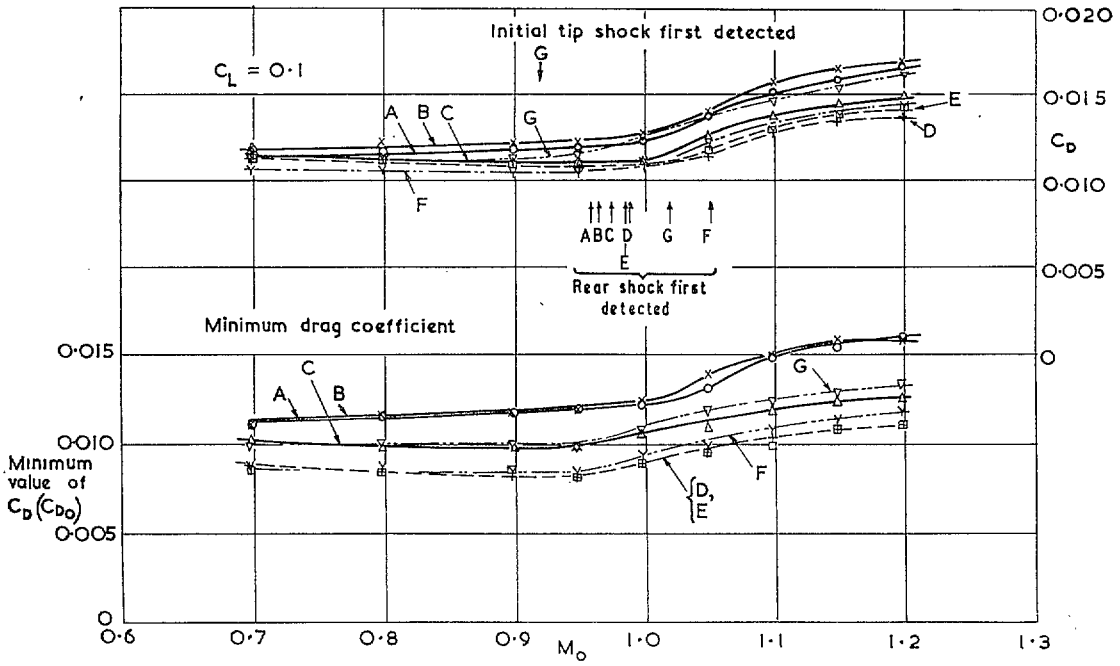

FIG. 45a. Minimum drag coefficient and drag at constant lift.

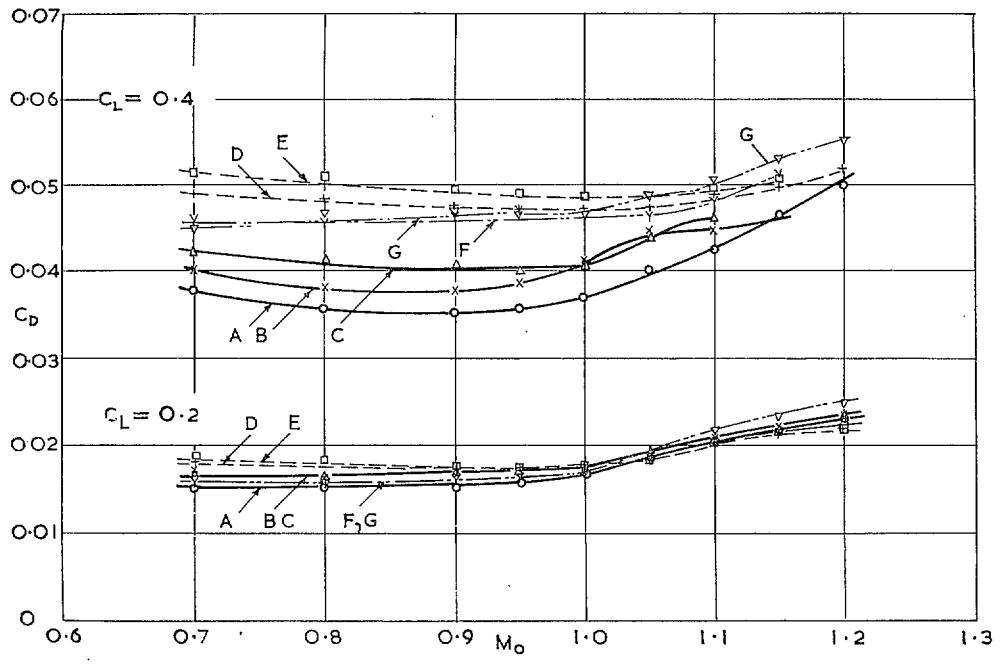

(b)

FIG. 45b.

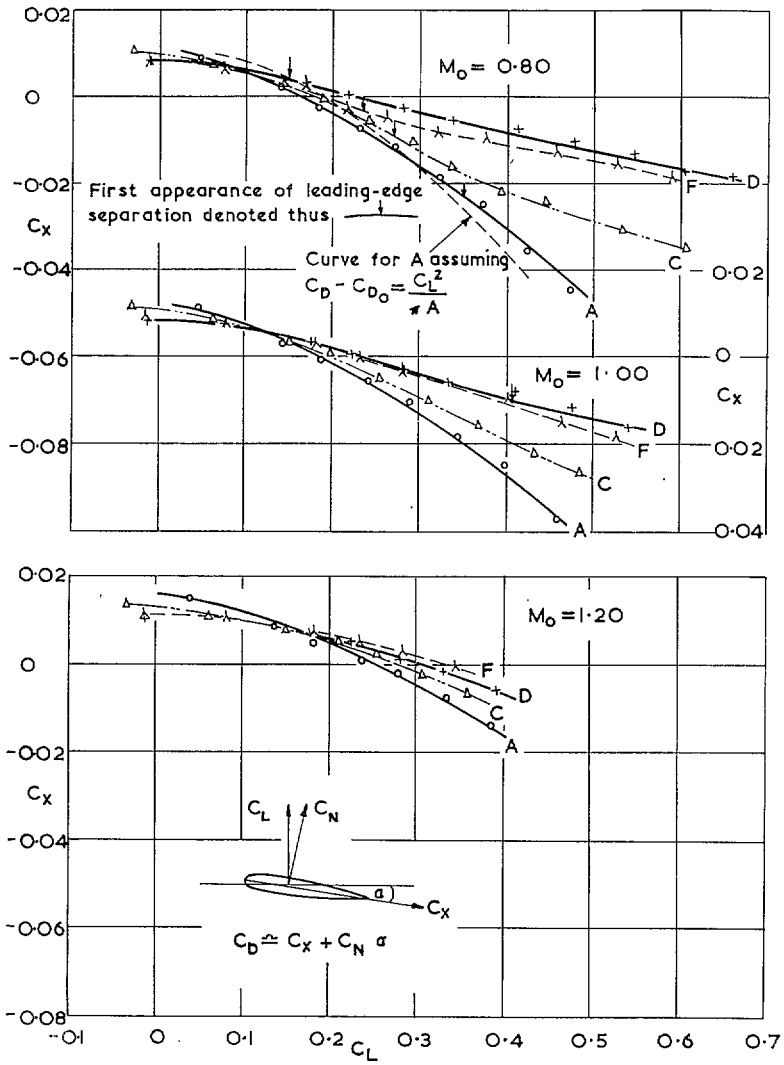

FIG. 46. Axial force variation with wing lift.

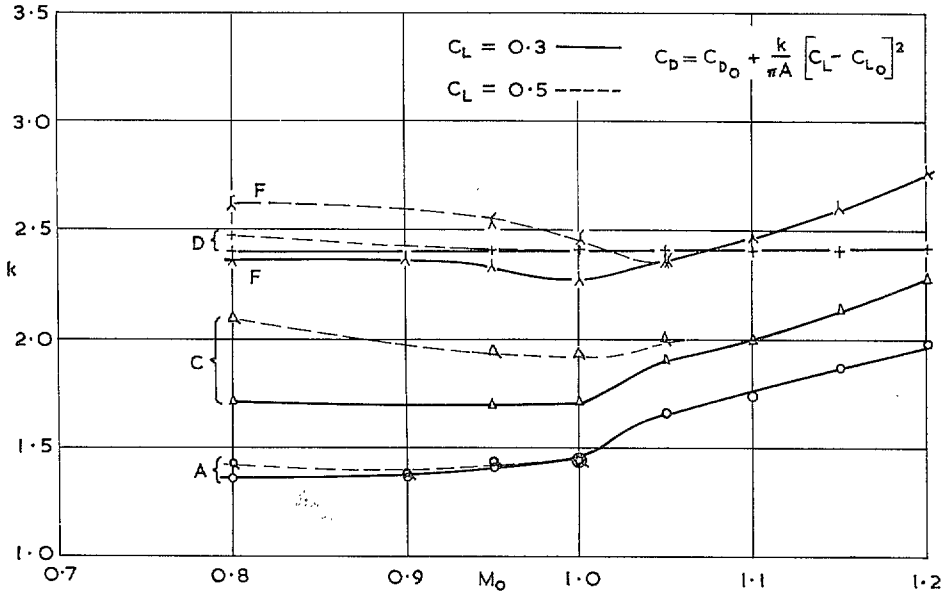

FIG. 47. Lift-dependant drag factors for four typical model states.

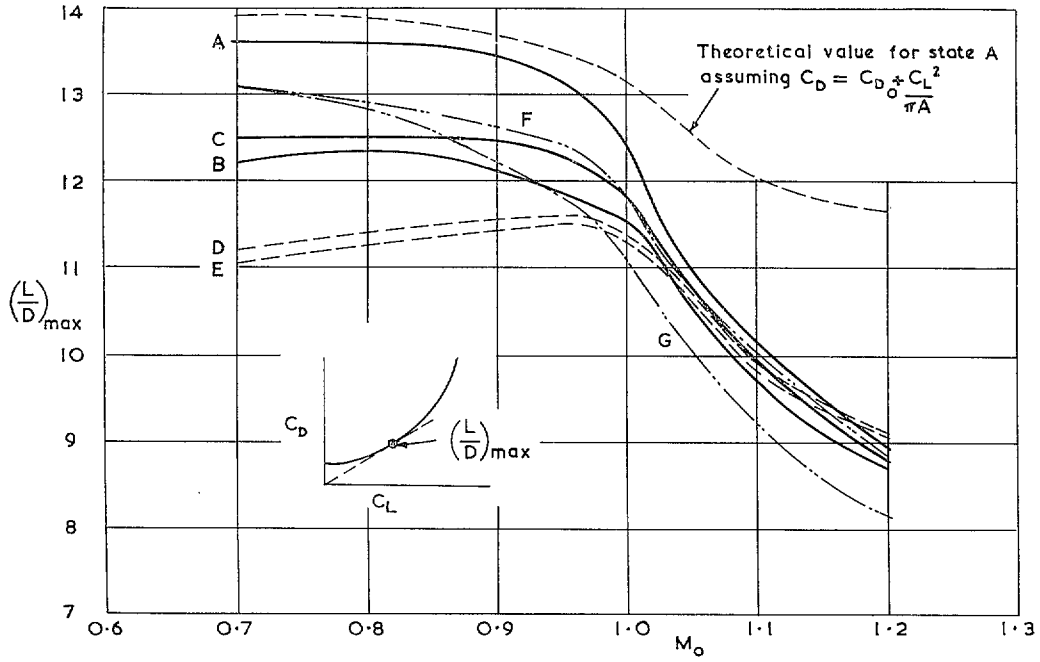

FIG. 48. Effect of model state on lift/drag ratio.

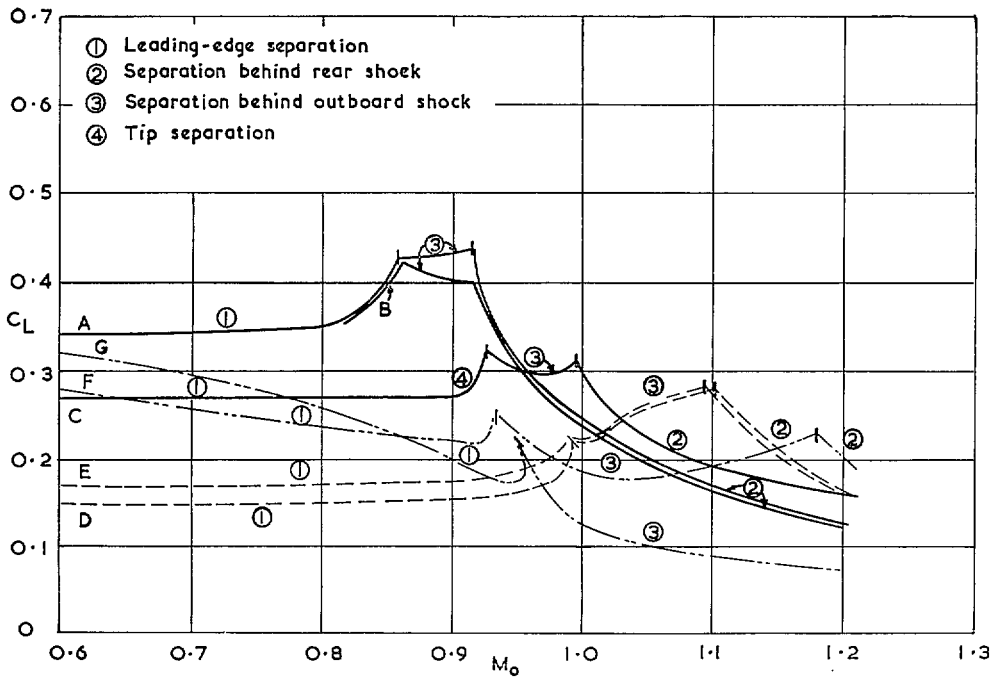

FIG. 49. The lower separation boundaries for the seven model states.

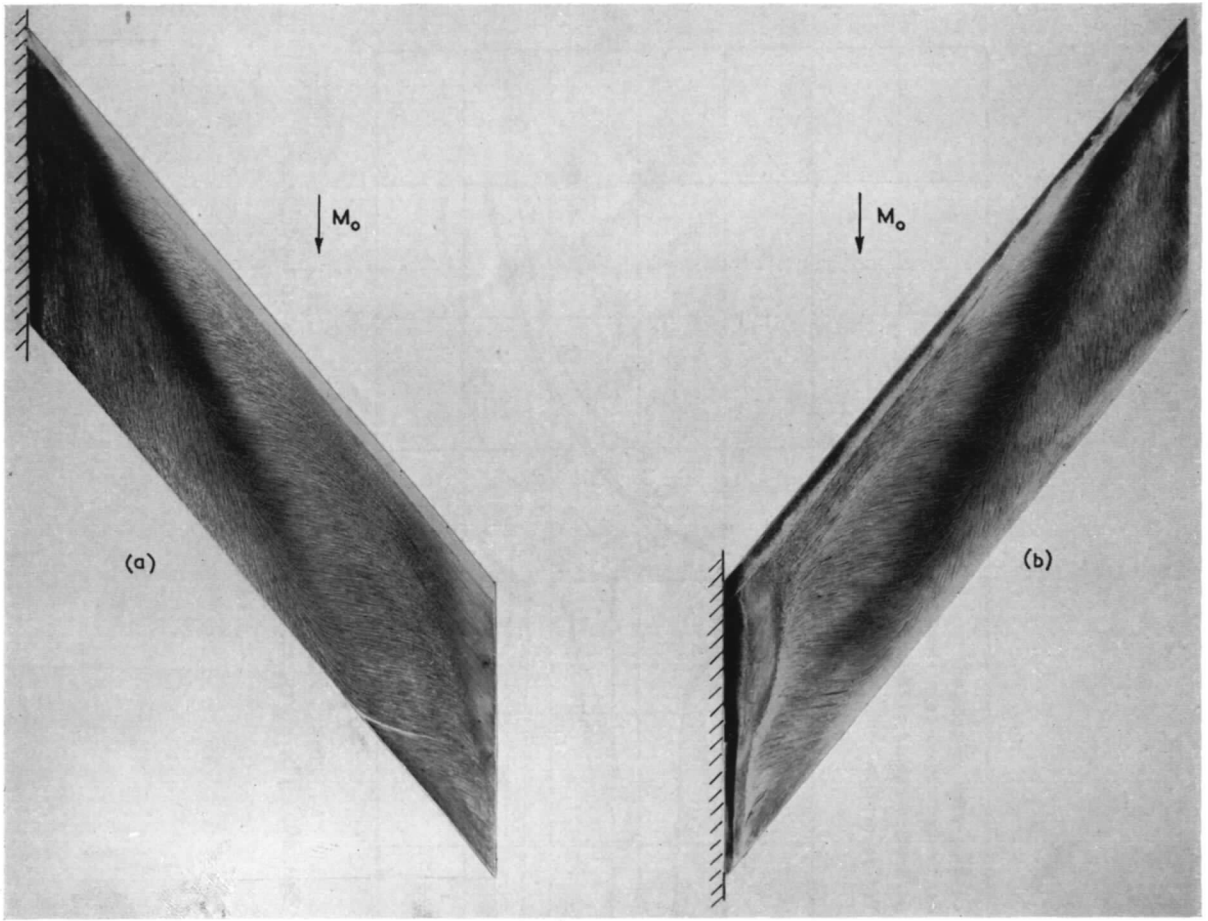

FIG. 50a and b. Comparison of flow patterns on sweptback and sweptforward wings at $M_0 = 0{\cdot}8$, $\alpha = 9{\cdot}6$ deg. (State D).

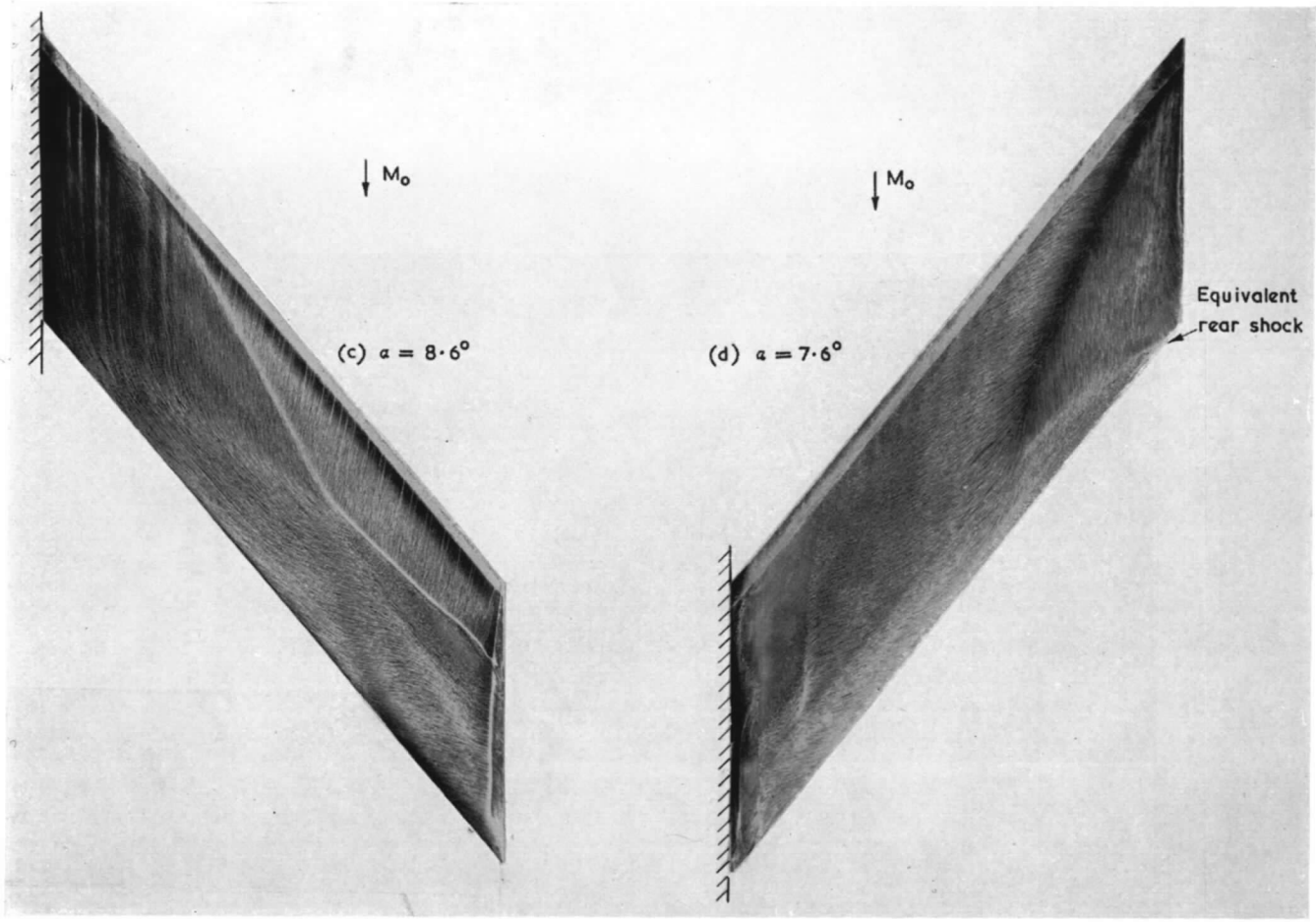

FIG. 50c and d. Comparison of flow patterns on sweptback and sweptforward wings at $M_0 = 1{\cdot}20$. (State D).

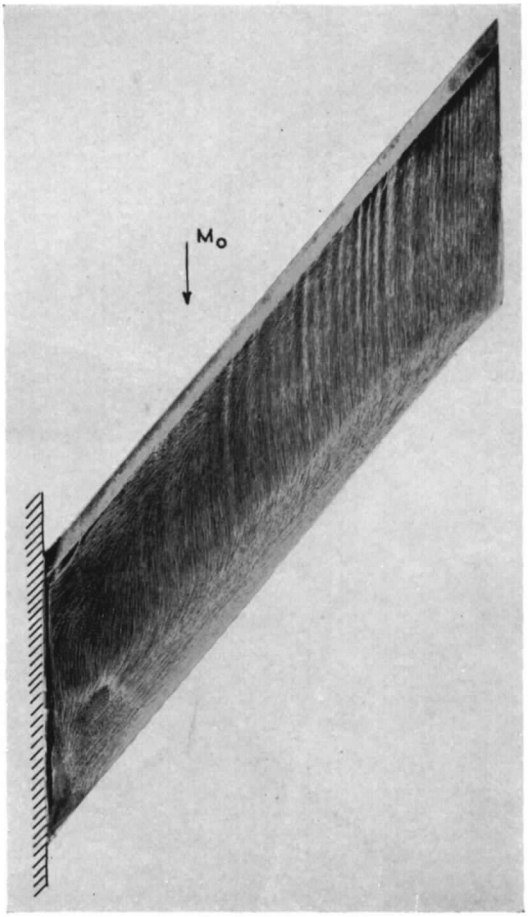

FIG. 50e. Flow pattern on sweptforward wing (State D) at $M_0 = 1{\cdot}20$, $\alpha = 3{\cdot}6$ deg.

(83976) Wt. 67/1876 K.5 3/62 Hw.

Publications of the Aeronautical Research Council

ANNUAL TECHNICAL REPORTS OF THE AERONAUTICAL RESEARCH COUNCIL (BOUND VOLUMES)

1941 Aero and Hydrodynamics, Aerofoils, Airscrews, Engines, Flutter, Stability and Control, Structures. 63*s.* (post 2*s.* 3*d.*)

1942 Vol. I. Aero and Hydrodynamics, Aerofoils, Airscrews, Engines. 75*s.* (post 2*s.* 3*d.*)
Vol. II. Noise, Parachutes, Stability and Control, Structures, Vibration, Wind Tunnels. 47*s.* 6*d.* (post 1*s.* 9*d.*)

1943 Vol. I. Aerodynamics, Aerofoils, Airscrews. 80*s.* (post 2*s.*)
Vol. II. Engines, Flutter, Materials, Parachutes, Performance, Stability and Control, Structures. 90*s.* (post 2*s.* 3*d.*)

1944 Vol. I. Aero and Hydrodynamics, Aerofoils, Aircraft, Airscrews, Controls. 84*s.* (post 2*s.* 6*d.*)
Vol. II. Flutter and Vibration, Materials, Miscellaneous, Navigation, Parachutes, Performance, Plates and Panels, Stability, Structures, Test Equipment, Wind Tunnels. 84*s.* (post 2*s.* 6*d.*)

1945 Vol. I. Aero and Hydrodynamics, Aerofoils. 130*s.* (post 3*s.*)
Vol. II. Aircraft, Airscrews, Controls. 130*s.* (post 3*s.*)
Vol. III. Flutter and Vibration, Instruments, Miscellaneous, Parachutes, Plates and Panels, Propulsion. 130*s.* (post 2*s.* 9*d.*)
Vol. IV. Stability, Structures, Wind Tunnels, Wind Tunnel Technique. 130*s.* (post 2*s.* 9*d.*)

1946 Vol. I. Accidents, Aerodynamics, Aerofoils and Hydrofoils. 168*s.* (post 3*s.* 3*d.*)
Vol. II. Airscrews, Cabin Cooling, Chemical Hazards, Controls, Flames, Flutter, Helicopters, Instruments and Instrumentation, Interference, Jets, Miscellaneous, Parachutes. 168*s.* (post 2*s.* 9*d.*)
Vol. III. Performance, Propulsion, Seaplanes, Stability, Structures, Wind Tunnels. 168*s.* (post 3*s.*)

1947 Vol. I. Aerodynamics, Aerofoils, Aircraft. 168*s.* (post 3*s.* 3*d.*)
Vol. II. Airscrews and Rotors, Controls, Flutter, Materials, Miscellaneous, Parachutes, Propulsion, Seaplanes, Stability, Structures, Take-off and Landing. 168*s.* (post 3*s.* 3*d.*)

Special Volumes

Vol. I. Aero and Hydrodynamics, Aerofoils, Controls, Flutter, Kites, Parachutes, Performance, Propulsion, Stability. 126*s.* (post 2*s.* 6*d.*)
Vol. II. Aero and Hydrodynamics, Aerofoils, Airscrews, Controls, Flutter, Materials, Miscellaneous, Parachutes, Propulsion, Stability, Structures. 147*s.* (post 2*s.* 6*d.*)
Vol. III. Aero and Hydrodynamics, Aerofoils, Airscrews, Controls, Flutter, Kites, Miscellaneous, Parachutes, Propulsion, Seaplanes, Stability, Structures, Test Equipment. 189*s.* (post 3*s.* 3*d.*)

Reviews of the Aeronautical Research Council

1939–48 3*s.* (post 5*d.*) 1949–54 5*s.* (post 5*d.*)

Index to all Reports and Memoranda published in the Annual Technical Reports

1909–1947 R. & M. 2600 6*s.* (post 2*d.*)

Indexes to the Reports and Memoranda of the Aeronautical Research Council

Between Nos. 2351–2449	R. & M. No. 2450 2*s.* (post 2*d.*)
Between Nos. 2451–2549	R. & M. No. 2550 2*s.* 6*d.* (post 2*d.*)
Between Nos. 2551–2649	R. & M. No. 2650 2*s.* 6*d.* (post 2*d.*)
Between Nos. 2651–2749	R. & M. No. 2750 2*s.* 6*d.* (post 2*d.*)
Between Nos. 2751–2849	R. & M. No. 2850 2*s.* 6*d.* (post 2*d.*)
Between Nos. 2851–2949	R. & M. No. 2950 3*s.* (post 2*d.*)
Between Nos. 2951–3049	R. & M. No. 3050 3*s.* 6*d.* (post 2*d.*)

HER MAJESTY'S STATIONERY OFFICE

from the addresses overleaf

Printed and published by
HER MAJESTY'S STATIONERY OFFICE

To be purchased from
York House, Kingsway, London W.C.2
423 Oxford Street, London W.1
13A Castle Street, Edinburgh 2
109 St. Mary Street, Cardiff
39 King Street, Manchester 2
50 Fairfax Street, Bristol 1
35 Smallbrook, Ringway, Birmingham 5
80 Chichester Street, Belfast 1
or through any bookseller

Printed in England

S.O. Code No. 23-3270